DESIGN & ANALYSIS OF MICROFLUIDIC SYSTEMS FOR DROPLET GENERATION VIA FLOW FOCUSING & ELECTROGENERATION

DESIGN & ANALYSIS OF MICROFLUIDIC SYSTEMS FOR DROPLET GENERATION VIA FLOW FOCUSING & ELECTROGENERATION

By

SIAWASH SHINWARY SYED, B.ENG.

B. Eng. (McMaster University, Ontario, Canada)

A Thesis

Submitted to the School of Graduate Studies

In Partial Fulfillment of the Requirements

For the Degree

Master of Applied Science

McMaster University

Master of Applied Science (2011) McMaster University

(Mechanical Engineering) Hamilton, Ontario

TITLE: Design & Analysis of Microfluidic Systems for Droplet Generation Via Flow Focusing & Electrogeneration

AUTHOR: Siawash Shinwary Syed, B.Eng. (McMaster University)

SUPERVISOR(S): Professor P. R. Selvaganapathy,

NUMBER OF PAGES: xv, 119

Abstract

Microdroplets have large and varied areas of application ranging from document printing to complex lab-on-chip devices. Lab-on-chip systems often require precise volume control as well as high throughput operations. Microdroplets fulfill these requirements and have become a staple in these devices. Out of the several ways droplet generation could be initiated in the microscale, electrical and flow control are of most interest. The work presented in this thesis involves the design and characterization of two individual devices capable of droplet generation utilizing these two methods.

The first design involved the generation of gel microdroplets utilizing the flow focusing technique. This device proved to be robust and reliable producing large volumes of uniformly mixed droplets. A microfluidic mixing section was developed for creating uniformly mixed droplets of two miscible solutions. The mixing obtained was analyzed using fluorescent tagging and was thus deemed to be uniform. Furthermore, long term operation of this device was analyzed and determined to be a feasible route for the manufacture of large quantities of droplets. The device was operated for over 30 hours creating gel droplets ranging from 40-200 μm in diameter with acceptable polydispersities for use in drug release studies.

The second device involved the design and characterization of a system for the electrogeneration of microdroplets. This novel device involved the injection of droplets via high voltage and high frequency signals into a cross-flow of oil. The droplet generation was characterized and different droplet generation modes were observed. With

the careful selection of parameters ideal conditions were obtained to generate monodisperse droplets of sizes ranging from under 5 to over 100 μm in a highly repeatable manner.

To conclude, two separate microfluidic droplet generation devices operating in distinct modes were designed and analyzed. These devices are robust, reliable, and flexible with some applications being tested.

Acknowledgements

I would like to express my appreciation to my supervisor Dr. P. R. Selvaganapathy for giving me the opportunity to work with him in this exciting area of research. Without his help, guidance, and ideas working in such a different area of engineering would have been impossible. He always encouraged me throughout this work when it seemed like it was impossible, for these things I am deeply grateful for all Dr. Ravi has done.

I would also like to thank those who have collaborated on this project and provided a great deal of help in its' completion. Leah Kesselman who helped me on the flow focusing project with all the chemistry and drug release studies, without her this project would have been impossible to complete. My thanks go to Dr. Hoare whose ideas started the flow focusing project and helped shape it to what it finally became. The moral support, help and equipment kindly provided by Dr. C. Y. Ching greatly aided the completion of this project, without him beautiful droplet pictures would not be possible.

I would like to thank Lisa for providing me with love and encouragement and Sinan with providing me with great advice. Arash, Geetha, Pouya, Wen, Peter and Salman for providing invaluable assistance on the project and sharing with me their knowledge and experience. Lastly, a big thanks my lab members Bo, Shihad, Ali, and Michael for providing an engaging and fun working environment. Without those listed this work would have been impossible, they have my appreciation and gratitude forever and I will look upon the time I spent working with them fondly.

Table of Contents

List of Figures

Chapter 1 Motivation & Organization

1.1 Motivation

Microdroplets have a long list of uses, the most important of which are in drug delivery, biological studies and medicine. Microparticles and gels formed by droplets are sought in drug delivery due to their monodispersity which effectively controls their drug release rates. Similarly, in biological studies, microdroplets are used to conduct large sets of screening experiments on small sample volumes consuming small quantities of valuable and expensive reagents. A variety of commonly used methods such as inkjet printing and emulsification are capable of microdroplet production. However, with these methods, control over droplet size is limited and droplets that are produced have large size distributions. Microfluidics overcomes many of these limitations offering the possibility of handling small volumes of fluid at reasonably high throughput. Out of the techniques currently available for microdroplet generation the most promising are control through fluid shear or by the application of a high voltage electrical signal. Although these methods have been established it is desirable to adapt and develop them further to improve performance and capability. The work presented in this thesis is an attempt to combine dynamic droplet size control with high frequency production. In addition, the ability to generate droplets composed of mixtures of two reacting species is desirable to applications such as drug discovery and microfluidic reactors. The devices developed in this thesis offers the ability to control droplet sizes while maintaining narrow size

distributions thus enabling the usage of these droplets for drug release and biomaterial encapsulation.

1.2 Sequence of Chapters

The organization of the thesis is outlined in the following:

Chapter 2 provides an introduction to droplets and the physics of droplet formation. The uses of these droplets are next discussed while also providing an introduction to microfluidics. Finally the uses and the various techniques that can be utilized to generate of microdroplets are reviewed.

Chapter 3 provides an outline of the materials and microfabrication techniques utilized when building and operating the devices. Additionally, the fabrication procedures are presented and device assembly is explained.

Chapter 4 presents the design of a microfluidic device for generation of mixed microdroplets composed of reacting solutions in large quantities using the flow focusing technique. The optimized design is analyzed and its' capabilities are determined. Micrographs are studied and data is presented on device capabilities and performance. Furthermore, results are analyzed and explained using theory and literature.

Chapter 5 presents the design of a microfluidic device for generation of microdroplets via the application of a high voltage electric signal. The optimized design is analyzed and droplet generation utilizing varying waveforms is studied.

Chapter 6 concludes this work and highlights the contributions made. Possibilities for future work and further design revisions to increase the capabilities of the devices are presented.

Chapter 2 Introduction

2.1 Droplet Formation

A falling cylinder of fluid in air will eventually break up into droplets as pictured in **Figure 2.1**, the question arises why does it not remain a cylinder? Lord Rayleigh [1] answered this question when he performed fluid mechanics analysis on the instabilities present in fluid jets. The formation of droplets is due to the flow instabilities occurring in any fluid. Although the surface tension acts to hold the fluid together, the increasing length of the jet and propagation of instabilities cause the surface energy to become very high. As with everything else in nature, the system tends to minimize energy and in this case the surface energy of droplets is less than that of a fluid cylinder. A detailed and involved mathematical analysis gives a better understanding of droplet formation.

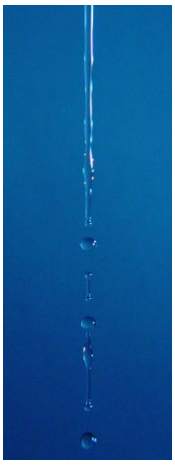

Figure 2.1 : *Droplet formation [2].*

The steady and perturbed states of a fluid jet are illustrated in **Figure 2.2**. Using the Navier-Stokes and continuity equations and adding the effects of perturbation fields present within the fluid, the following relationships are obtained [2].

$$\frac{\partial \widetilde{u}_r}{\partial t} = -\frac{1}{\rho}\frac{\partial \widetilde{p}}{\partial r}$$

$$\frac{\partial \widetilde{u}_z}{\partial t} = -\frac{1}{\rho}\frac{\partial \widetilde{p}}{\partial z} \quad (2.1)(2.2)$$

$$\frac{\partial \widetilde{u}_r}{\partial r} + \frac{\widetilde{u}_r}{r} + \widetilde{u}_z = 0 \quad (2.3)$$

Where *u* is flow velocity, *p* is the pressure, *r* is the radial axis, *z* is the vertical axis, and tilde indicating that the effects of perturbations are being considered. Substituting perturbation velocities and pressures into the equations above yields a Bessel function of the order 1. This Bessel function can be solved to give a wave dispersion function. Using the fastest propagating mode it is possible to determine a characteristic time for the breakup of a fluid jet [2]:

$$t_{breakup} \simeq 2.91\sqrt{\frac{\rho R_0^3}{\gamma}} \quad (2.4)$$

With this relation it is possible to calculate the time in which a fluid jet will collapse and form a droplet.

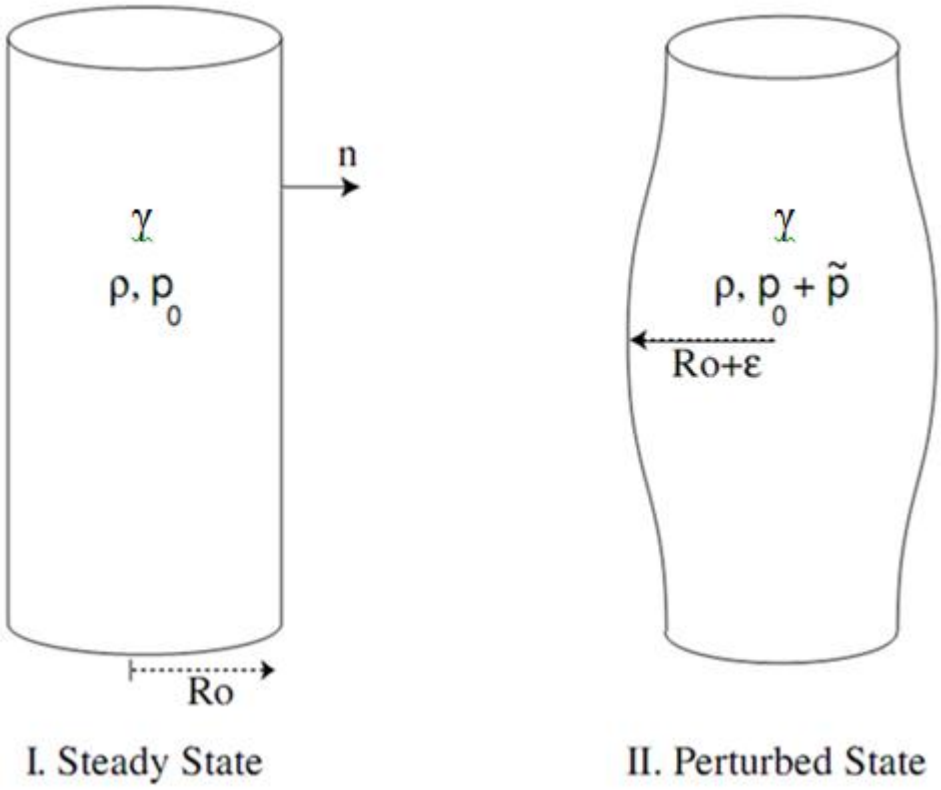

Figure 2.2 : *Steady and perturbed states of a fluid jet [2].*

Using dimensional analysis it is possible to obtain a relationship for the critical length formed by a jet before breakup into droplets. It is reasonable to assume that the critical length will be related to the jet velocity, density, surface tension, and radius. Using these parameters in dimensionless analysis it is possible to obtain:

$$\frac{L_{crit}}{R} \sim U\left(\frac{\rho R}{\gamma}\right)^{\frac{1}{2}} \quad (2.5)$$

With experiments it is possible to obtain a direct relationship between the critical length and the dimensionless number presented. These relations help give a better understanding into the fundamentals of droplet formation. That is to say that the formation of droplets is

essentially due to the propagation of instabilities in the fluid jet which become too great after some length and cause the jet's collapse into droplets. It is reasonable to assume by introducing instabilities into a fluid it would be possible to cause droplet formation and perhaps to even control it.

2.2 Microfluidics & Applications of Microdroplets

Microfluidics is a promising new area of engineering dealing with the handling of sub picolitre volumes of fluids [3]. Microfluidics is synonymous with lab-on-a-chip devices capable of performing laboratory operations in a very small environment [4]. This area has arisen as a result of increased interest in the areas of biochemical screening, protein crystallization [5], enzymatic kinetic assays, DNA amplification [6], DNA sequencing, and many other applications in chemical and biological studies. In particular the use of microdroplets is appealing to microfluidics[7] due to its ability to compartmentalize reactions, have precise control over reacting volumes and parameters such as temperature [8], and the ability to perform thousands of operations simultaneously on thousands of droplets [9]. Typically it is easy to imagine droplets being manually generated by a pipette, however for high throughput systems and smaller volumes such a technique does not provide enough quantity or precision [10]. Additionally it is possible to generate emulsions of large amounts of droplets (disperse phase) suspended in a carrying phase which can be called the continuous phase. However although these methods can produce bulk solutions, typical emulsion production methods produce larger variation in droplet sizes or what is known as high polydispersities [3].

Pneumatic and rotary atomizers also provide a method to generate droplets in bulk but are limited in sizes [11]. In order to create droplets in varying size ranges as well as in large quantities for lab-on-chip or drug release applications we look to microfluidics.

One of the main applications for microdroplets is for usage in lab-on-chip systems [12]. Lab-on-chip systems aim to shrink down the processes traditionally done in a larger scale laboratory into single automated microfluidic device that does not require a highly trained professional for operation. Such a system would significantly reduce the lab footprint of certain processes whilst at the same time performing the same tasks and reducing costs. **Figure 2.3** demonstrates some of the processes that could be integrated onto a single microfluidic chip in order to perform complex laboratory procedures. Advantages of using such systems include a reduction of up to 100000 times of the volumes of expensive reagents being utilized and as a result increasing the number of experiments possible [12]. An example of an integrated lab-on-chip system is protein crystallization [13]. Many biomedical applications require knowledge of the tertiary structure of a protein, however in order to determine the structure of a protein one must utilize X-ray diffraction on a crystallized sample of said protein.

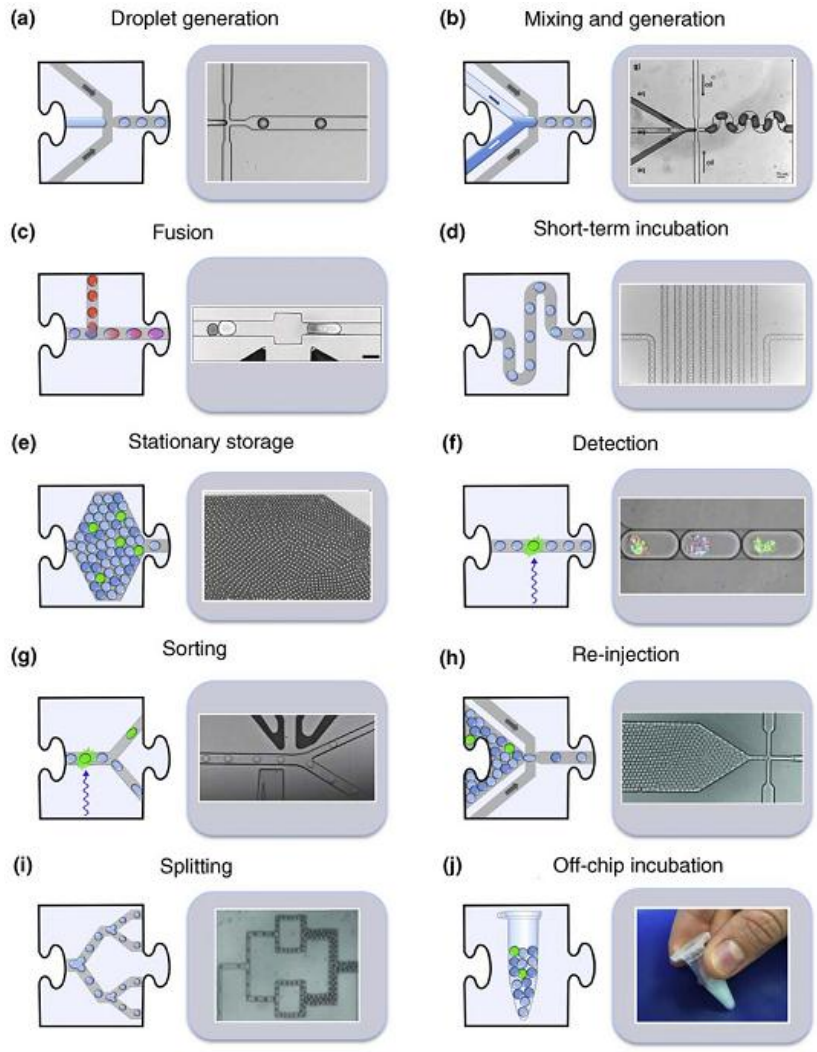

Figure 2.3 : *Lab-on-chip processes [12].*

A crystallized protein is not so easily obtained, it requires a specific chemical environment. In order to achieve crystallization a series of experiments must be conducted where protein in a solution is subjected to varying pH levels, salt concentrations, protein concentrations, and temperatures. Currently such processes are done on a large scale using microwell plates with advanced systems controlling experimental conditions with the usage of expensive large scale robotics. As shown in

Figure 2.4 Zheng *et al.* [13] demonstrated that these protein crystallization experiments could be completed in a lab-on-chip system. This significantly reduced the amount of reagents utilized down to nanolitre volumes. Many other processes such as biomaterial encapsulation [14], combinatorial chemistry and drug discovery [15] are similar to protein crystallization and require large numbers of experiments to be completed with expensive reagents. These types of experiments would greatly benefit through the usage of novel lab-on-chip devices.

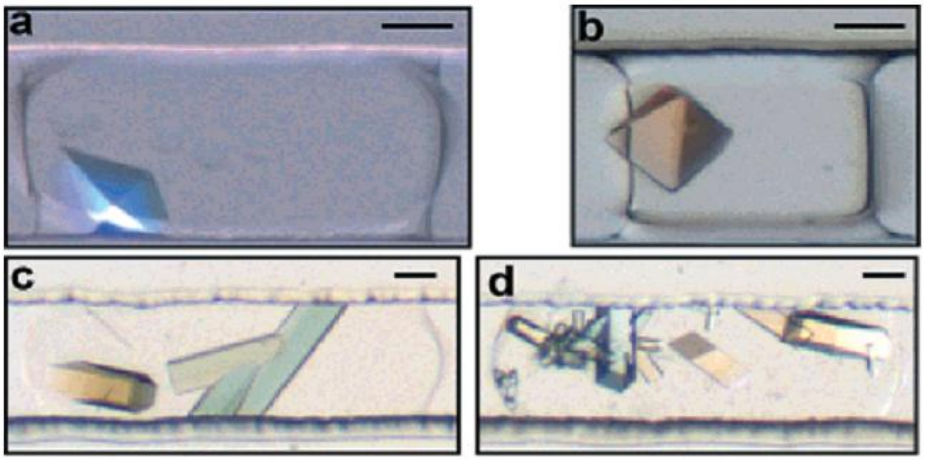

Figure 2.4 : *Protein crystallization in a microfluidic chip (scale bar is 50 μm) [13].*

The usage of biodegradable polymer microparticles as a drug release method provides several key advantages over traditional means. One such advantage is that these particles can be easily implanted into the subject and release drugs over long durations of time [5].Typically particles in the size ranges from 1-100 μm are of interest for drug release since they are less likely to be endocytosed by macrophages and quickly sequestered to the spleen. This increases their endurance and usefulness inside the patient. Long term release in itself provides several advantages, one being that there is an

avoidance of drug concentration spikes experienced by the subject's body. The drug concentration spikes are typical with more traditional methods of drug delivery such as injections or pills. It follows from **Figure 2.5** that the drug release can be controlled by varying particle sizes. This figure was obtained by measuring the drug release from 300 mg of particles with the mean diameter listed. Furthermore it is possible to change the particle morphologies such as introducing porosity or creating hollow shells to analyze the drug release. For the reasons stated, microparticles are a very interesting development in drug release analysis.

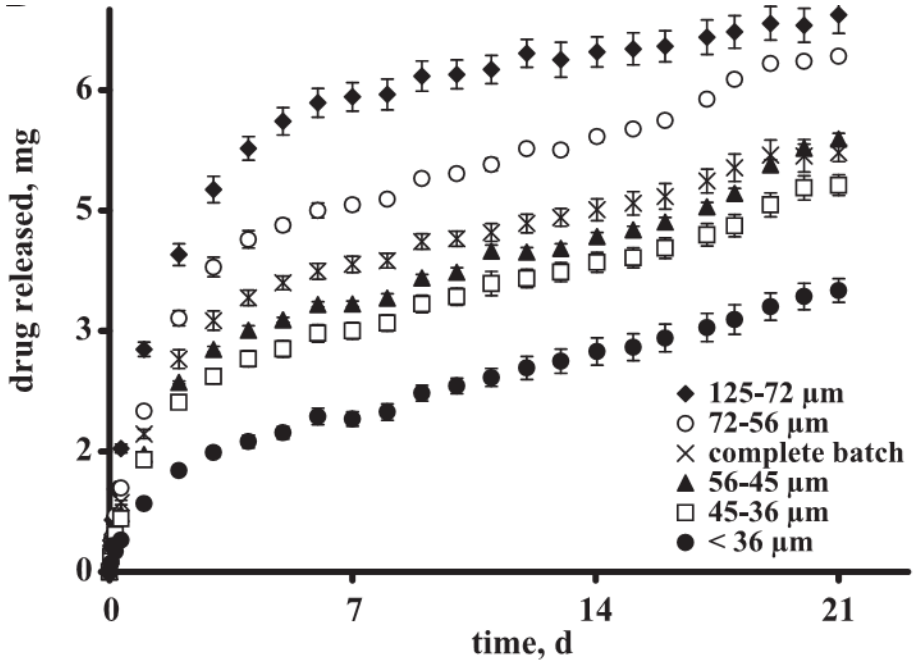

Figure 2.5 : *Drug release of varying polymer microparticles sizes vs time [16].*

Additionally microgels that are not solid have varying applications not possible with the usage of dry particles such as the encapsulation of living cells [17]. All of the areas discussed involve droplets or spherical microparticles. For some applications

changing the droplet sizes rapidly and extracting them on demand are important whilst others require generation of droplets in vast quantities. It was determined that an investigation and design of devices for both sides of the spectrum would be beneficial. The first device is one that is capable of generating droplets in a more discrete manner but at higher frequencies than what has currently been investigated in drop on demand studies which operate in frequencies typically slower than 1 Hz. Additionally this device would require the ability to change droplet sizes dynamically with little transition, an electrical signal provides a fast responding driving force ideal for this case. Another device will focus on the generation of a mixture of reacting polymers that will turn into a gel ideal for holding drugs that are to be delivered to patients. This device would produce the vast quantities of monodisperse gel droplets required to perform drug release studies. Both of these devices are required to generate droplets in sizes ranging from a few to hundreds of microns. This size range is of interest due to being in the same range as cells as well as reasons previously discussed.

2.3 Droplet Generation Techniques

Due to their wide ranging applications several microdroplet generation techniques have been developed. Perhaps the most well developed and best established technique is inkjet printing. This technique involves the usage of a piezoelectric [18] or heat source [19] to produce high pressure and force fluid out of a nozzle generating a microdroplet. Other methods involve the creation of bulk emulsions through sonication [20] or the use of a mixer [21]. Although emulsion production techniques and inkjet printing are capable

of microdroplet generation, control over size and variation in size remains limited. To overcome these limitations a novel approach was developed that utilized flow focusing to generate highly monodisperse droplets of varying sizes [22].

2.3.1 Flow Focusing

Possibly the simplest method to generate droplets in microchannels is through the usage of a viscous shearing force [23]. As demonstrated in **Figure 2.6**, to generate droplets via a shear force a flow of a continuous phase is introduced perpendicular to the flow of a disperse phase. The vicious drag force of the continuous phase causes droplets of the disperse phase to be sheared off [24]. Modifications done by Choi *et al.* [17] to this basic design allow for the creation of polymerized alginate droplets.

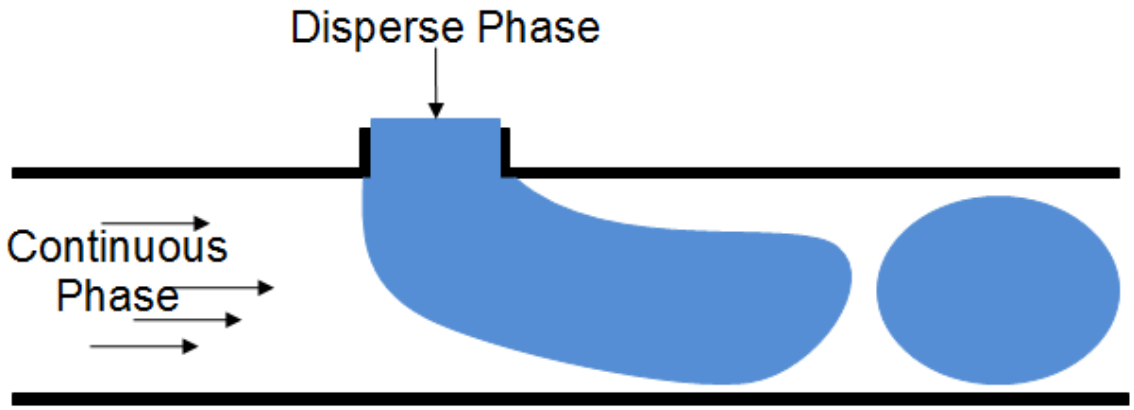

Figure 2.6 : *Typical droplet shearing setup.*

It is seen in **Figure 2.7** that the disperse phase channel involved the combination of alginate and a $CaCl_2$ solution to generate plugs that are mixed in winding section and subsequently cross-linking into alginate gel. This work demonstrated that this method is

capable of making monodisperse alginate microgels above sixty microns in diameter. Furthermore by introducing a third flow in the disperse phase this method can be used to encapsulate cells or other biological materials in an alginate gel in situ. More recently, work has been conducted on creating alginate gels in such devices [14] involving flow or the usage of common techniques such as inkjet printing [25]. Although in this case spherical gels were created other works have looked on the creation of hollow structures [26]. All of these studies involve the usage of the ionically cross-linked alginate system which is not ideal for applications inside the body since ionic cross-linking can easily be broken by ions present in the blood stream [27].

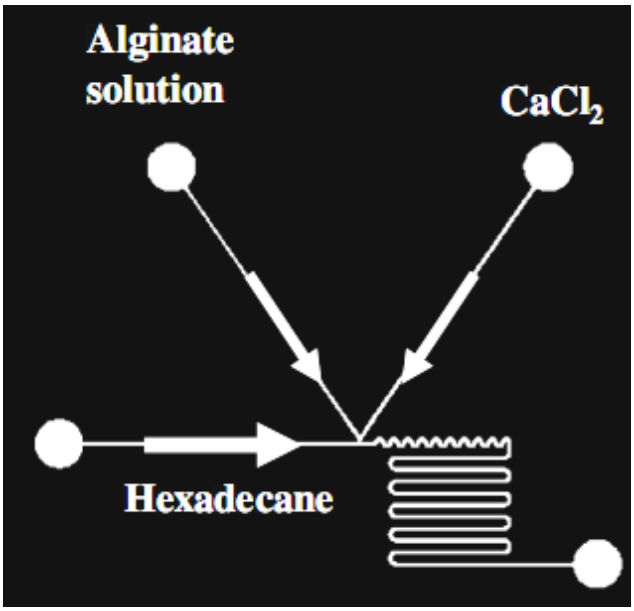

Figure 2.7 : *Setup used to generation alginate gel droplets* [17] .

Perhaps one of the most widely studied methods for droplet generation is flow focusing. First introduced in a microfluidic set up by Shelley *et al.* [22] it has since been

adapted into a wide range of geometries to generate droplets of oils [28], aqueous solutions, polymers, gases [29] and gels. As suggested in the name, flow focusing uses fluid flow to initiate the breakup of droplets [30]. The most basic flow focusing setup is pictured in **Figure 2.8** where a continuous phase surrounds the flow of the disperse phase on either side and focuses this flow through a nozzle to generate droplets. Initially this method was used to generate monodisperse water droplets in oil [31], and in essence creating a controlled water oil emulsion. It was demonstrated that flow focusing is capable of making droplets ranging from over a hundred micrometres to several hundred nanometres in diameter [30]. Due to the ability of having great control over the droplet generation via the flow rates and channel geometries [32] flow focusing has become a prominent method for droplet generation.

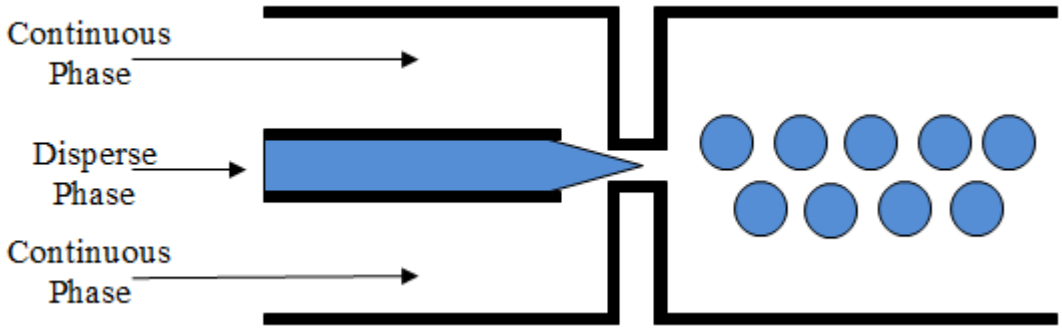

Figure 2.8 : *Basic flow focusing setup with a disperse phase and a continuous phase.*

The mechanism of droplet breakup in flow focusing is ultimately dependent on the interplay between the surface tension of the disperse phase holding everything together and the continuous phase applying a viscous drag and pressure. This forces the disperse phase through a nozzle and introduces surface instabilities [33]. These surface instabilities

introduced by the flow allow for a controlled breakup[34] of the disperse phase fluid producing monodisperse microdroplets.

Due to its robustness and versatility this method of droplet generation has been adapted to create monodisperse gel droplets. One such case involves the usage of the polymer alginate in a flow focusing device [35]. Alginate is a linear copolymer readily available and easily synthesized using common sea algae. This polymer is nontoxic and biodegradable making it an ideal choice for usage in biomaterial encapsulation applications [17]. The setup utilized by Xu et al is shown in **Figure 2.9** [35]. This design involved the integration of alginate, DI water, and $CaCl_2$ streams being focused by octyl alchohol to generate droplets of the three solutions. These droplets due to their composition will react and gel further downstream. This study provides an excellent method for alginate microgel generation with very low coefficients of droplet size variance.

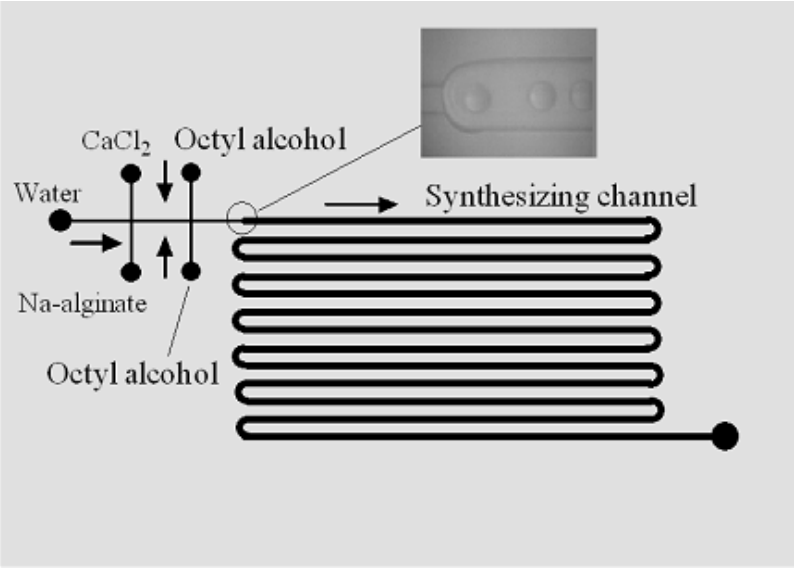

Figure 2.9 : *Device used to create alginate gels [35].*

The vast majority of studies done in creating polymer or gel particles using flow focusing involve polymerization post cross-linking. Common methods of polymerization include solvent evaporation [36], thermal cross-linking, UV cross-linking [37], and submerging generated droplets into a cross-linking solution. All of these methods involve the generation of microdroplets first with the polymerization occurring as a post processing step. In the case of ionic, thermal, or UV cross-linking it is possible to cause polymerization to occur on chip downstream by introducing heat, light or ion sources. Alternatively when using ionic cross-linking polymers it is possible to insert ions into the continuous phase to initiate polymerization as the droplets are being generated. With these methods it is possible to create microgels or polymer microparticles with high monodispersity provided the polymerization technique utilized is appropriate.

Although the methods discussed provide many ways of creating microgels, several shortcomings arise when dealing with these designs. Many of the cases involve polymerization in the post processing step, in the case of UV and thermal this could denature or kill any biological specimens contained in the droplet. This makes these methods undesirable for such applications. In addition, post processing steps often increase the time and material costs associated with droplet generation. Thus, it is desired to perform the cross-linking in situ without the need of any external energy sources.

The approaches used to create alginate microgels hold the most promise for a robust microgel flow focusing chip due to in situ cross-linking. Choi et al [17] introduced a novel microfluidic device for on chip alginate microgel generation. Although this method is quite capable, the flow rates used [17] are significantly lower than those

present when using a flow focusing setup [22]. The reduced flow rate makes this technique undesirable for high throughput droplet generation.

The study presented by Xu et al [35] provides a great method for creating microgels. However, in the present application for creating drug delivery microgels, it is desired to generate microgels of A/B polymer systems without the need of introducing a third central stream to act as a buffer which would possibly affect the mixing and the gel composition negatively. It is desired to design a device where any two polymers system can be utilized including "smart" polymers that are typically covalently cross-linked. The advantages of having the polymers in contact is the possibility of having a more uniform gel by the enhanced mixing introduced as well as the device being capable of being operated with various A/B polymer systems. For the reasons stated, the design of a new novel microfluidic system that is capable of in situ microgel generation via flow focusing using covalently cross-linking polymers or any other A/B polymer system would be highly beneficial.

2.3.2 Electrogeneration

Another method to control droplet generation is through the application of an electrical signal. As with any system dealing with electrical signals such a system could possibly provide the ability to change parameters very quickly. This is very attractive for generating droplets on demand or for changing droplet sizes very rapidly during continuous production. Many applications previously discussed such as micro reactors or lab-on-chip systems would greatly benefit from the ability to both dynamically and

rapidly control volumes for chemical reactions. Furthermore, electrical signals also offer a method to provide a sustained and constant force to drive droplet generation with little variation or drift in this force. The promise this method holds has resulted in significant investigations on a process known as electrospraying where droplets can be generated in bulk.

Electrospraying is a process where droplets are generated via a method very similar to aerosol with the key difference being that instead of pressure an electric field is the driving force. Electrospraying is an evolution of the process known as electrospinning. Electrospinning was a phenomena that was initially patented in 1934 [38] and is a process that can generate nanofibres. The experimental setup used for both electrospray and electrospinning is virtually the same and is illustrated in **Figure 2.10** [39]. It consists of a conductive needle that is connected to the working electrode and the grounded collecting plate is placed some distance opposite to the needle. The solution which is going to be spun or sprayed is fed to the needle via a pump and the electric potential is provided by a high voltage power supply. The electrospinning process is very simple; consisting of an electrostatic force elongating a polymer solution at the needle tip [40].

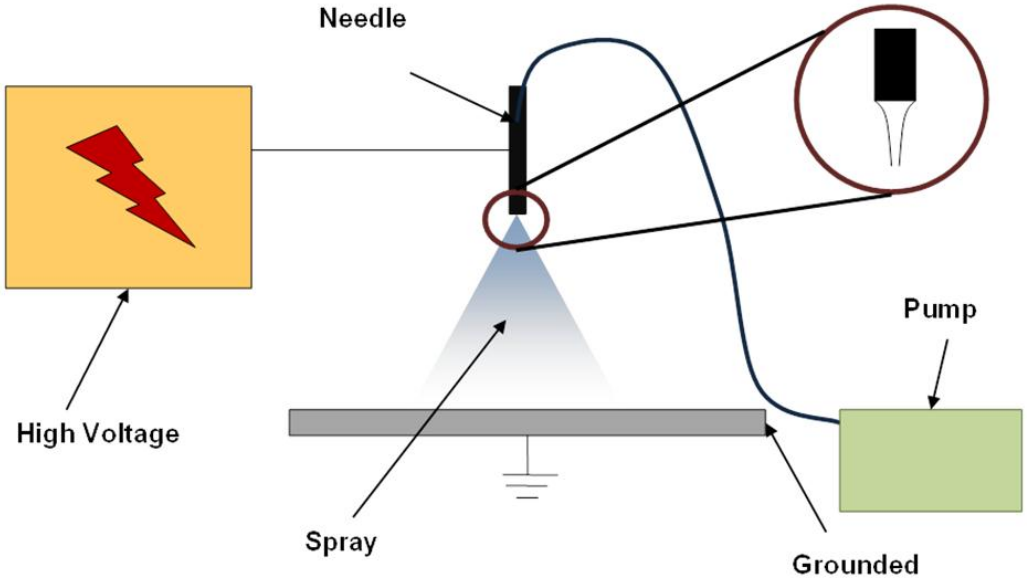

Figure 2.10 : *Typical electrospray experimental setup.*

The application of high voltages in this process that go up to 30 kV causes the formation of what is known as a Taylor cone (shown in **Figure 2.10**). The Taylor cone forms due to the interactions between the electrostatic repulsion at the surface caused by charging, the electrostatic force between the fluid and the ground due to the electric field, and the surface tension. Once the electrical forces overcome surface tension at the tip of the cone, a jet is ejected from the Taylor cone and as the jet travels through the atmosphere towards the ground the solvent will evaporate leaving behind a polymer nanofibre. Many modifications have been made to this setup to produce varying morphologies of fibres [38] , furthermore it is even possible to use this method to create a fine spray of droplets [41].

To move from creating fluid jets to creating a fine spray of droplets a few key parameter must be adjusted [42]. Various modes of droplet generation exist such as

dripping mode, microdripping mode, and cone-jet mode. The cone-jet mode is of the most importance due to its ability to generate large quantities of droplets through a fine spray. It has be determined that this method is capable of generating droplets from under a micron in diameter at frequencies as high as 10^{10} Hz [43]. There is a large amount of literature in this area [44-48] with the most interesting work dealing with the generation of microparticles. A. Jaworek [46] conducted an extensive survey of the work that has been done on electrospraying. It was determined that the main method of controlling the electrospray process was through the viscosity and the electrical conductivity of the solution which could vary from 10^{-4} to 10^{-8} S/m. Additionally, it is determined that by creating a fine spray of a polymer solution it is possible to create polymer microparticles via solvent evaporation. Many modes of operation exist for electrospray with microdroplets being generated primarily in the spraying mode [41].

Using electrospray to create microgels or microparticles is very useful for applications such as drug release and biomaterial encapsulation. Wang *et al.* [42] showed that decreasing the viscosity of the solution being spun caused the transition from fibres, to bead on fibres, and finally to spherical particles as illustrated in **Figure 2.11** and **Figure 2.12** illustrates their attempt to change particle size by varying voltage; it is found that the droplet size does not appreciably change when even doubling the applied potential difference. Despite inability to vary size significantly they did demonstrate particle generation at high flow rates of up to 1 mL/hour with varying morphologies [42]. Xie *et al.*[47] took this electrospraying one step further by encapsulating drug proteins in these particles. Although they demonstrated the ability to vary the size, the particles were

still limited to diameters less than 10 um. Furthermore, studies have been done on parallelization of this process [48] and to generate droplets of varying sizes with low polydispersity [45]. However, by applying high voltages for prolonged periods of time the fluid becomes excessively charged and reaches what is known as the Rayleigh limit of charge [48]. Reaching this limit causes larger droplets to become unstable and undergo fission thus leading to the small diameter droplets. In order to gain more control on the charge injected and thus droplet generation process the application of high voltage pulses is attractive.

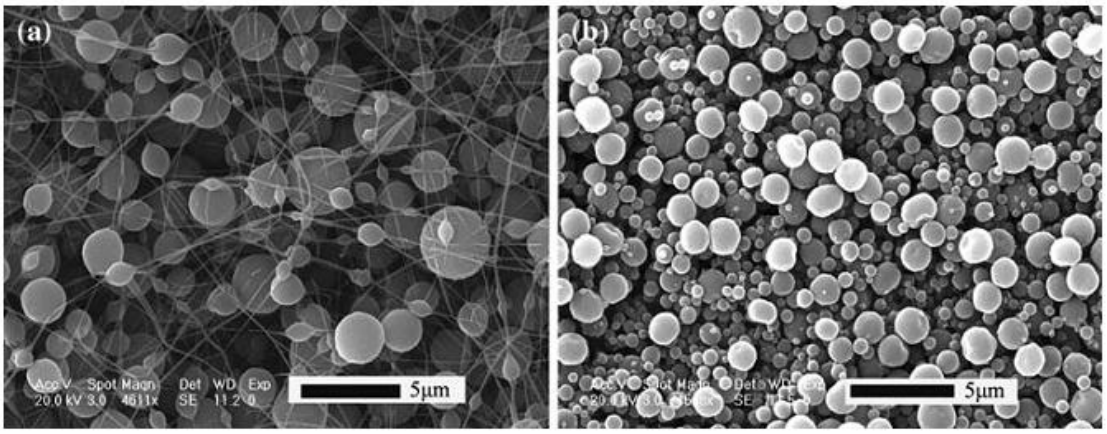

Figure 2.11 : *Differing morphologies obtained when decreasing the polymer concentration from a) 14 %wt to b) 10 %wt [42].*

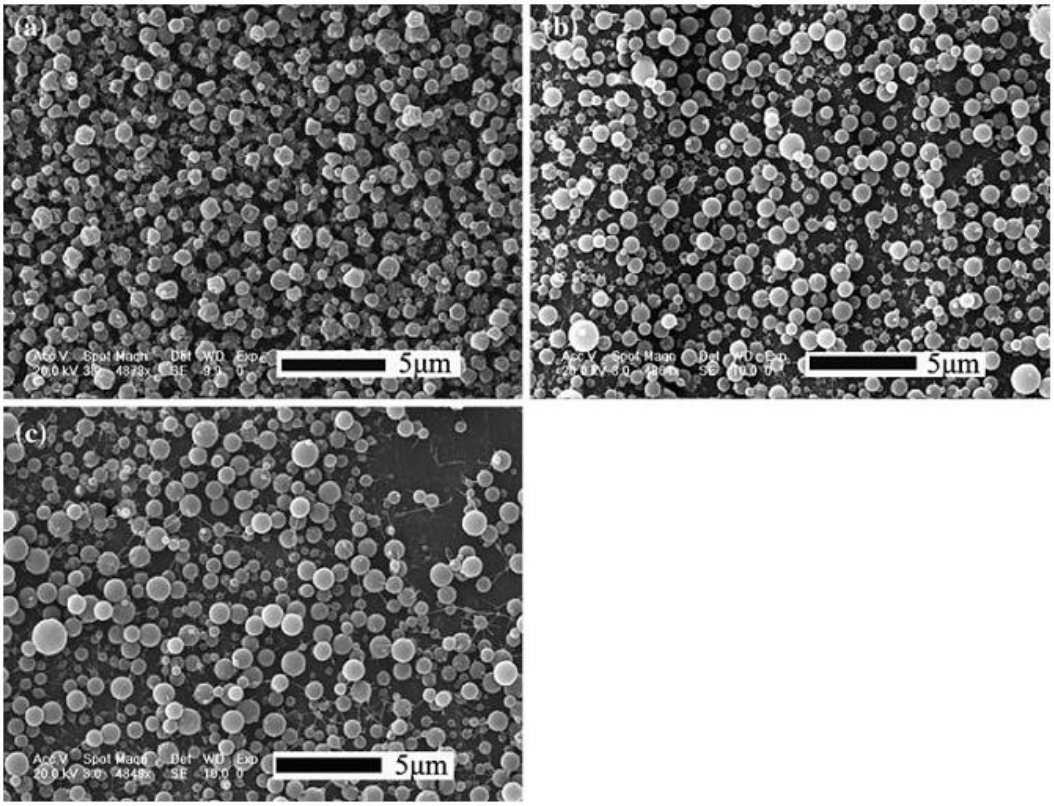

Figure 2.12 : *Effect of changing the voltage on particles generated a) 10 kV b) 15 kV c) 20 kV [9].*

Atten *et al.*[49] demonstrated better control over the droplet size via the application of pulses (**Figure 2.13**) rather than a DC signal. The setup is almost identical to the traditional electrospinning setup pictured in **Figure 2.10** with the exception that the experiments are conducted in oil rather than free air and that no flow rate is present at the needle. This work demonstrated control over size by applying high voltage pulses with varying potentials and pulse widths to a static fluid meniscus. Voltages applied in this case although in excess of 2000 V, are still considerably less than the potentials applied in electrospray cases [44-48]. This method provides greater control over droplet size [49]

however for many applications it is desired to perform the same process but on a smaller scale.

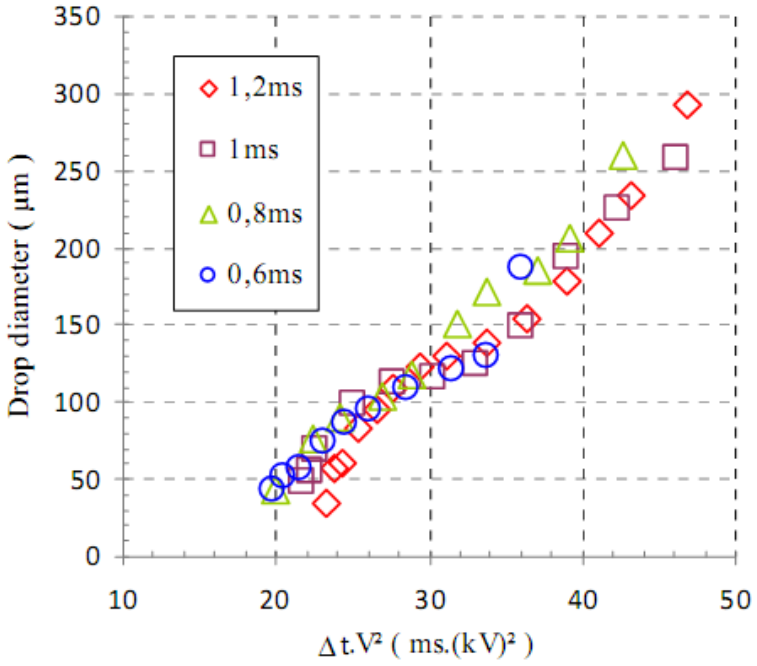

Figure 2.13 : *The variation in droplet diameter vs. the product of the pulse width and the square of the applied potential difference [10].*

He *et al.* [50] did similar work with the key difference being that the droplets were generated in a microfluidic channel. In this case a microchannel connecting oil and water reservoirs were utilized as illustrated in **Figure 2.14** where high voltage pulses less than 1 kV with a period of 20-50 ms are applied. Using this setup it was possible to generate droplets ranging in size from 5-25 µm but at higher polydispersities than what is desirable for many applications. In depth analysis on the effects of the voltage pulse on the droplet diameter was not completed although some previous simulations do exist on fluid jets [51]. Although this method is promising due to the smaller experimental setup when

compared to electrospraying process, further work needs to be completed to test the viability of this method of droplet generation for lab-on-chip applications.

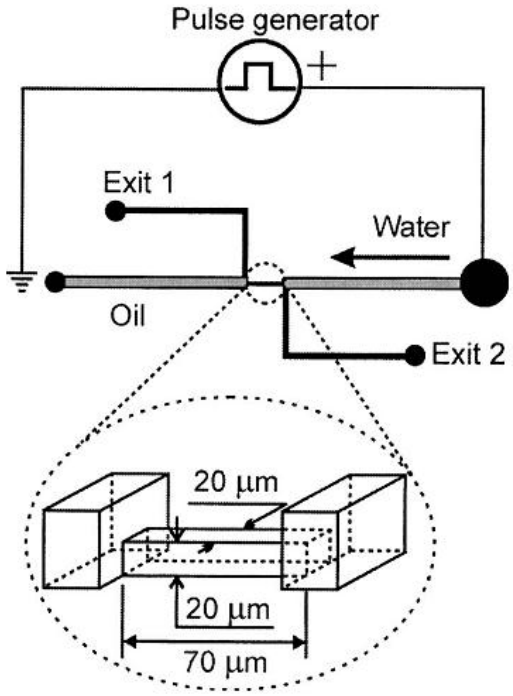

Figure 2.14 : *Schematic of setup used by He et al [11].*

The methods discussed in this section provide a mean to generate droplets, microgels, and microparticle but all have shortcomings. Electrospray provides a method to generate large quantities of droplets however the lab footprint is very large and to cause variation in the droplet sizes viscosities or conductivities need to be changed. This is not ideal since changing the working fluids is often not possible. Similarly, work completed by Atten *et al.* [10] overcomes the limitations of size control whilst using a similar electrospray setup. However, the sizes were much larger being over 50 µm with the frequency of droplet generation less than 1 Hz caused by the usage of a static

meniscus. He *et al.* [50] significantly reduced the experimental setup footprint by conducting droplet generation in a microfluidic channel. However, yet again the droplet sizes were of a limited size range of 5-25 μm with higher frequency generation not being attempted or investigated. Due to the many applications previously discussed requiring large quantities of these droplets it is desirable to design and characterize a system that can generate droplets at higher frequencies whilst simultaneously having dynamic control over droplet diameter. Therefore a microfluidic system that utilizes the high voltage pulses to control droplet diameter at high frequencies to generate large quantities of droplets could be a solution to these short comings.

2.4 Summary

This chapter introduced the concepts of droplet formation and microfluidics. Many applications in microfluidics require the handling of small volumes of fluids in an isolated manner. Microdroplets are an ideal vessel for these applications due to the ability to manipulate and experiment on multiple vessels isolated in a bulk fluid at the same time reducing reagent expenditure.

Although several microdroplet production techniques exist they are currently limited. The work in this thesis will focus on increasing the capabilities of devices that utilized flow focusing and electrogeneration as a means of generating droplets.

Chapter 3 Materials & Fabrication

3.1 Materials

3.1.1 PDMS

PDMS (Polydimethylsiloxane) is a widely used organic silicone polymer. PDMS is a two part polymer with vinyl and hydrosiloxane groups. When a cross-linking agent is introduced to the uncured PDMS base a reaction is catalyzed which results in the formations of long polymer chains and thus the solidification of the compound. PDMS has gained widespread usage as a structural material for microfluidics since it is transparent, inert, and is an easily mouldable viscous liquid when not cured [52]. These properties have made this material and ideal candidate for fabrication of microfluidic devices with minimum feature sizes that range from a few to hundreds of micrometers. In these devices Sylgard 184 PDMS kits were used at a ratio of 10 base to 1 curing agent in order to create microchannels.

3.1.2 Paraffin Oil

Paraffin oil (mineral oil) is an organic non-polar compound that is primarily composed of alkanes and has the basic chemical formula of C_nH_{2n+2}. As oil it is composed of a mixture of the heavier alkanes with its viscosity varying depending on the density of oil used. Paraffin oil is non-toxic, often colourless, transparent, and insulating liquid. It has a wide range of usages ranging from being a food additive to being utilized as a

lubricant. The high relative dielectric constant (2.2) of this oil has enabled its usage in various electronics systems both as a coolant as well as an electrical insulator. These properties make this oil an ideal material for usage in microfluidic devices where transparency and electric isolation are important. This oil was used in both flow focusing and droplet generation via electrogeneration as the continuous phase.

3.1.3 Methylene Blue

Methylene blue is a polar water soluble chemical compound with the chemical formula of $C_{16}H_{18}N_3SCl$. It is used in chemical processes as well as in medicine, due to its strong blue color it has seen wide spread usage in applications such as tissue staining. In these experiments it is used as a dye in order to obtain better images of microdroplets as well as a means to increase the electrical conductivity of DI water in a controlled manner. This material was added to DI water and used as the disperse phase for experiments dealing with electrically generated droplets.

3.1.4 Span80

Sorbitane monooleate (Span80) is an oil soluble surfactant. This compound is relatively safe being utilized in oral pharmaceuticals as well as in food products. Surfactants are amphiphilic chemicals meaning they have both hydrophobic and hydrophilic ends. Typically these compounds cause the lowering of surface tension or interfacial tension of the liquids in which they are present [53]. The chemical structure is illustrated in **Figure 3.1**, it is observed that the left end of the structure is hydrophilic and

will dissociate when in contact with water and become negatively charged. Span80 is primarily used as an emulsifier, an agent that stabilizes water-oil emulsions. The hydrophilic end will adhere to water droplets with the other end of molecule sticking out and acting as a protective barrier, preventing the coalescence of two adjacent water droplets. In this work Span80 was used in oil to reduce probability of droplet coalescence.

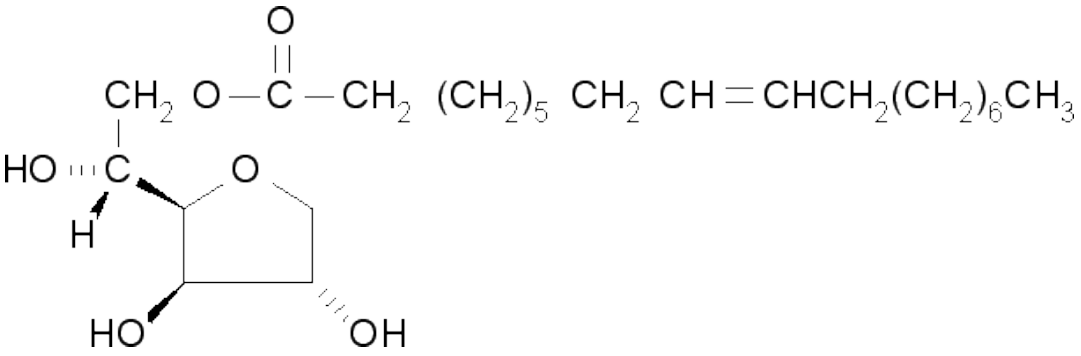

Figure 3.1 : *Chemical structure of span80 [Sigma Aldrich].*

3.1.5 Hydrazide-Functionalized Carboxymethyl Cellulose (CMCA) & Aldehyde-Functionalized Dextran (DEXB)

CMC is derived from cellulose and is biodegradable as well as being non-toxic. Similarly, Dextran is also biocompatible being composed of many units of glucose molecules. Both of these polymers have usages in medicine as well as in the food industry and are easily available from large scale chemical suppliers such as Sigma Aldrich. The functionalization of these polymers is possible by the addition of hydrazide and aldehyde groups through chemical processes [54]. Functionalization allows for cross-linking to occur when the two are mixed together. This causes the formation of a hydrophilic polymer matrix and hence a gel. When cross-linked they form a smart polymer that

responds to external stimuli that are in this case different buffers [55]. Hydrogels that can respond to external stimuli are attractive for usage in drug release applications due to their ability to adsorb the drugs and release them when the external environment is changes. These two polymers were used in solution in the flow focusing device as the disperse phase.

3.2 Device Fabrication & Assembly

3.2.1 Soft Lithography

Soft lithography was used to fabricate the microchannel in both cases. This process is the most widely used method for creating microchannels and was first introduced by Xia *et al* [56]. In this case soft lithography's replica moulding technique was used in conjunction with PDMS, this method can reproduce features down to a few micrometers very accurately, quickly and with a low cost. Replica moulding is typically a 4 step process consisting of mould fabrication, casting, replica removal, and bonding of replica to a substrate to provide sealed channels [52].

Typically in this soft lithography moulds are fabricated through photolithography which is a well-established and widely used process for patterning structures out of a photoresist on a substrate (typically a silicon wafer). After the mould is fabricated a polymeric material (usually PDMS) is cast and allowed to cure via the application of heat. After this process is complete the cured replica is removed from the mould and bonded to a substrate to seal channels. Additional steps may be required for the placement of inlets and outlets or other items required for device functionality.

3.2.2 Flow Focusing Device Fabrication & Assembly

The process flow for the fabrication of flow focusing devices is outlined in **Figure 3.2**. Due to the minimum feature size of the flow focusing device designs being less than 100 μm the best method for mould fabrication is through the usage of photolithography. Photolithography is a process by which selective parts of a polymer are removed from the substrate by the usage of a developer and UV radiation. This work utilized the photoresist SU 8 – 2075 (Microchem, MA, USA) and a 3 inch diameter silicon wafer as the substrate (University Wafers, MA, USA). The completed mould is pictured in **Figure 3.3**. This process is well documented; the full recipe is posted in the appendix.

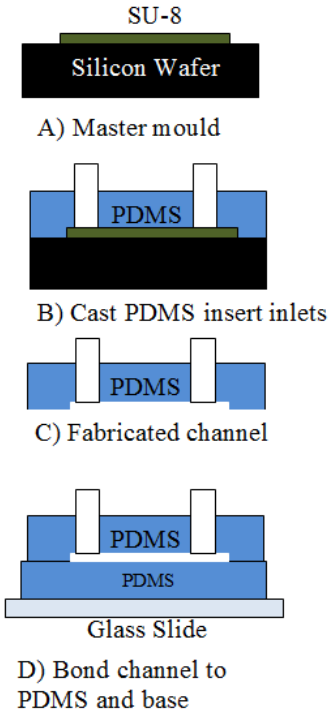

Figure 3.2 : *Process flow for device fabrication and assembly.*

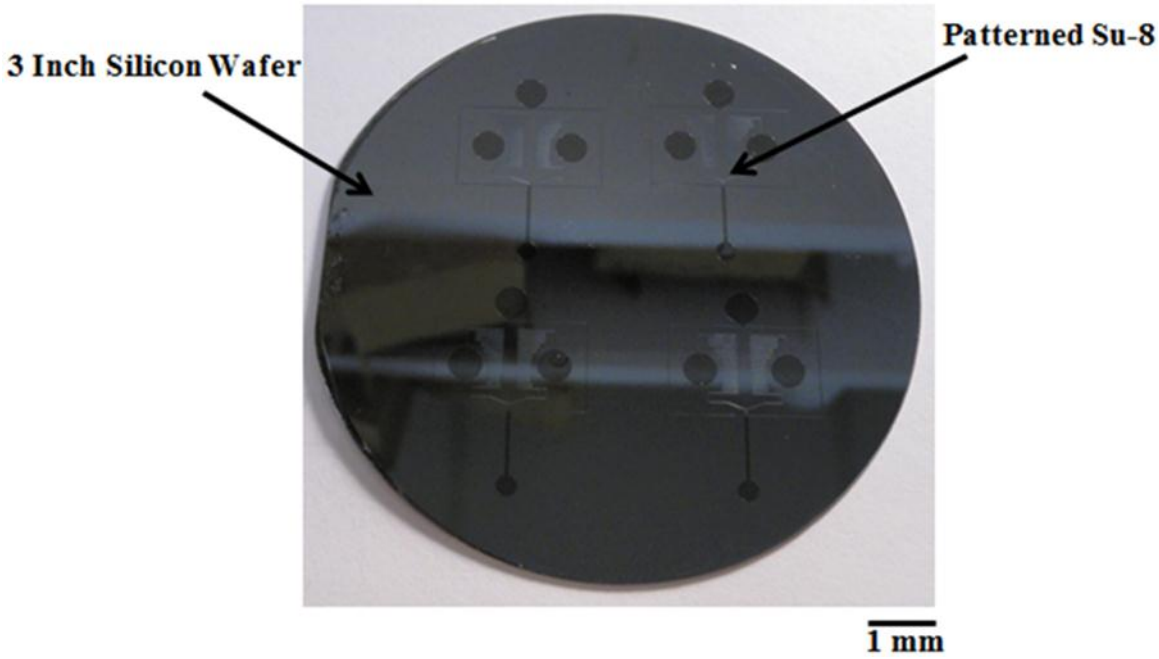

Figure 3.3 : *Mould prepared via photolithography.*

Prior to casting, Masterflex 0.8 mm inner diameter (4 mm OD) (Cole Palmer, Ontario, Canada) silicone inlets were placed on the wafer at the reservoirs. This enabled strong bonding to occur between PDMS and interconnect tubing. The PDMS was then cured on a hotplate at 65 degrees Celsius for 2 hours. After curing the devices were carefully cut and subsequently peeled off the wafer. Next, interconnects were cleaned of excess PDMS utilizing a needle and an outlet was obtained using a 1 mm diameter biopsy punch. Oxygen plasma surface treatment is one of several techniques that exist for bonding cured PDMS pieces. Work done by Eddings *et al.* [57] was used as a reference and oxygen plasma surface treatments proved to be the most reliable, rapid, and robust bonding technique for the flow focusing device. This process involved exposing the PDMS surface containing the channels and a blank PDMS slab to oxygen plasma. The

PDMS pieces are exposed for a period of 30 seconds at a plasma power of 40 W. This resulted in surface activation and enabled molecular bonds between two different pieces of PDMS.

After surface activation these two pieces were brought in contact and left over night for 24 hours. The final step involved bonding the bottom of the device to a rigid support (glass slide) utilizing uncured PDMS glue and subsequent placement on a hot plate at 65^{o} for two hours. The fully fabricated device is shown in **Figure 3.4** with features having been replicated to sub-micron precision from the mould.

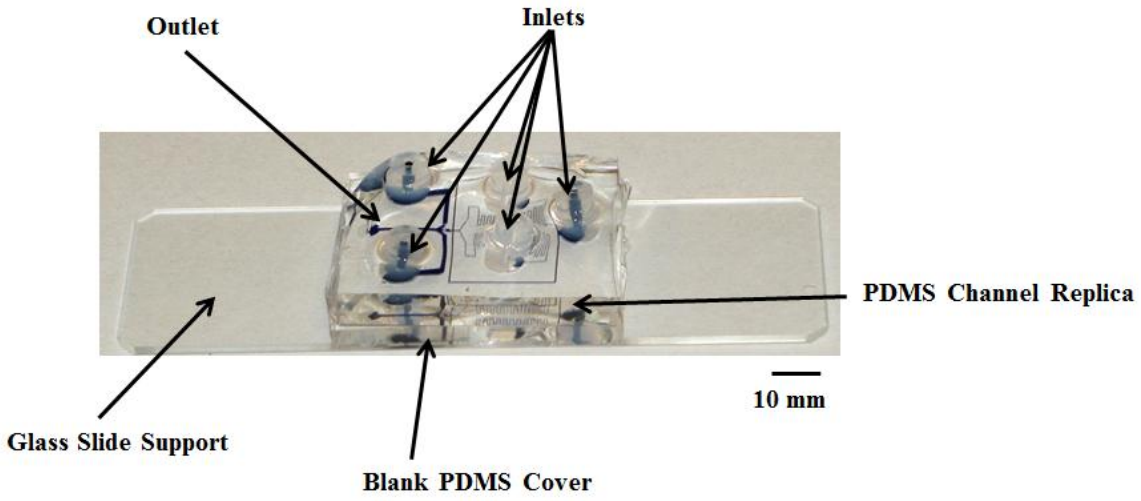

Figure 3.4 : *Fabricated flow focusing device.*

3.2.3 Electrogenerated Droplet Device Mould Fabrication

The process flow for the fabrication of the electrically generated droplet devices is outlined in **Figure 3.5**. Since the channels used in this device were much larger with the minimum feature sizing being 800 um, a 3D printer was utilized to fabricate the moulds.

The 3D polymer printer was characterized with regards to its ability to print small channels and the data is present in **Figure 3.6**. Examining this figure we were able to determine that this 3D printer can print a minimum feature size of 200 um. Since this device has features larger than 200 μm a 3D model was constructed in AutoDesk Inventor software and fed to the printer, **Figure 3.7** shows a mould once printed.

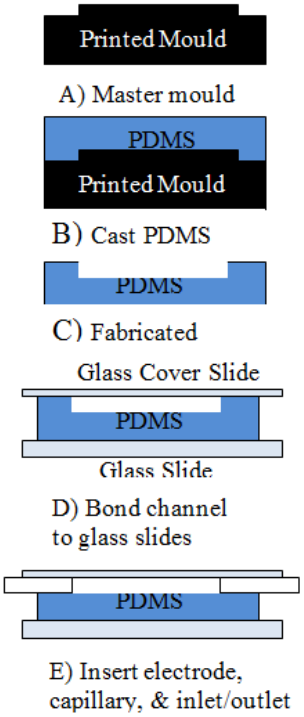

Figure 3.5 : *Process flow for fabricating devices for electrically generated droplets.*

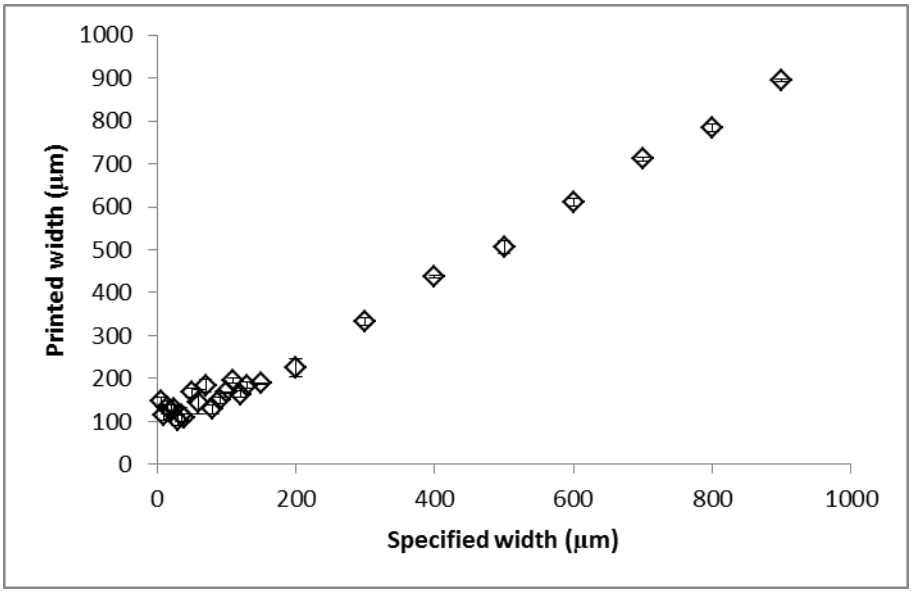

Figure 3.6 : *The specified channel width plotted against width printed by the 3d printer.*

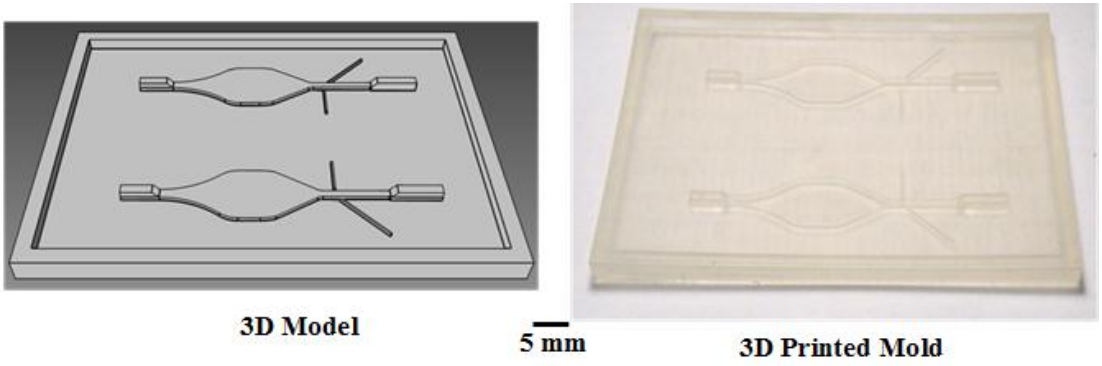

Figure 3.7 : *3D model and final mould after printing.*

PDMS was cast on the 3D polymer printer mould and left overnight to cure rather than being placed on the hotplate since the mould shows signs of deformations when heat is applied. After curing the devices were carefully cut and subsequently peeled off the mould. The device was next bonded using PDMS glue to a rigid support (glass slide) at 65^{o} for 2 hours with the open channels facing upward. The channels were closed with the usage of uncured PDMS glue to bond a glass cover slip to the device on the hot plate at

65^{o} for 2 hours. Next the borosilicate glass inlets were inserted into the appropriate locations and sealed off utilizing uncured PDMS glue. Finally, the droplet injection capillary and a stainless steel 27 G1/2 needle ground electrode were placed into the device in the appropriate slots, no sealant was required. The taper present in the droplet injection capillary was created using an etching process previously developed [58]. This process involved the submersion of a fused silica capillary with a 365 μm OD and 50 μm ID (Polymicro, AZ, USA) into bilayer of paraffin oil and 49% hydrofluoric acid solution. The hydrofluoric acid solution is at the bottom of the bilayer and etches the capillary into a tapered form due to the interfacial interactions between the fused silica capillary, oil, and hydrofluoric acid solution. The final product of device fabrication is pictured in **Figure 3.8** with features having been replicated to sub-micron precision from the mould.

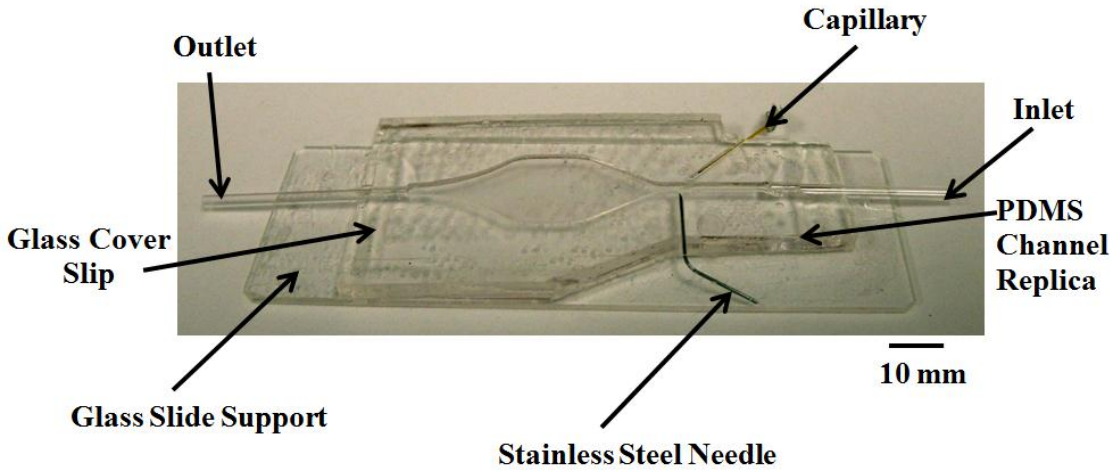

Figure 3.8 : *Fabricated device for droplet generation via electrogeneration.*

3.3 Summary

In this chapter the materials and fabrication of the devices were presented. For experimentation a varying list of chemicals and structural materials were being utilized. Both devices required the usage of soft lithography for manufacture in conjunction with rapidly prototyped moulds. The master moulds were fabricated utilizing photolithography and a 3D polymer printer. Device assembly was a relatively simple process involving the sealing of channels utilizing glass and PDMS glue or cured PDMS and oxygen plasma. The devices constructed are robust, reusable, and relatively inexpensive.

Chapter 4 Flow Focusing Device Design & Characterization

4.1 Introduction

As mentioned in Chapter 2, microfluidic devices capable of generating droplets followed by reaction polymerization inside them have been developed in the recent past [59]. For instance, microfluidic devices that produce alginate droplets cross linked by calcium have used co-flow of three streams of fluid through a flow focusing nozzle to produce droplets [35]. Of the three streams, the first is the alginate polymer, the second is a buffer, and a third contains calcium ions vital to cross-linking. The middle stream containing the buffer was introduced in this design to overcome the main disadvantage of reacting systems which is initiation of reaction before the generation of droplets at the nozzle. However, the introduction of the buffer stream dilutes the eventual chemical composition of the droplet and may cause non-uniform mixing. Additionally ionic cross-linking is undesirable due to the presence of counter-ions in the body causing premature dissolution the gel. Covalently cross-linked polymers such CMCA and DEXB [55][60] do not have this problem. Alternatively other groups have used initiator induced polymerization processes to form hydrogels after the formation of droplets. However, these processes require the exposure of droplets to cross-linking catalysts such as heat and UV-radiation [37] which is not desirable when encapsulating proteins or cells in these microgels.

This chapter presents the design, development and testing of a microfluidic flow focusing device to generate monodisperse microgel particles for drug release trails and other applications. Monodispersity is required as it is better assembled into structures as well as having a lower immune response when compared to polydisperse particles. The device designed is required to be capable of droplet generation of reactive chemical mixtures without a buffer stream. The device is required to generate monodisperse droplets of fixed sizes ranging 40-200 μm regardless of the reactive nature of the fluid streams utilized.

4.2 Device Design

4.2.1 Working Principle

A typical flow focusing device consists of a "chip" with several inlets and outlets. Inlets for the continuous and disperse phases and an outlet for emulsion produced. In forming microgels the reactant polymers are usually kept in separate microchannels, brought together and allowed to co-flow over a section to ensure mixing and then flow focused through a nozzle to generate droplets.

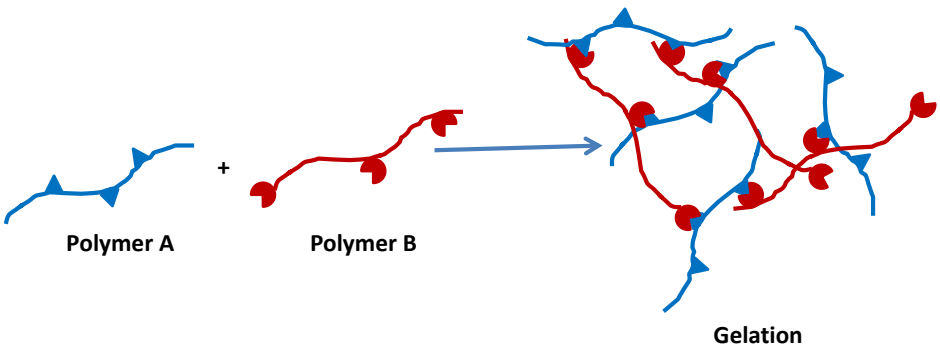

Figure 4.1 : *Covalent cross-linking.*

The preferred method for formation of the microgels to be used in the drug release study was through reaction crosslinking of large polymers as shown in **Figure 4.1**. The polymers used (CMC & DEX B) have long chain lengths and high molecular weights as previously stated in Chapter 3. This imposes a challenge to the construction of the microfluidic device. If the gelation time is too long then the droplets formed will merge and introduce polydispersity. If the gelation time is too short then large chunks of gel form and the channels can get clogged. Therefore stable and reliable operation over long periods of time for this gelling system is difficult to achieve and has not been shown in the past. A simple schematic for the cross-linking is pictured in **Figure 4.1**, two long chained polymers come together and interact, forming covalent bonds between the chains and subsequently a polymer matrix is assembled. This polymer matrix becomes a solid if the solvent is extracted or a gel if the solvent remains trapped in the matrix of polymers with longer chains. Due to the low Reynold's number experienced in microchannels (<1 in this case) the flows are laminar and thus there is very little mixing of the A and B polymers when they are made to flow side by side in a microchannel.

The main mechanism for mixing in microchannels is through molecular diffusion. Diffusion is the movement of matter across concentration gradients and is given by Fick's Law [61]:

$$J = -AD\frac{dC}{dx} \qquad (4.1)$$

where J is the mass flux, D is the diffusion coefficient, A is the area, dC/dx is the concentration gradient. From Fick's Law it is clear that in the microscale since the

distance over which the concentration gradient exists is decreasing the apparent mass flux would increase. However the residence time as well as the length and area at which diffusion must occur over are also significantly reduced. The diffusion lengths and times are as follows[61]:

$$t_r = \frac{L}{v} \quad (4.2) \qquad\qquad L_d = \sqrt{4Dt_r} \quad (4.3)$$

where t_r is the residence time, v is the velocity, L is the mixing length, L_d is the distance over which diffusion will occur, and D is the diffusion coefficient. In order to compute these values the diffusion coefficient is needed and was determined using the Einstein-Stokes equation as followed [62]:

$$D = \frac{kT}{6\pi\mu r} \quad (4.4)$$

where D is the diffusion coefficient, k is the Boltzmann constant, T is the absolute temperature (298 Kelvin), μ is the viscosity of water, and r is the molecule radius (1-28 nm determined by light scattering). The diffusion coefficient for mass transfer was determined to be 2.44×10^{-10} to 8.73×10^{-12} m^2/s. Combining the equations for diffusion length and residence time the following relationship can be obtained:

$$L = \frac{vL_d{}^2}{4D} \quad (4.5)$$

This relationship is useful for estimating a mixing length. Using a diffusion length of 50 μm and a flow velocity corresponding to 0.06 mL/hour (typical widths and flow rates in literature) a mixing length of 0.7-18 cm was calculated. Therefore it is clear that at this flow rate inside the microfluidic device, effective mixing between two streams will

take a significant amount of time or length. Therefore, various designs were considered to enable continuous droplet formation over long periods of time while ensuring that the reactants are mixed homogeneously and the microgels produces are uniform.

4.2.2 Experimental Setup

Three primary solutions were utilized during the operation of the flow focusing device. The first being bulk oil solution consisting of heavy paraffin oil (Caledon Labs, Georgetown, Ontario) mixed with 1 %wt of Span80 (Sigma Aldrich). The oil solution was manually mixed for several minutes. The remaining two solutions were of the polymers hydrazide-functionalized carboxymethylcellulose (CMCA) and aldehyde-functionalized dextran (DEXB) which were synthesized using procedures previously developed by Hudson *et al.*[63] and Ito *et al.* [60] . The CMC A solution had a concentration of 10 mg/mL while the DEX B solution was double at 20 mg/mL. These solutions were mixed utilizing a vortex mixer for 8 hours and then filtered through 0.45 μm pore syringe filters.

The experimental setup for droplet generation is illustrated in **Figure 4.2**. The microfluidic device (**Figure 3.4**) was held by a retort stand under a microscope with a LED ring light (AmScope, LA, USA) being placed below. The primary oil (60 mL syringe) and polymer (3 mL syringes) flows were controlled by KDS Legato 270 (GeneQ Inc., Quebec, Canada) high precision syringe pumps capable of providing high linear forces necessary to flow through the small microfluidic channels. A KDS 100 syringe pump provided flow for the secondary 60 mL oil syringe which was connected to a Y-

junction to provide equal amounts of flow to the separator channels. A Nikon Coolpix P6000 mounted on the microscope was utilized to capture images every 5 minutes over the experiment duration at a shutter speed of 1 ms in order to eliminate motion blur caused by fast moving droplets. Droplets were collected at the outlet in a sealed 250 mL Nalgene container over the duration of the experiment. After droplet generation, the microgels formed were allowed to settle via gravitation and the oil supernatant was removed from the container. Gels were washed 5 times with pentane (10 mL pentane/0.5 mL microgels), to obtain complete removal of surfactant and oil and the gel was stored in the fumehood for a period of 48 hours to allow for pentane evaporation to occur. Microgels were centrifuged and resuspended in water, phosphate buffered saline (10 mM buffer concentration, , pH 7.4, 0.15M total ionic strength) or citrate buffer (10 mM buffer concentration, pH 4, 0.15M total ionic strength); ionic strength was increased as required by addition of NaCl.

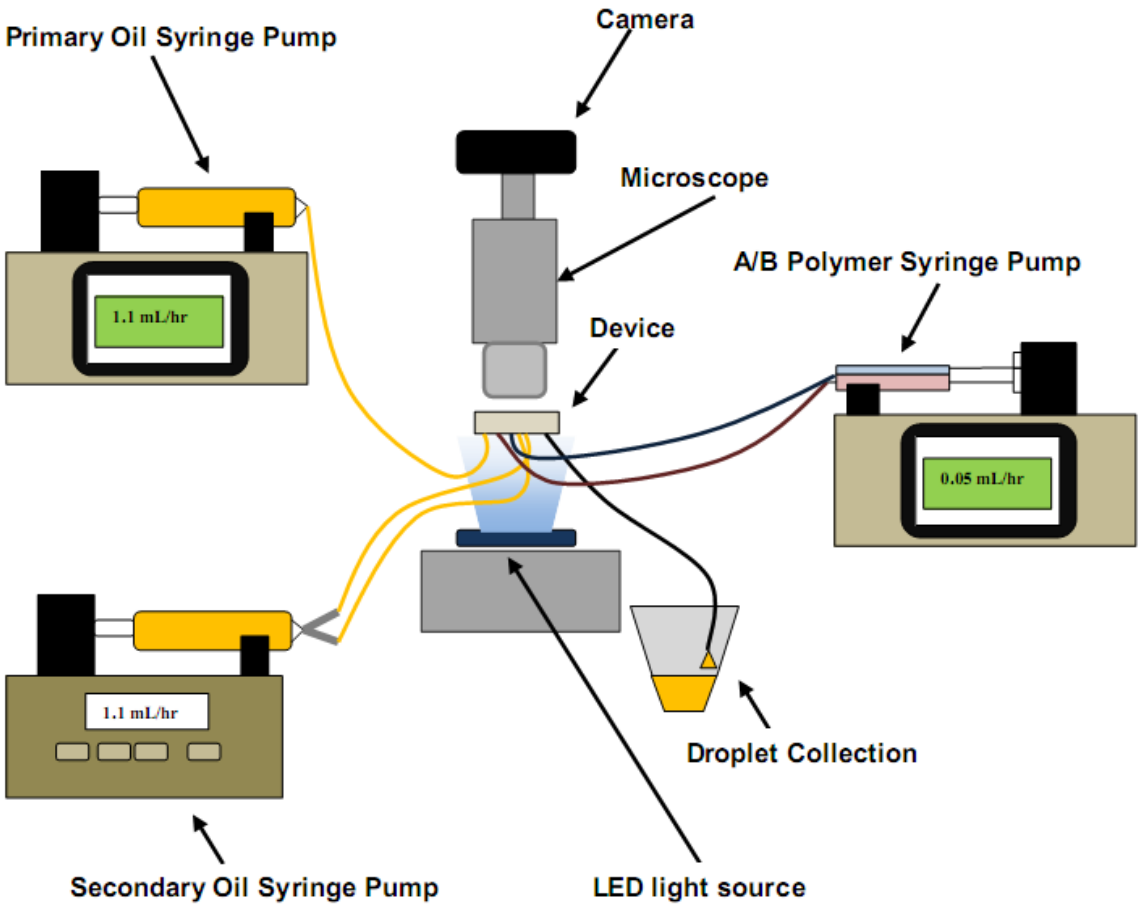

Figure 4.2 : *Experimental Setup.*

Droplet sizes were measured in ImageJ image analysis software. A Meiji (Cole Palmer, Ontario, Canada) stage micrometer with 10 μm divisions was used as a scale for measurements. Droplet diameter measurements were made by manually measuring the length of the droplet midsection in ImageJ using its measurement tool. With pictures having pixel resolutions lower than 1 μm the largest amount of error was due to the manual measurements. The 95% confidence interval of the measurements was determined to be +/-0.52% of the measured value. Three droplets were measured per image, with

droplets being selected that were closest to the left the right and the center of the ImageJ. A possible selection bias exists towards selecting larger droplets when two droplets were present in the center of the image due to user bias. This possibly increased the apparent polydispersity due to the inability to measure the entire population.

Interfacial tension between oil and polymer solutions was assumed to be the same as between oil and water since the solutions were 98.4% water. This value was determined previously by Santini *et al* [53] for various concentrations of Span80 in paraffin oil. Viscosity of the paraffin oil at 40 degrees Celsius was provided by Caledon Labs which was correlated to room temperature by making appropriate measurements utilizing a Cannon 400 K175 viscometer.

4.2.3 Design Iterations

The drug release trial required about 2.6 mL of microgels at various diameters in the range of 20-100 um. This is a significant amount of volume that would have to flow through a microfluidic device. To create such large volumes of microgels microfluidically, three options are available: parallel operation of several devices simultaneously, a new device design containing multiple droplet generation locations on the same chip, and lastly long term operation of a single device. Due to equipment limitations and desire to monitor the experiment in progress it was not possible to run several devices simultaneously. Similarly a new device design involving multiple nozzles would be extremely complicated for reaction polymerization. It was determined that the operation of a single device for durations in excess of 24 hours was the best option to

create an adequate volume of droplets. Additionally, in order to analyze the drug release characteristics of uniformly mixed microgels it is desired to test several different sizes. In order to obtain uniformly mixed microgels a mixing section is required.

Most importantly it is necessary to obtain monodisperse droplets. Monodisperse microgels produce identical release profiles and are desired to engineer the dose release in drug delivery. Thus the device must maintain stable droplet generation through extended durations.

In order to determine the most appropriate mixing section, offering the most stable droplet generation, several designs were evaluated. The device that was initially designed (**Figure 4.3**) consisted of mixing sections of lengths of 38 mm (with and without mixing baffles A & B), and 5 mm (with and without mixing baffles) pictured in C. This was done to ensure that the mixing sections were sufficiently long in order to create uniformly mixed droplets with little variation in composition over the population. In addition, the first devices had the reactant polymer solutions A and B meeting head-on prior to entering the mixing section as shown in **Figure 4.4**. This design was soon found to be not optimal. During the initial filling of the device, one of the polymer solutions would reach the intersection first and flow into the opposite microchannel and into its reservoir where it would react with the second polymer and cause device clogging.

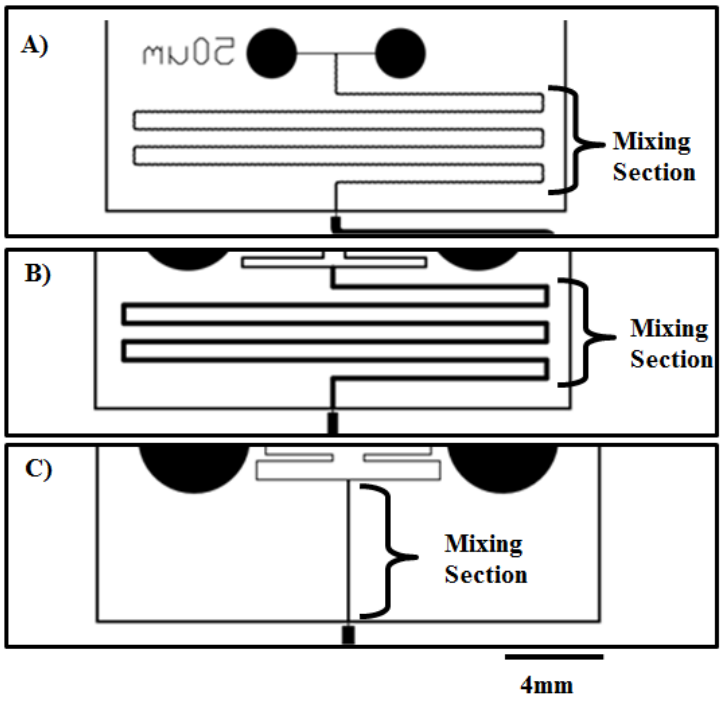

Figure 4.3 : *Initial designs with long mixing sections with lengths of A)B) 38 mm C)5 mm.*

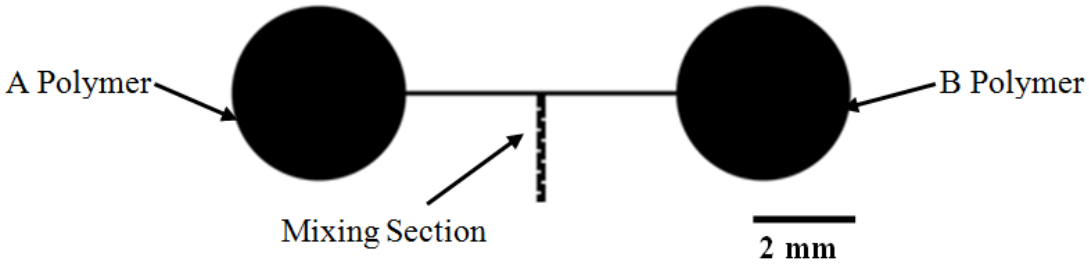

Figure 4.4 : *Initial design with A and B polymers meeting immediately after inlet and outlet reservoirs.*

To understand why this happened we look at the hydraulic resistance [64]:

$$R_h \propto \frac{64}{Re}\left(\frac{l}{d}\right)\left(\frac{v^2}{2g}\right) \qquad (1)$$

where *Re* is the Reynold's number, *l* is the length of the channel, *d* is the hydraulic diameter, *v* is the flow velocity, and *g* is the gravitational constant. The parameter that affects the resistance the most in this case is the length since the other parameters are not significantly changed before or after the location where polymers meet. Thus in order to prevent reactants from reaching the opposite reservoir and clogging the device, the hydraulic resistance prior to the mixing channel was increased by the introduction of a winding channel prior to the mixing section as shown in **Figure 4.3 B**. This modification significantly reduced the occurrence of one polymer flowing into the reservoir of the other reactant. However, these devices failed as well due to gel formation and clogging in the mixing section. We found that irrespective of the presence or absence of mixing baffles, reaction still occured at the interface between CMCA and DEXB solutions in the mixing section. This reaction caused gel to form along the interface and possibly adhere to the channel surfaces long before a uniform mixture is obtained. Accumulation at the spot of initial adhesion leads to accumulation of gelled material and eventually causes clogging. To avoid this phenomenon, the mixing length was reduced to what is shown on **Figure 4.3 C**. This modification provided better results as full clogging was not observed but the droplet generation was still unsteady since gelation still occurred and accumulated to some extent in the mixing section before being dislodged in the flow. This caused cyclic behaviour temporarily reducing the flow and then once the pressure forced out the gel there was a sudden flow increase until the flow once again became normal and gelation occurring again. Although this design reduced clogging, it was not optimal for

stable operation. Therefore, the mixing section was significantly reduced in subsequent designs.

The design illustrated in **Figure 4.5** was the first attempt to significantly reduce the mixing section. Here the source channels of the reactant polymers approach the intersection prior to the mixing section not head on but orthogonal to each other. This design proved to be relatively stable even enabling the operation of the device for prolonged periods of time. Nevertheless, stability without uniform mixing and distribution of polymers A & B would not be very useful. In order to determine the distribution of these polymers, dyes (red and blue food colouring) were introduced in both of the polymers. It was observed that in the orthogonal junction configuration depicted in **Figure 4.5**, there was a periodic movement (freq <1 Hz) of one of the polymer solution (CMCA) into the source channel of the other polymer before the mixing length. When this happened the droplets produced were of a single polymer and had homogeneous color distribution in them. In between these periodic cycles there was co-flow of both the polymer solutions into the short mixing channel and the droplet generated contained both the polymers. This showed the when the reacting polymers approach each other at 90^{o} angle prior to the mixing section, the interface between them is still not stable and shifts periodically. This shifting leads to erratic droplet production; although the stability is maintained over long durations as clogging is eliminated. The reason could be due to the pulsatile nature of the syringe pumps used. This pulsatility leads to varying forces across the interface between the two polymers that could locate it in different positions. In order

to eliminate this situation the two designs illustrated in **Figure 4.6** were tested involving the introduction of polymers with parallel flow directions.

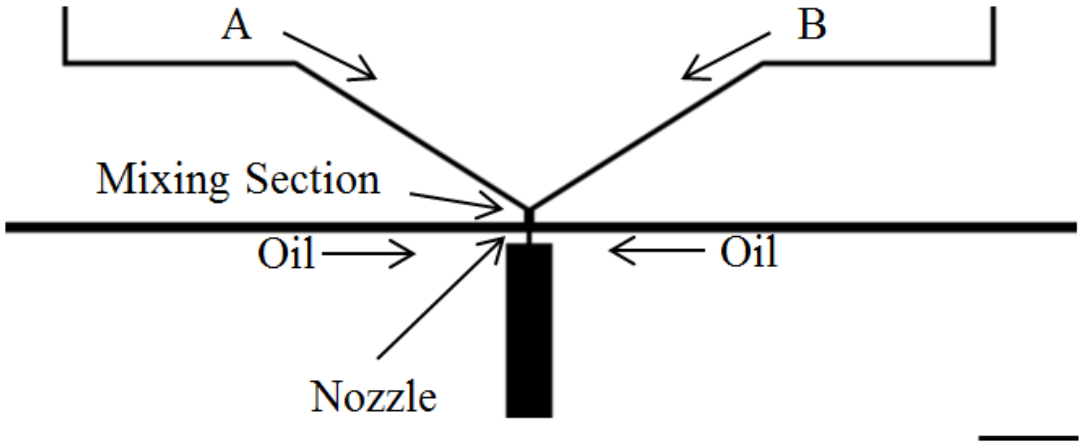

Figure 4.5 : *Design with nearly no mixing length (scale bar is 1 mm).*

The design shown in **Figure 4.6 a** where the mixing section is completely eliminated did not clog, but proved to be unstable generating droplets with high polydispersity. As the mixing section is eliminated, the reactants are introduced directly into the oil stream and this leads to formation, in some instances, of individual interfaces at the mouths of the source channels which produce individual droplets of reactants A or B. After a while, these individual interfaces merge as they are co-located and this leads to droplet formation with both reactants in them. **Figure 4.6 b** proved to be the best design capable of generating droplets with little change in sizes and no clogging due to reaction. This design allows for a short stabilization length which is crucial for the polymer solution to co-flow and equilibrate their velocities and flow profile by allowing the polymers to co-flow parallel to each other stabilizing the flow and the composition prior

to being focused through the nozzle. Thus, this design was chosen to be optimal to generate large quantities of microgels for drug release studies. One drawback of this design is that the residence time in the mixing section is reduced. This could cause poorly mixed droplets that would be detrimental for formation of uniform spherical microgels. Therefore, mixing of the reactant solutions both before and after droplet formation was characterized in the following sections in this optimal design.

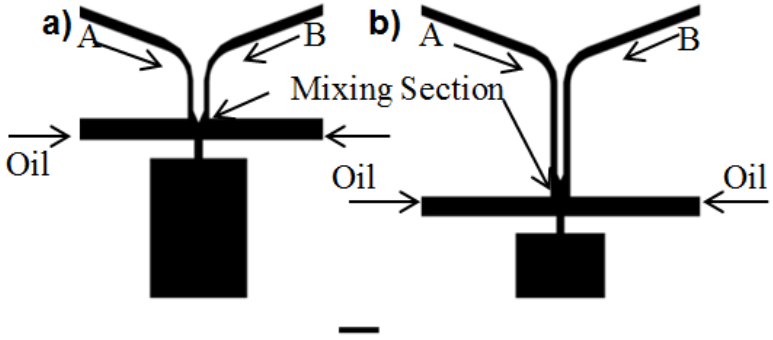

Figure 4.6 : *Final Designs (scale bar is 200 μm).*

4.2.3 Optimal Design

The design of the optimal device consisting of five inlets and one outlet is shown as a schematic in **Figure 4.7**. Here the polymers A and B are introduced at the junction prior to the stabilization section through a winding source channel which provides enough hydraulic resistance to prevent any backflow. The source channels at the junction also meet such that they flow parallel to each other into the stabilization section rather than meeting head-on or orthogonally. This ensures that any fluctuation in the pressures or

flow rates introduced by the syringe pumps do not cause a significant backflow into the source channels.

The device was fabricated using a process flow as described in Chapter ***3***. The fabricated device is shown in **Figure 3.4** and **Figure 4.7**. All of the inlets are connected to tubing supplying the working solutions via a simple tubing connection setup. The outlet is simply a segment of Cole Palmer PTFE tubing. Prior to experimentation the tubing was cleansed using DI water in an attempt to reduce the amount of debris present. Similarly when flowing working solutions in the device, the polymer channels are primed with DI water for one hour in order to allow for flows to reach steady state prior to the introduction of polymers into the channels.

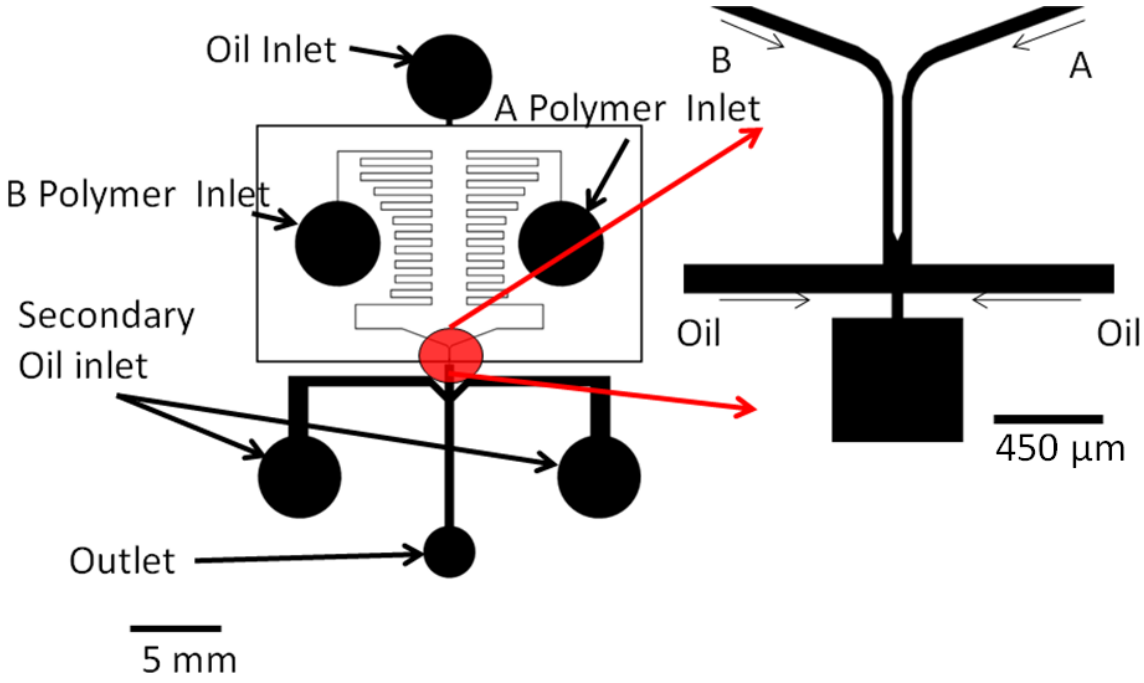

Figure 4.7 : *Schematic of the device with exploded view.*

The flow focusing area is shown in the exploded view in **Figure 4.7**. The focusing flows come in perpendicular to that of the disperse phase due to the increased complexity of the device that required careful placements of the inlets. It is seen clearly in the exploded view that the two polymer solutions flow in different 50 μm channels and then meet for a length of 150 μm before being focused by the oil flowing through a 100 μm channel. The length of the mixing section was optimized to ensure that the flow becomes stable before the droplet formation, yet no appreciable gelation occurs. The focused stream passes through a 40 μm nozzle and droplets are formed immediately downstream of the nozzle. It is known that the size of the droplets formed correspond to the same order of magnitude as the nozzle dimension and can be varied over a small range through the changes in flow rates [28], [32]. Since the drug release study required droplets in the range of 40-200 um, a 40 μm nozzle was chosen. The spacing between droplets was increased in order to prevent droplet coalescence by secondary oil flows being introduced by additional oil channels downstream as shown in **Figure 4.8**.

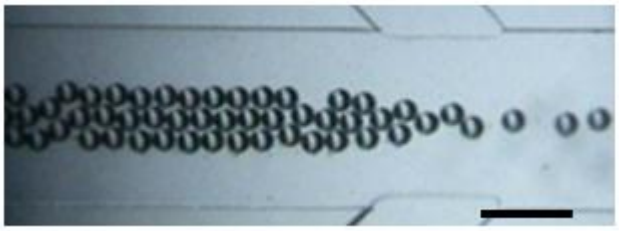

Figure 4.8 : *Secondary oil flow increasing adjacent droplet distance (scale bar is 200 μm).*

4.3 Device Characterization

4.3.2 Long Duration Device Operation & Bulk Microgel Manufacture

Utilizing the final chip design previously mentioned, microgels were generated continuously to demonstrate the long term operation of the device. As seen in **Figure 4.9** three different sizes of droplets were generated all exceeding 24 hours. After generation the microgels were collected in a Nalgene container and separated from the oil via the process mentioned earlier in the experimental Setup section and suspended in DI water. All three runs of the microgel generation demonstrated the long term stability of the device, there was very little drift in droplet size over large amount of time. The two larger runs ran for a total of ~32 hours generating the required amount of microgels, however the third run due to the significantly lower flow rate utilized to generate a smaller size operated for approximately 50 hours to generate adequate microgel volume (3.0 mL). In order to determine the characteristics further testing was required on the droplets generated.

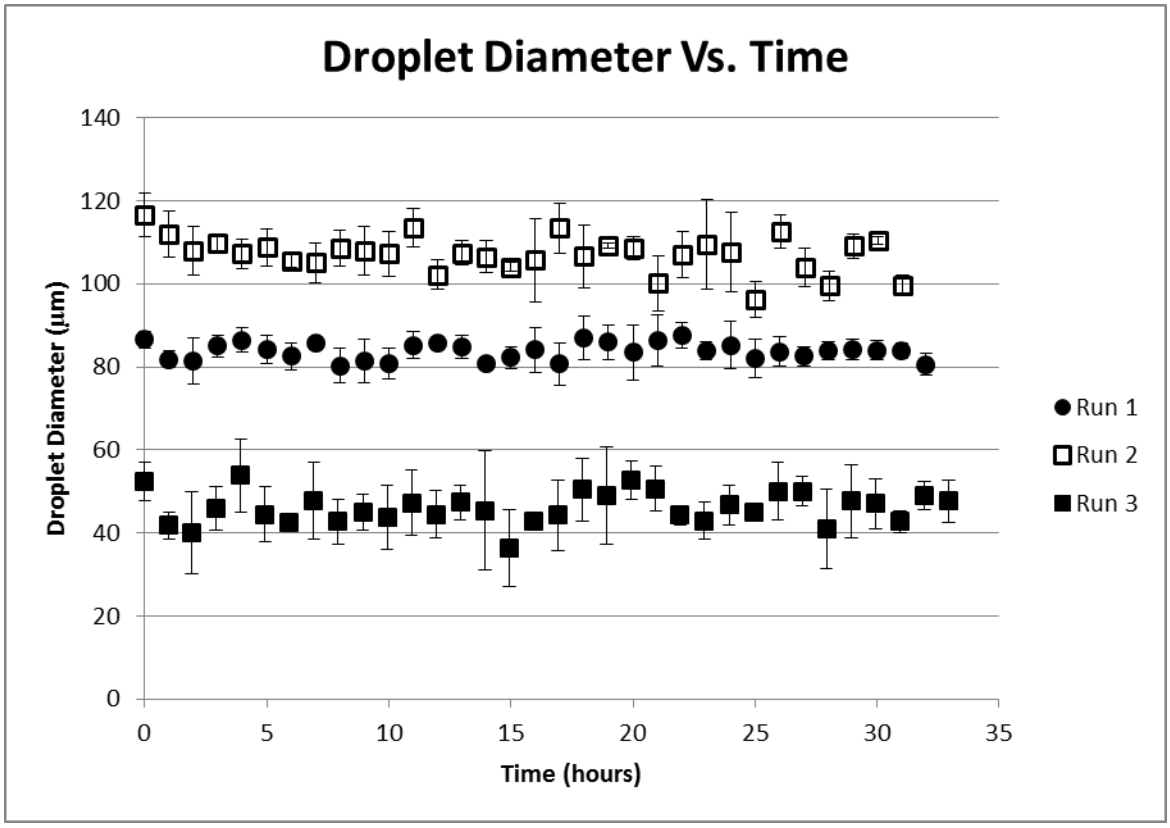

Figure 4.9 : *Long term microgel generation. Run 1) 1.1 ml/hour oil flow rate 0.06 ml/hour polymer flow rate. Run 2) 1.1 ml/hour oil flow rate 0.08 ml/hour polymer flow rate. Run 3) 1.1 ml/hour oil flow rate 0.03 ml/hour polymer flow rate.*

4.3.1 Droplet Mixing Analysis

The most suitable design was chosen to be analyzed and operated over long term to generate adequate volume of microgels for drug release studies. The device was operated under polymer flow rates of 0.06 mL/hour and an oil flow rate of 1.1 mL/hour. These operating conditions were chosen as it was observed that under these flow rates stable and continuous droplet generation was possible with what appeared to be little variation in size. Under these flow rates the droplets generated were 80 µm in diameter (**Figure 4.10 A**). Assuming that the droplets were monodisperse, a droplet generation

frequency of 280 Hz can be calculated for the given polymer flow rate. Although, this experiment demonstrated that the device design is suitable for producing monodisperse droplets from a co-flow of reactants, various parameters of importance to its application in drug delivery such as compositional uniformity, microgel polydispersity and the stability of device over long operating times are to be determined.

The chemical uniformity is of primary importance because if they are non-uniformly mixed some areas of the droplet will be in liquid form and dissolve once suspended in different media causing non spherical microgels. Droplets were generated using the device design (**Figure 4.7**) using 10 mg/mL CMCA and 20 mg/mL DEXB as the polymer solutions. After generation the droplets were separated from the oil phase and suspended in DI water. **Figure 4.10** shows 50 μm microgels that were generated in this device and are composed of a mixture of CMCA and DEXB suspended in various DI water, citrate buffer, and phosphate buffer solutions. As observed in **Figure 4.10** the droplets can be verified to be gels as they do not dissolve in water. Additionally they show swelling/shrinking in various solutions such as citrate buffer, phosphate buffer, and DI water. Therefore they can be confirmed to be "smart" microgels. It is clear that this method is capable of making gels rather than liquid droplets since the droplets did not dissolve when suspended in DI water or other aqueous solutions and maintained their shape and integrity. In order to analyze the chemical uniformity of the microgels a fluorescent tag was added to the CMCA during the microgel formation. The fluorescent microgels thus formed are displayed in **Figure 4.11**.

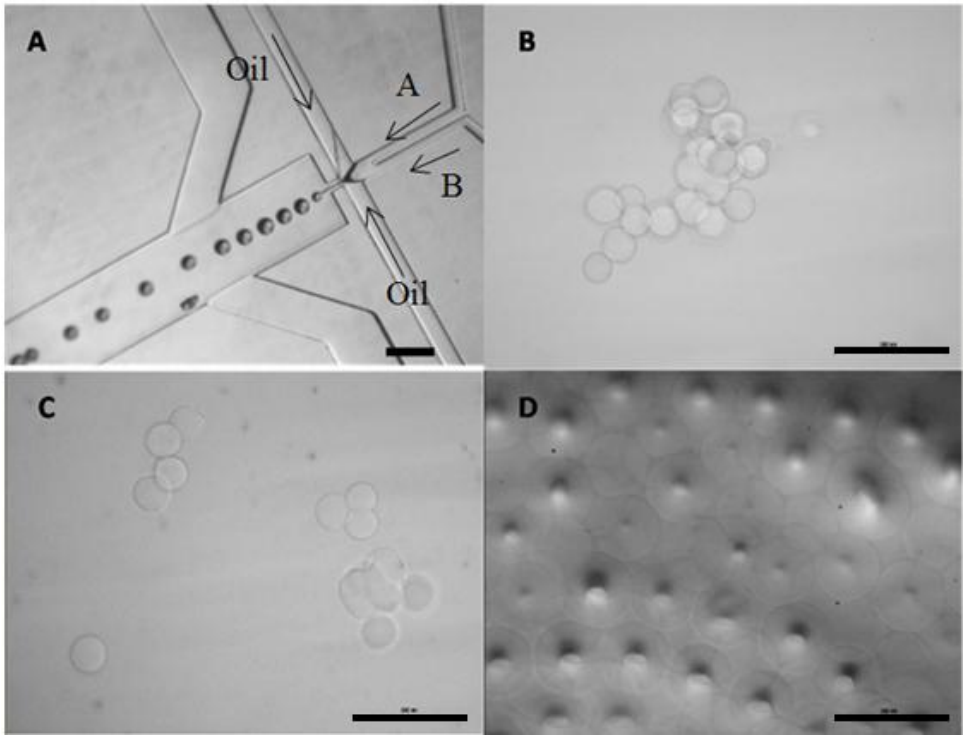

Figure 4.10 : *Microgels generated in different solutions (scale bar is 200 μm). A) Demonstrates microgel generation utilizing paraffin oil in the device. B) Microgels suspended in phosphate buffer solution. C) Microgels suspended in citrate buffer solution. D) Microgels suspended in DI water.*

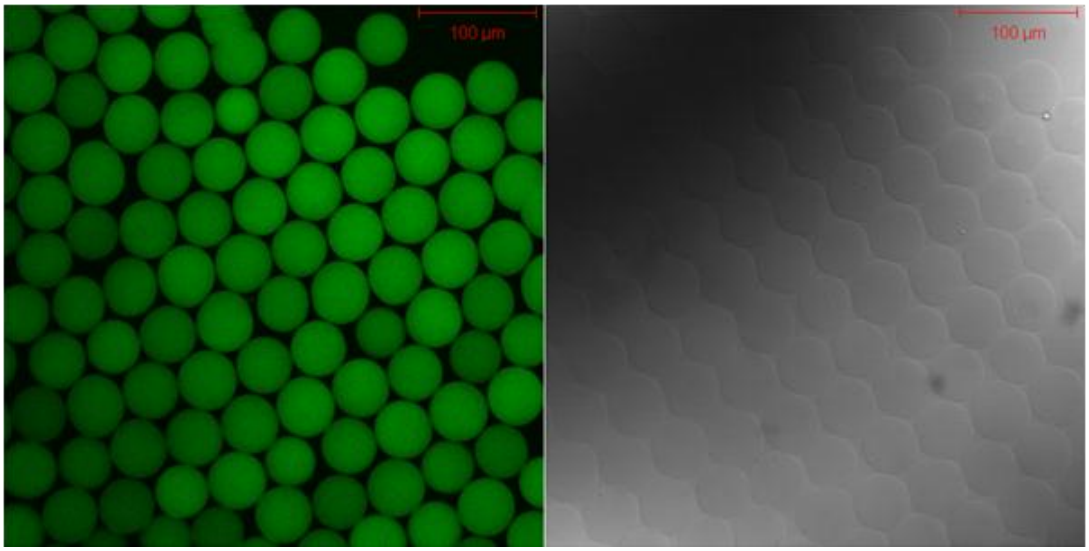

Figure 4.11 : *Fluorescent images of microgels created using fluorescently labeled FITC-CMCA and DEXB. The left image is fluorescence measured at 488 nm on a confocal microscope.The right image is visible light.*

Measuring the pixel intensity values it was confirmed that the fluorescence was uniform for microgels created via this method as shown in **Figure 4.12.** Since only one polymer is fluorescently labeled any unmixed region would not fluoresce. It is reasonable to conclude that the resulting microgels generated are a uniform mixture based on the fluorescent data obtained. The reason for achieving such uniform mixtures is not due to the short stabilization length but rather due to the flows occurring inside the droplets.

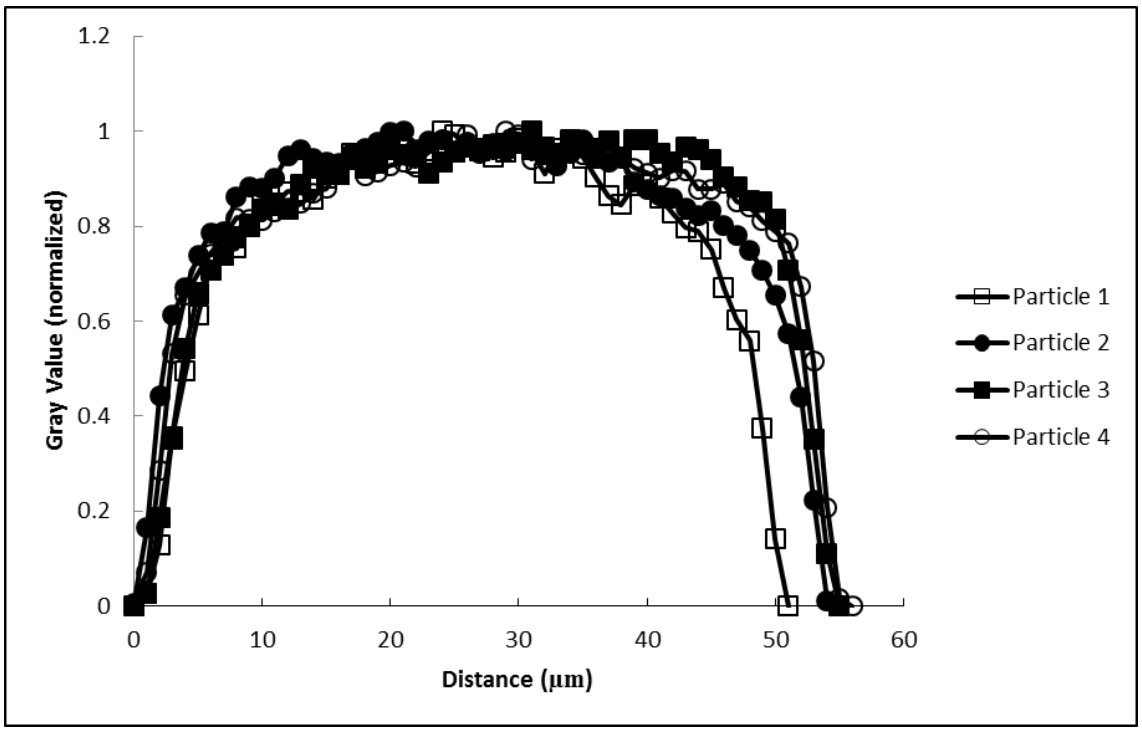

Figure 4.12 : *Fluorescence intensity measured across different particles in fluorescently labeled microgels.*

It can be determined that the mixing prior to droplet generation is insignificant (**Figure 4.13)** by utilizing Reynold's and Péclet numbers. The Reynold's number was calculated to be 0.05 to 0.2 when using the A/B polymer stabilization section width as the characteristic length (100 μm), kinematic viscosity of water (8.96 x 10^{-7} m^2/s), and

average channel flow rates 0.002 to 0.1 ml/hr. At such low Reynold's numbers highly laminar flow is expected and thus mixing is purely diffusional across the interface [64]. To determine the extent of diffusion the Péclet number is used and is as follows [65]:

$$Pe_L = \frac{LU}{D} \quad (4.6)$$

where L is the characteristic length, U is the flow velocity, and D is the mass diffusion coefficient (calculated to be 8.73×10^{-12} m^2/s) .The characteristic length that will be used is the length across the channel prior to the nozzle and the average velocity in this channel will be used. The Péclet number for operational flow rates (0.002-0.1 mL/hour each channel) used in experiments range from 5000 to 15000. For such large Péclet numbers the mixing length can be approximated to be the product of the Péclet number and the characteristic length, the mixing lengths are determined to be 50 to 150 mm [65]. Thus it can be concluded that no significant mixing of the polymers will occur over the short section which they meet

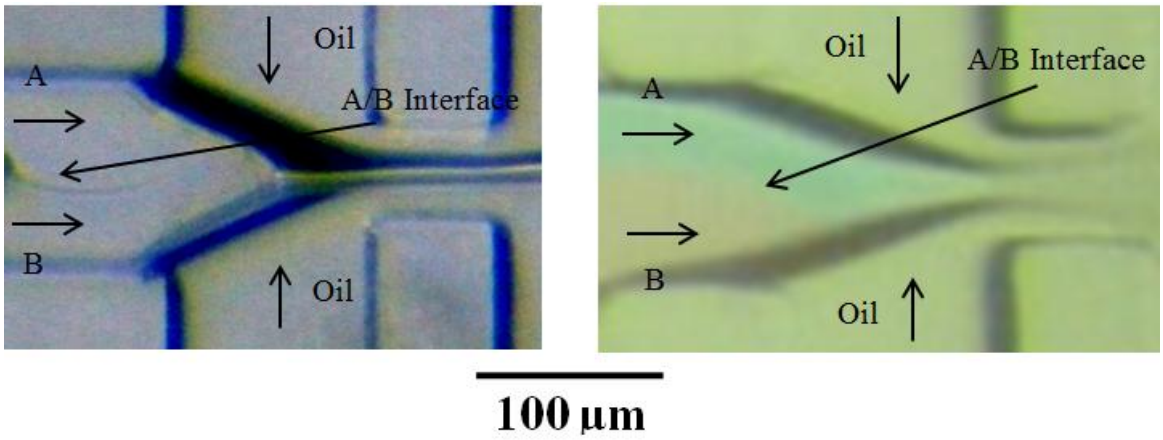

Figure 4.13 : *The stabilization section without and with die, it is observed no significant mixing is occurring.*

To explain the uniform mixing observed in these experiments we draw comparisons to literature dealing with mixing in microdroplets. François Blanchette [66] modeled the internal flows generated inside moving droplets which are in contact with the external channel as well as those suspended surrounded by a second immiscible phase. The flows resulting from the latter case are illustrated in **Figure 4.14** as streamlines, it is observed the significant recirculation is present in a droplet flowing in a carrying fluid. The internal flows occurring in a droplet arise from the perturbations caused by the droplet into the carrying fluid **(Figure 4.14).** These perturbations in conjunction with the flow of the carrying fluid cause differing tangential stresses on the surface of the droplet causing the recirculation observed. This is analogous to the situation microgel droplets face when flowing inside the microchannels; although the channel is rectangular the Reynolds number is similar to the study done by Blanchette. Therefore, this type of recirculatory flows within the droplets can be used to explain the uniform mixtures obtained in the microgels.

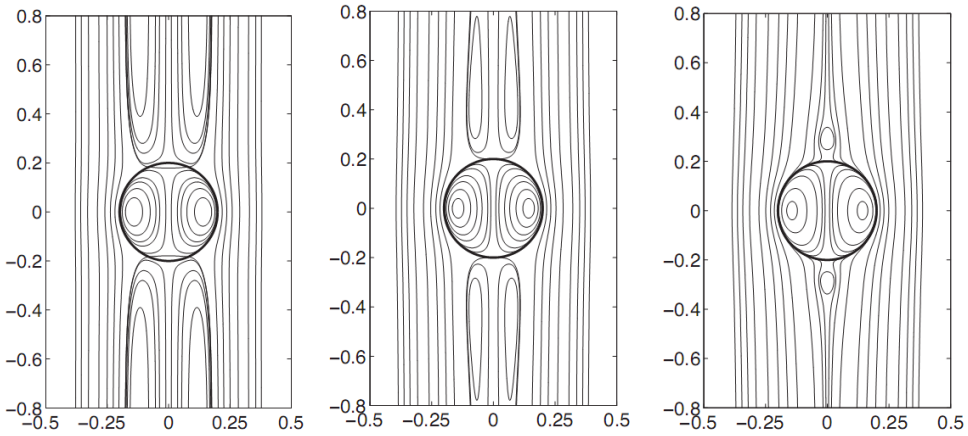

Figure 4.14 : *Streamlines for a drop flowing inside a capillary. The drag force on the droplet is proportional to ε A) ε = 0. B) ε = -2/5 drop moves at maximum velocity of unperturbed pipe flow. C) ε = -4/5.[Reproduced from*[66]*]*

In contrast, Nisisako *et al.* [67] demonstrated that it is possible to take advantage of microfluidics to create hemispherical particles. This study generated droplets of two immiscible organic phases and subsequently half of the droplet is polymerized causing the creation of hemispheres. The work done in this thesis involves the usage of miscible liquids and more closely resembles the case studied by Blanchette *et al.*

Results obtained in **Figure 4.12** demonstrate uniform fluorescence and hence uniform mixing was obtained. This uniform mixture is caused by a combination of the convective flows and diffusion occurring inside the droplets. These phenomena act together improving the mixture obtained in microdroplets. A simple experiment was completed in order to determine the extent of diffusion for a microdroplet. The results are shown in **Figure 4.15** where two droplets of approximately 1 mm diameter of CMCA (red) and DEXB (blue) placed on a bilayer of oil were coalesced. After approximately 15 minutes the resulting droplet appeared to be largely uniform with some gradient present in color. This droplet was determined to be fully gelled via removal from oil and suspension in DI water. Although dye is not linked to the CMCA and DEXB these results show that diffusion occurs rapidly once in the droplet. Since the droplets are suspended in the oil phase for tens of ours the polymer diffusion should be significant. Additionally work previously discussed [4] can directly be applied to the flow focusing device and used to explain the uniform mixtures obtained.

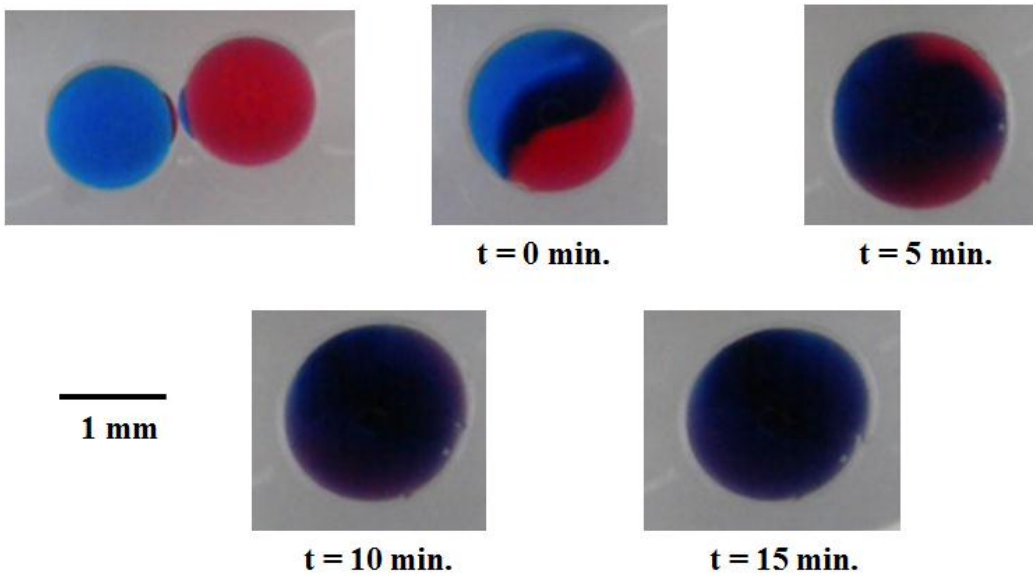

Figure 4.15 : *Diffusion observed in a droplet composed of the miscible CMC (Red) and DEX B (Blue) solutions.*

4.3.2 Droplet Size Analysis

Analyzing the device's capabilities and size ranges possible is an important factor when considering its usage. In order to assess the potential of the device the polymers CMCA and DEXB were utilized under normal operation with paraffin oil at various flow rates ranging from 0.02 to 0.2 mL/hr for polymers and 1 to 1.2 mL/hour for oil in the device design previously illustrated **Figure 4.7**. **Figure 4.16** shows that in this microfluidic device, the diameter of the droplet generated and hence the microgel formed varies linearly with the polymer flow rate when the oil flow rate is held constant. A linear relationship is expected since volume is linearly dependant on the flow rate. The droplets generated will retain their diameter once fully reacted to be microgels of the same size. This system can be used for microgel generation from sizes from 140 μm down to sizes

40 μm by varying the polymer flow rate from 0.02 mL/hour to 0.1 mL/hour. Generating droplets above 140 μm is possible but was not examined in detail in this work since smaller droplets were of more interest. Generation of droplets under 40 μm is possible by decreasing polymer flow rates.

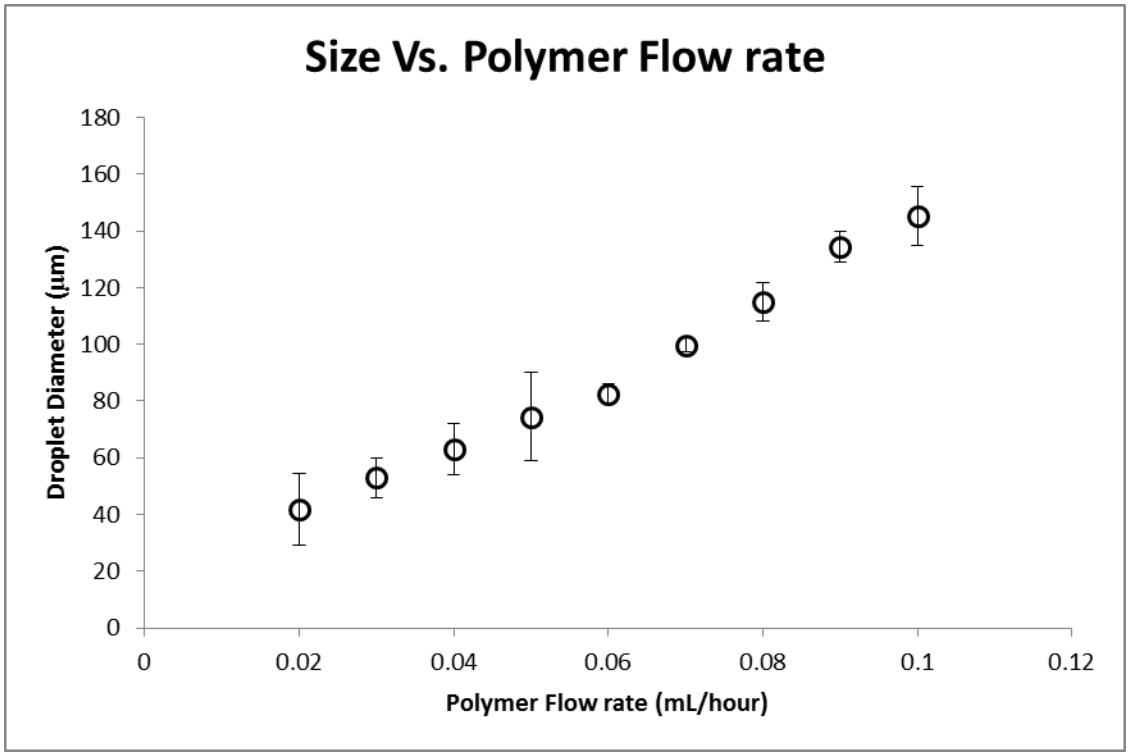

Figure 4.16 : *Droplet diameter vs. the polymer flow rate when the oil flow rate is fixed at 1.1 ml/hour.*

Additionally, the effect of the flow ratio (oil/polymer flow rate) on the droplet sizes generated was investigated. The results, as shown in **Figure 4.17**, makes evident that the droplet sizes decrease as the flow ratio in increased parabolically. This demonstrates the ability of the device to generate a wide range of microgel sizes, however

when generating very small droplets under 10 μm as shown in **Figure 4.18**, the droplet generation is unstable.

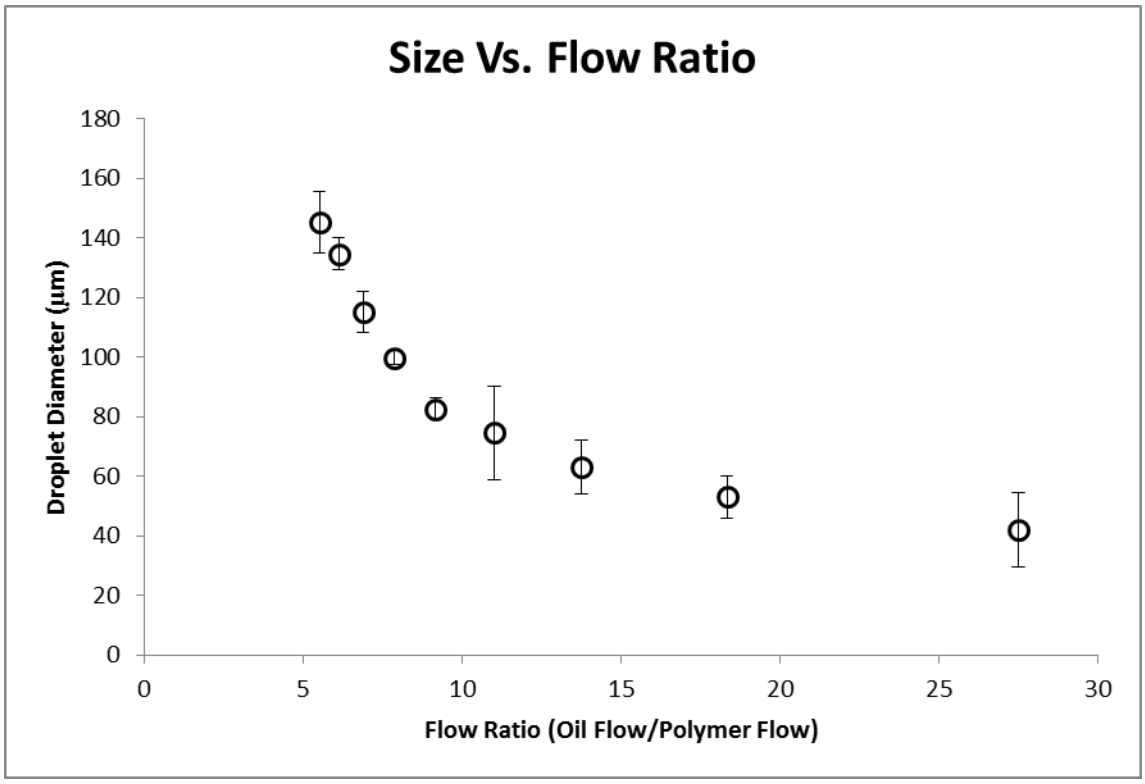

Figure 4.17 : *Size of microgels generated vs. flow ratio (oil flow rate / polymer flow rate).*

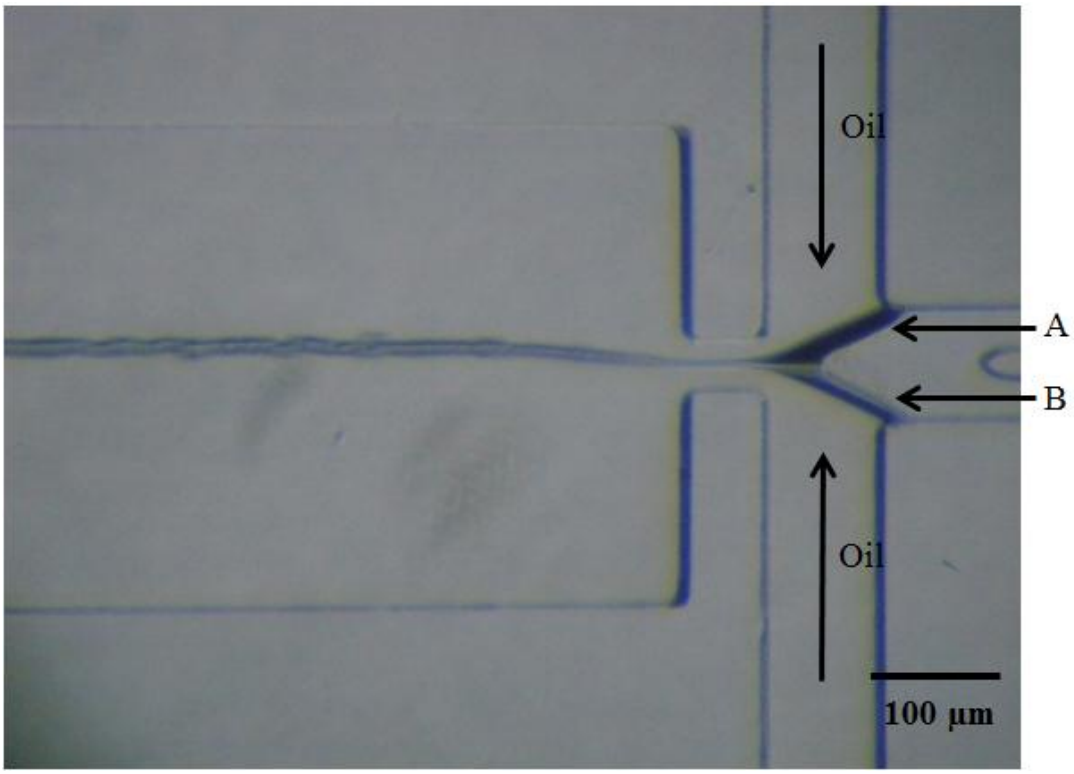

Figure 4.18 : *Very small microgels generated when oil flow rate is 1.1 ml/hour and polymer flow rates are 0.002 ml/hour.Due to their rapid generation, the appear as a continous stream.*

At very high flow ratios the device appears to have two stable regimes of droplet formation which it alternates between. **Figure 4.19** demonstrates this instability as the device alternates between forming small droplets and large droplets. At these low polymer flow rates (0.002 mL/hour), the Péclet number is merely 4. Therefore the diffusion in the short stabilization section becomes significant and gelation at the interface begins to impact the droplet formation. The cyclic nature is due chemical reaction causing some gelling at the stabilization channel. This gel eventually limits the flow causing the droplet sizes to decrease. However since the syringe pumps apply a constant flow rate this blockage causes a pressure rise until the gel is forced out and a

temporary rise in flow rate and droplet size is observed. In order to get past this limitation the oil flow rate must be increased to obtain higher flow ratios without reducing the polymer flow rates (and thereby reducing Péclet number and possibly entering the unstable regime of droplet generation). Increasing the oil flow rate is currently not possible in the device configuration as the bond strength at the interconnects and the PDMS device is not strong enough. To overcome this a lower viscosity continuous phase can be used or alternatively the mixing section can be reduced.

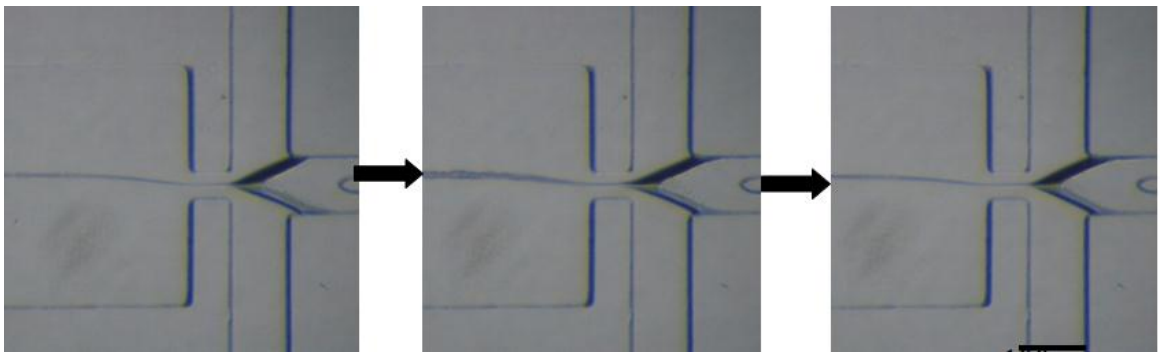

Figure 4.19 : *Cyclic unstable droplet generation observed over a period of approximately a minute at low polymer flow rates (scale bar is 100 µm).*

Statistics of the droplet sizes were also evaluated for the long duration experiments to obtain a measure of the polydispersity of the generated microgels. It can be seen in **Figure 4.20**, **Figure 4.21**, and **Figure 4.22** that the polydispersity of the microgels obtained via this method is larger than droplets generated using general flow focusing setups that do not involve reactions [22]. This can be explained for several reasons, the first being that the regime of droplet generation at the high flow rates being utilized is in the "jetting mode" [30].

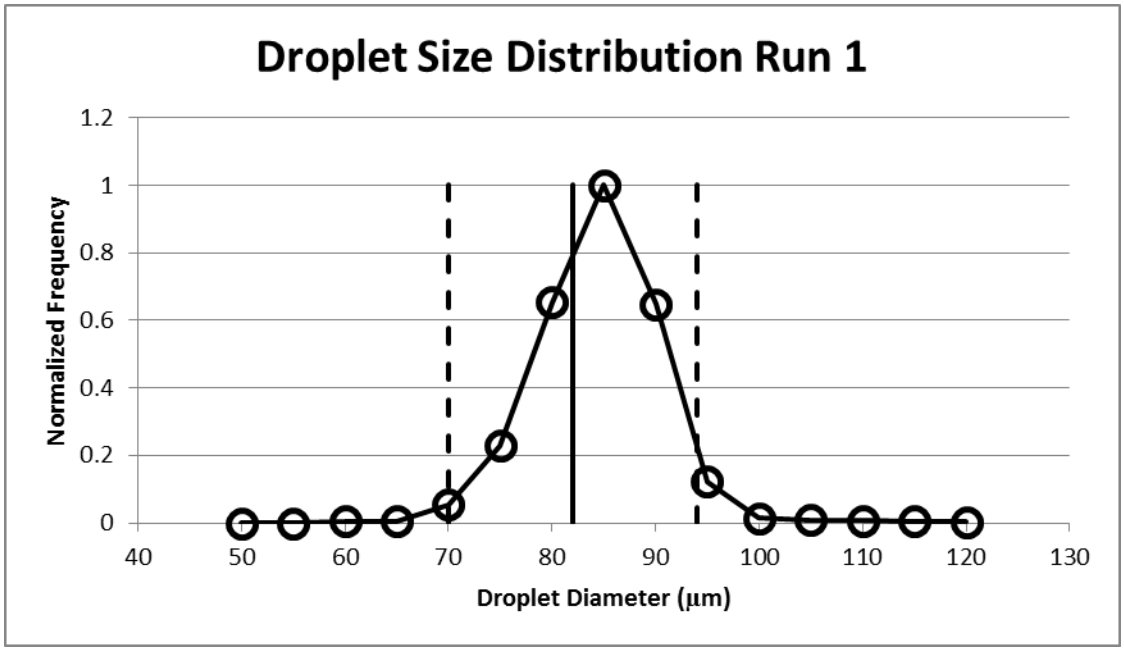

Figure 4.20 : *Droplet size distribution for Run 1 with a 1.1 ml/hour oil flow rate 0.06 ml/hour polymer flow rate. The mean (solid line) is 82.1 µm while the dashed lines represent 2 standard deviation distant (σ = 6.0 µm).*

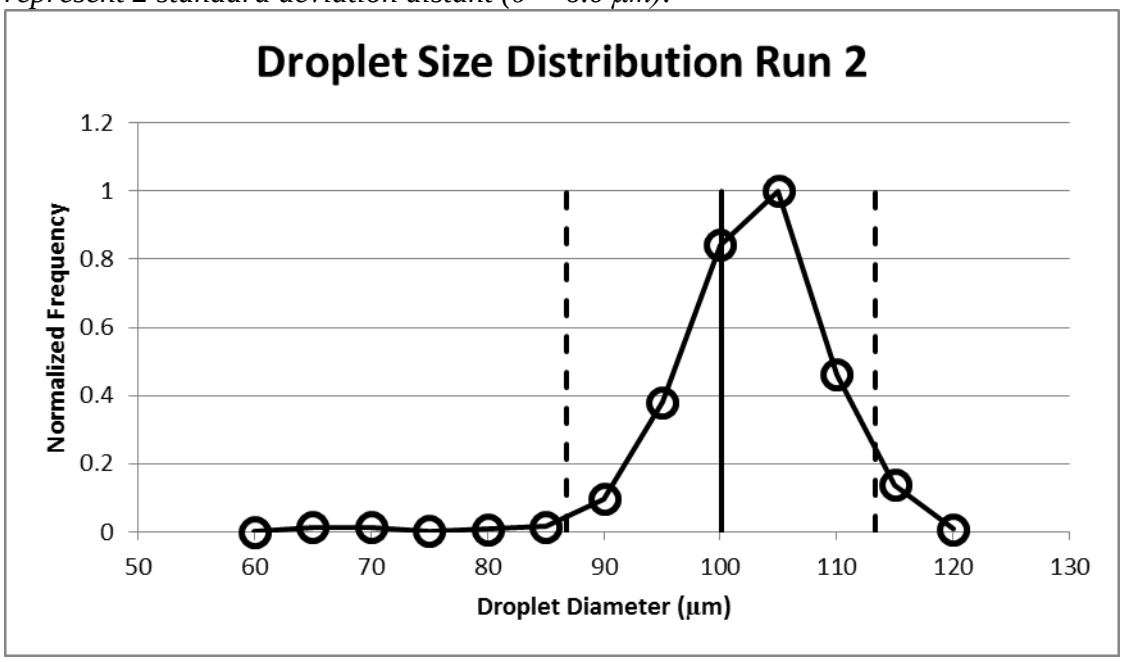

Figure 4.21 : *Droplet size distribution for Run 2 with a 1.1 ml/hour oil flow rate 0.08 ml/hour polymer flow rate. The mean (solid line) is 100.1 µm while the dashed lines represent 2 standard deviation distant (σ = 6.6 µm).*

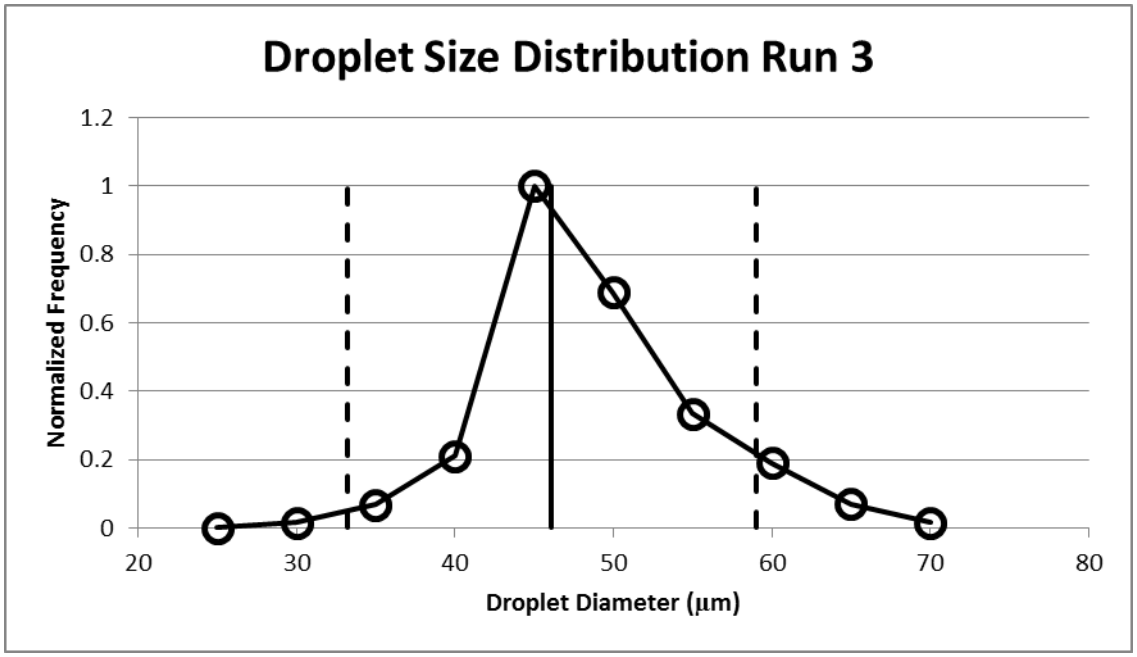

Figure 4.22 : *Droplet size distribution for Run 3 with a 1.1 ml/hour oil flow rate 0.03 ml/hour polymer flow rate. The mean (solid line) is 46.4 µm while the dashed lines represent 2 standard deviation distant (σ = 6.7 µm).*

To understand why the device is operating in the jetting mode we need to use the capillary number that has been defined as the following for microfluidic device [30]:

$$Ca = \frac{\mu_O a Q_c}{\gamma h \Delta Z}\left[\frac{1}{W_{OR}} - \frac{1}{2W_c}\right] \quad (4.7)$$

where μ_O is the viscosity of the oil, γ is the interfacial tension between the continuous phase and the disperse phase, h is the channel height, and the remaining variables explained in **Figure 4.23**.

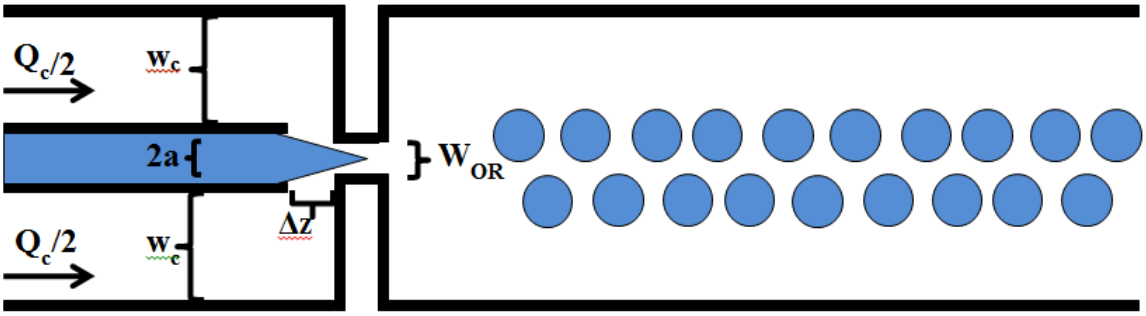

Figure 4.23 : *Geometric parameters for capillary number utilized in flow focusing.*

The capillary number computed for these experiments is 0.73. In this region of capillary numbers it has been determined by Shelley *et al.* [30] that jetting is likely to occur which is what was observed in the experiments. In the jetting regime the droplet generation is more polydisperse [30], from the capillary number it is observed that the capillary number must be lowered to move the droplet generation into a more monodisperse regime of droplet generation. The parameter most easily changed in these experiments is the oil flow rate. However, when decreasing the flow rate one must also reduce polymer flow rate in order to maintain a high flow ratio to achieve the same microgel size. This is undesirable due to the increase in the operation time to generate same volume of microgels as well as the reduced Péclet number causing possibly unstable operation as previously discussed.

Although jetting is one reason for the polydispersity observed, other factors do exist. One such factor is that droplet coalescence still occurs although at a much reduced frequency. As seen in **Figure 4.24** there are many similarly sized droplets with a larger droplet spaced some distance away from the previous droplet. It is possible that two adjacent droplets merged to create a larger droplet followed by a gap. Although the

separating oil flow was meant to introduce additional spacing between the droplets, it is farther downstream and does not prevent merging in the vicinity of the nozzle. Another source for polydispersity is due to the direct contact between A and B polymer solutions. This direct contact indicated that reaction occurs prior to droplet generation. This situation is likely to cause momentary viscosity changes leading to varying shear forces and thus slight changes in droplet size. All of the listed factors contribute to the polydispersity of microgels generated using this method.

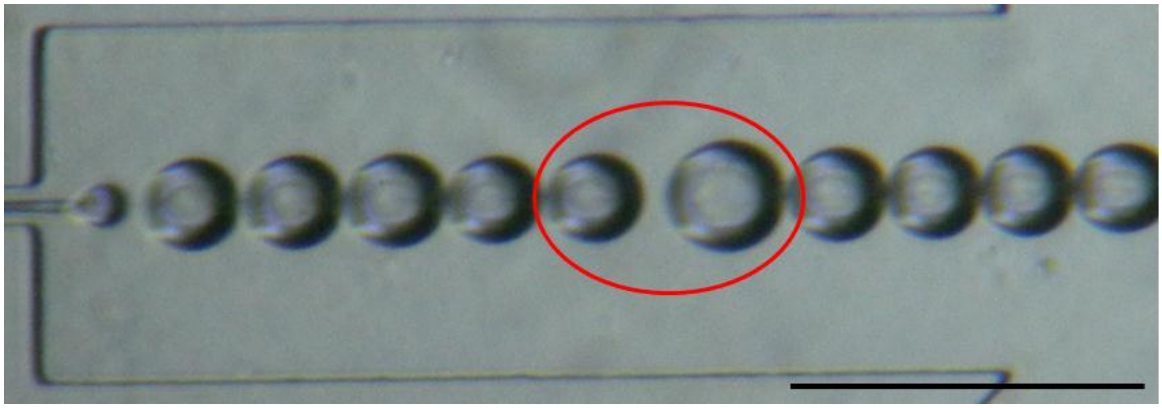

Figure 4.24 : *Possible coalescence of two droplets and subsequent gap (scale bar 450 μm).*

4.4 Summary

It has been demonstrated that a novel microfluidic device for microgel generation has been designed, tested, and analyzed. This device design allows for the generation of a uniformly mixed droplet of any A/B polymer system and was tested using CMC/DEXB as well as lupamin /glutaraldehyde. In order to evaluate the device performance long term microgel generation runs were conducted and it was determined that this system can operate for extended durations with little drift in microgel size. The droplets were verified

to be polymerized by being suspended in DI water as well as buffer solutions. Mixing was tested by fluorescently tagging one of the CMC solution and subsequently analyzing the emission of the droplets. Once it was determined that uniformly mixed microgels were created the device was operated for durations exceeding 30 hours. The droplet generation was stable over these long periods of time with the longest experiment taking longer than 45 hours to complete. Once the data was analyzed it was determined that drift was not present during the droplet generation and the droplets generated had a standard deviation of about 10% with respect to the diameter. This was adequate in order to use these microgels for drug release studies.

This device has proven to be robust and flexible being currently being utilized for microgel creation for drug release, gel encapsulated DNA, as well as potential uses in stem cell encapsulation. The microfluidic flow focusing device developed and designed in this work is versatile with the ability to work with many different polymer systems, provides control over droplet sizes, creates uniformly mixed droplets, can be operated for long time durations with little user interaction, with the microgels having acceptable monodispersity. Although this device has achieved a wide range of capability, rapid dynamic control over droplet size is still not possible. To achieve this droplet generation must be controlled via an electrical signal.

Chapter 5 Electrogenerated Droplet Device Design & Characterization

5.1 Introduction

The work in this chapter outlines the design and characterization of a microfluidic device for the generation of microdroplets via the electrogeneration process described in Chapter 2. The bulk of work done on this method is in the area of electrospray [11]. This technique is capable of large volume droplet production via an AC or DC high voltage signal. However it is not well suited for many applications since the sizes are typically limited to under 10 μm and control over size is difficult [42]. Work completed by Atten *et al.* [49] improves upon this method by introducing control over droplet sizes (50-200 μm) via pulsing. Unfortunately this technique does not examine high frequency droplet production and like electrospray is done on the macroscale with droplet generation occurring in a desktop setup.

While still focusing on droplet generation via high voltage pulses He *et al.*[50] were able to create droplets in a microfluidic channel. Although this method brought electrogeneration of droplets to microfluidics high frequency generation as well as control over sizes was not demonstrated. This section presents the design of a microfluidic device capable of droplet generations with the application of high voltage signals. Additionally high frequency droplet generation is examined and control over droplet sizes is demonstrated.

5.2 Device Design

5.2.1 Working Principle

Wright *et al.*[49] determined by simple analysis that in order to eject a droplet one must overcome the capillary pressure which is given by [69]:

$$P_{cp} = \frac{2\gamma}{r} \quad (5.1)$$

where P_{cp} is the capillary pressure, γ is the interfacial tension between the water/oil solutions, r is the capillary radius. In order to eject a droplet an electrostatic pressure pushing the fluid out must overcome the capillary pressure holding the meniscus in place. The electrostatic pressure was determined to be the following by Wright *et al.*:

$$P_e = {}^1/_2 \ \varepsilon E_n^2 \quad (5.2)$$

where P_e is the electrostatic pressure, ε is the permittivity of the insulating fluid, and E_n is the electric field normal to the meniscus surface. The maximum electric field for a curved surface such as a meniscus was determined to be the following [68], [69]:

$$E_{max} = \frac{2V}{r log\frac{4L}{r}} \quad (5.3)$$

where E_{max} is the maximum electric field, V is the potential difference, r is the meniscus radius, and L is the length between the surface and the ground. Equating the equations 1 and 2 and subsequently substituting into equation 3 it is possible to estimate the minimum voltage required to eject a droplet from a capillary. Using the dimensions of the final device design with a 50 μm meniscus radius and the physical properties of the working fluids a minimum voltage of ~150 V was calculated. Using this voltage as a guideline a

device can be designed for the generation of microdroplets. The device will consist of a primary oil channel that functions as a continuous carrier phase for the droplets being generated at an injecting site. Droplet generation is required to be high frequency whilst control over size is maintained.

5.2.2 Experimental Setup

The experimental setup is illustrated in **Figure 5.1** and consists of three primary components; signal generation, imaging, and pumping. The signal generation component provides high frequency high voltage signals to the device via a combination of a function generator and an amplifier. A Tektronix AFG 3022B function generator was utilized to produce various high frequency waveforms. These signals were then amplified by a Trek 10/10b HS high voltage amplifier. The limiting factor of the signal generation component is the amplifier which has a slew rate of 700 V/μs. Experimental limitations restricted the signals that could be applied to a maximum of 2000 V in amplitude and a minimum pulse width of 500 μs as in this case. The rise and fall time are under 1% of the lowest pulse duration period and the signal shape is not compromised. The working electrode is connected to the a syringe containing methylene blue solution and the ground is connected to a stainless steel needle placed approximately 600 μm away from the capillary as shown in **Figure 5.2**.

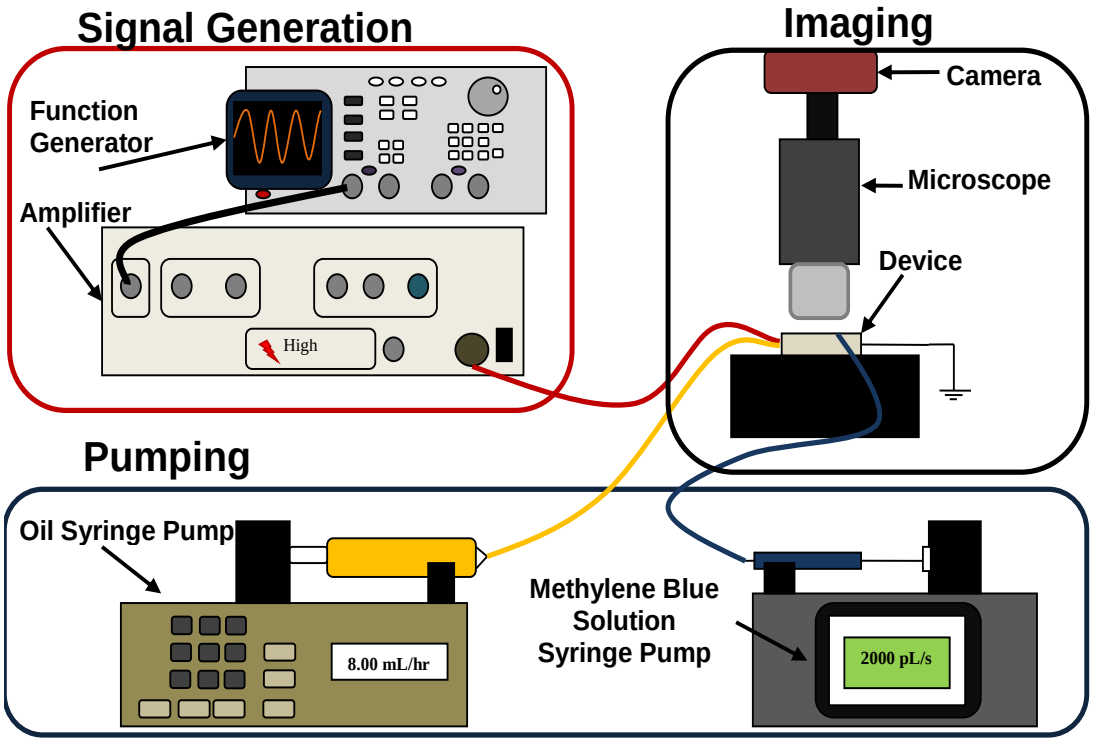

Figure 5.1 : *Experimental setup.*

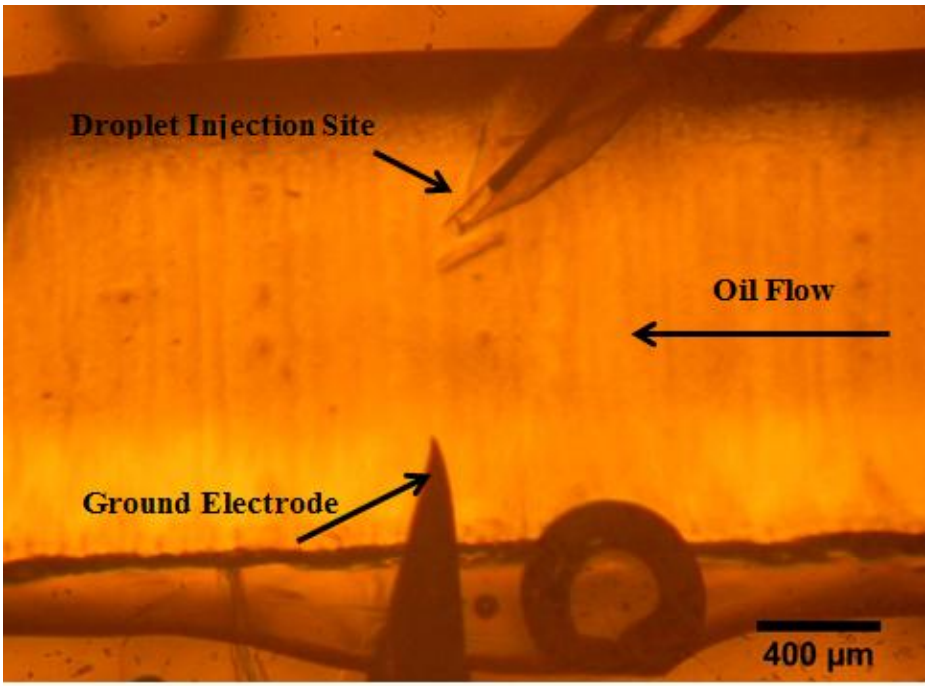

Figure 5.2 : *Placement of the ground electrode opposite the capillary.*

The flow component of the setup consisted of two syringe pumps providing linear actuation force to syringes connected to the microfluidic device. Initially to maintain flow in the capillary pictured in **Figure 5.2** the capillary pressure head was adjusted by the elevation of the syringe containing methylene blue solution. This was done since the syringe pumps available produced a pulsatile flow at extremely low flow rates. However, a KDS Legato 270 (GeneQ Inc., Quebec, Canada) high precision syringe pump was then purchased which provided pulse free flow for the 1 mL methylene blue syringe connected to the capillary. A Harvard Apparatus 22 infusion pump was used to provide flow to the 30 mL oil syringe. The experiment was allowed to reach steady flow conditions by waiting approximately 2 hours after set up. The oil solution utilized was the same 1 %wt Span80 in heavy paraffin oil used in the flow focusing experiments discussed in Chapter 4. A 1 %wt methylene blue (Sigma Aldrich, Ontario, Canada) DI water solution was prepared using laboratory scales for weight measurements and manual mixed.

Imaging on droplet generation was done with the combination of the microscope on a Signatone 1160 Series Probe Station and a camera. Initial experiments were recorded utilized a Nikon Coolpix P6100 camera mounted on the microscope. The usage of this camera resulted in motion blur due to high frequency droplet generation thus it was replaced by a Photron Fastcam Troubleshooter high speed camera. Videos were recorded 3 minutes after the electrical signal was changed or applied for consistency. The majority of videos were recorded in 1000 FPS to eliminate motion blurring and for better experimental observations on the droplet generation process.

Droplet diameter measurements were made by placing a line across the droplet midsection in ImageJ to measure the length. With pictures having pixel resolutions lower than 1 μm the largest amount of error was due to the manual measurements. The 95% confidence interval of the measurements was determined to be +/-0.52% of the measured value. In all cases measurements were done on the primary droplet. The primary droplet is the largest ejected droplet in each cycle of the waveform.

All physical properties remained the same as flow focusing experiments with the exception of the methylene blue solution. The viscosity, interfacial tension, and relative dielectric constant of the paraffin oil remained the same as the work conducted in the flow focusing chapter at 49.9 cSt, 0.003 N/m, and 2.2 respectively. The methylene blue solution was measured to have a conductivity of 2.56 mS/cm utilizing an Omega CDH-280 conductivity meter. This experimental setup was utilized in all experiments to determine the optimum design for a device capable of droplet generation via high voltage electrical signals.

5.2.3 Design Iterations

Initially the capillaries shown in figure were utilized for the injection of the disperse phase into the flowing oil channel. Design a) in **Figure 5.3** was the first tested but the large surface area near the capillary tip proved to be problematic, providing a large hydrophilic surface to which droplets and the meniscus would attach to. The next tests involved the nozzle shown in image b), this is a pulled glass needle that has a large taper and as a result minimized the surface area near the droplet injection points.

Although this design proved to be much better, the repeatability between devices was low because the inner diameter of the needle during the pulling process was very difficult to control. Next result design c) was developed in an attempt to maintain injection site dimensions. This design involved the usage of a PDMS microchannel as the injection point for the disperse phase. Although the diameter of the injection channel could be accurately controlled, the disperse phase was in contact with the top and bottom surfaces of the oil channel, which caused droplet generation to be very difficult.

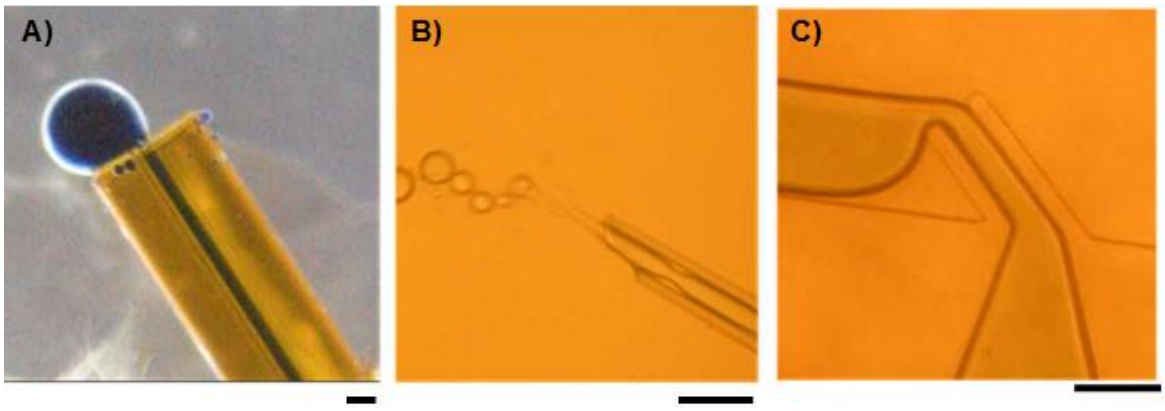

Figure 5.3 : *Capillary designs tested. A) fused silica capillary B) pulled glass needle C) PDMS injection channel (scale bars represent 100 μm).*

The final design for an injection point for the disperse phase is a fused silica capillary with a 365 μm OD and a 50 μm ID. The tip was tapered via an etching process developed by Geetha Mahadevan [58]. This process preserved the capillary inner diameter while etching the outer surface as shown in **Figure 5.4**. The taper is advantageous because it eliminated the probability of droplet adhesion to the surfaces near the meniscus. In addition, the usage of a commercially fabricated capillary insures that the ID remains the same when using new capillaries. During experimentation it was

determined that the shorter taper pictured on the left was more robust. This robustness came from its' increased strength since there was more material at the capillary near the tip. This is advantageous since same capillary can be removed, cleaned, and re-injected into a new channel without the risk of breakage at the tip. This capillary proved to be the best method as a droplet injection site and was used in the optimal device design.

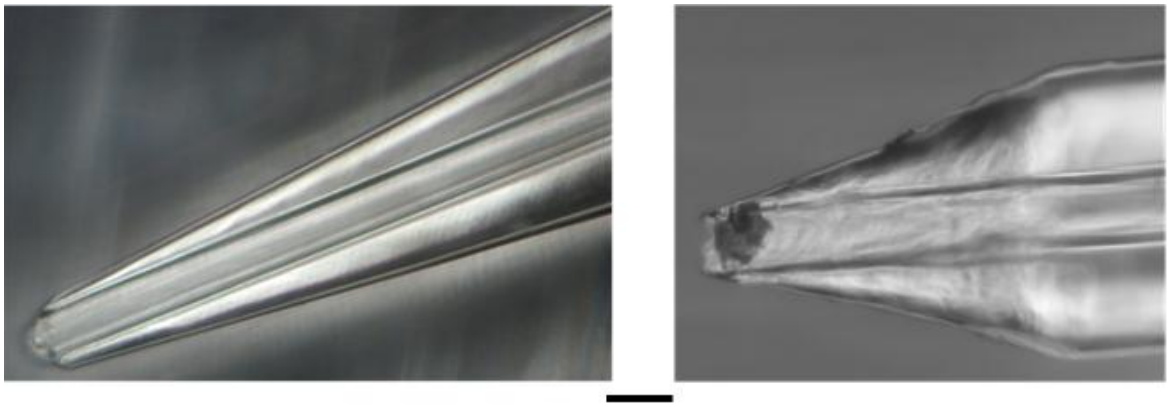

Figure 5.4 : *Etched fused silica capillaries (Scale bar is 50 μm).*

5.2.4 Optimized Design

The final design for a device to electrically generate droplets is proposed in **Figure 5.5**. The oil inlets and outlets are 2 mm square channels to allow the insertion of 1.8 mm diameter borosilicate glass capillaries as interconnects. The primary channel is of reduced dimensions at 1.5x0.8 mm in order to allow the flow to accelerate and clear away droplets generated more rapidly. The channel expands greatly to a width of 11.54 mm decelerating the flow and allowing for better imaging if required. The last features are the slots sized appropriately for the ground electrode which is a stainless steel 27 G1/2 needle and the capillary which has an outer diameter of 360 um. The capillary is positioned at 45

degrees away from the oil flow in the primary channel. The reason is that when placed perpendicular it was determined that some oil flowed into the capillary due to the impossibility of positioning perfectly and thus it is possible the capillary was facing the oil flow.

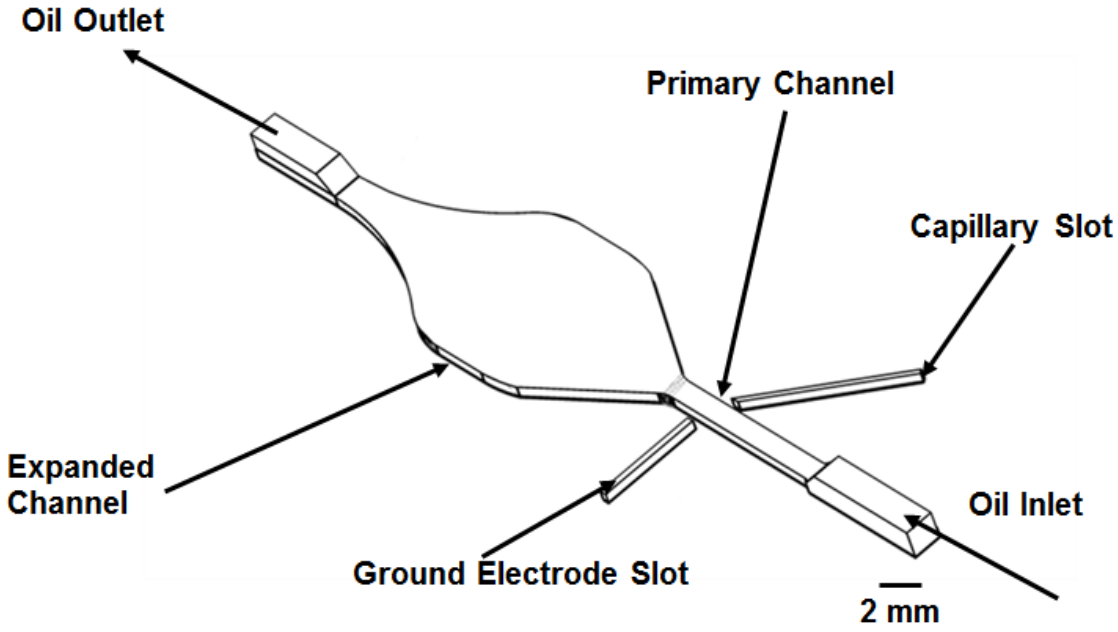

Figure 5.5 : Final design for droplet generation device.

5.3 Device Characterization & Analysis

5.3.1 Comparison of Droplet Generation with AC Waveforms

Droplet generation can be initiated by a variety of electrical waveforms. In order to obtain the optimized waveform for monodisperse droplet generation with a high degree

of control over droplet size, the droplet generation process was observed under the influence of square, pulse and ramping waveforms as shown in **Figure 5.6**.

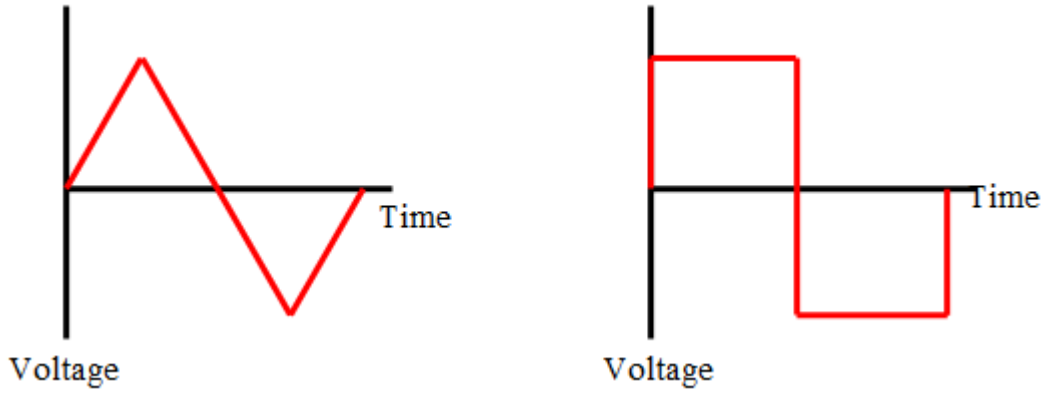

Figure 5.6 : *Waveforms used for droplet generation. Ramp (left) & square (right).*

Apart from the electrical signal applied, another factor that may influence the droplet generation is the shear force introduced at the interface due to the flow of the continuous phase. In order to evaluate the significance of the continuous phase flow in comparison with the surface tension forces the Weber number which is given in the following number was utilized:

$$We = \frac{\rho V^2 D}{\gamma} \qquad (5.4)$$

Where ρ is the density of the oil (895.5 kg/m^3), V is the fluid velocity (100-200 um/s), D is the meniscus diameter (50 μm), γ is the interfacial tension between water and oil (0.003 N/m). Using this simple calculation for channel flow rates of 4 and 8 ml/hour which in the microfluidic device translates to very high velocities the Weber number computed is on the order of 10^{-5}. This indicates that the surface tension forces are significantly more dominant than the inertial forces applied on the meniscus by the oil flow rate. The

modulation in surface tension introduced by the electrical potential will be the dominant factor influencing the generation of droplets as compared to the shear induced by the fluid flow. Thus, in the subsequent experiments the continuous phase (oil) flow will be maintained constant and the influence of the electric field will be studied.

In order to test the waveforms shown in **Figure 5.6** for droplet generation appropriate levels for parameters such as voltage and frequency are required. Previous experiments as shown in **Figure 5.3**, indicate that droplet generation process starts at 500V for these waveforms. This voltage is higher than that was calculated in the analysis previously presented in the Working Principle section (5.1). The model was developed for an electrically conducting droplet injection site placed a distance away from a flat plate ground electrode which is not the case in the device outlined in sections 5.3 and 5.4. Results obtained from preliminary testing also led to the usage of a static pressure of 1.08 kPa being applied to the capillary and an oil flow rate of 8 mL/hour being applied to the primary channel shown in **Figure 5.2**. A frequency of 30 Hz was initially chosen for experiments due to the lack of access to a high speed camera. This frequency allows synchronization between droplet generation and a 30 FPS commercially available camera (Nikon Coolpix P6100) and resulted in better quality footage.

As seen in **Figure 5.7** a 30 Hz square wave form at an amplitude of 500 V generates droplets in various locations along the depth and width of the channel with the additional generation of many satellite droplets with sizes considerably less than that of the primary droplet. A sine wave with the same frequency and voltage on the other hand ejected droplets and satellite droplets in a more ordered manner having two distinctly

located streams of droplets shown in **Figure 5.8**. Keeping voltage and frequency the same, it appears that a sine wave produces smaller and larger number of droplets than a square wave. This size difference could be due to the fact that a square wave form spends a prolonged period of time at the peak voltage causing a larger electrostatic pressure build up due to a higher RMS voltage and hence more volume of fluid being ejected as opposed to a ramping wave (**Figure 5.6**). It follows that smaller droplets are observed to be ejected in a single stream while utilizing a ramping waveform as shown in **Figure 5.9**. This could be due to the ramping wave form (30 Hz, 500 V) having a sharp rise and drop at the peak voltage and a lower RMS voltage value. A ramping wave's more gradual rise and fall could cause more sustained electrostatic forces causing more and smaller droplets to be ejected per cycle. To analyze droplet ejection in better temporal detail it was necessary to utilize a high speed camera.

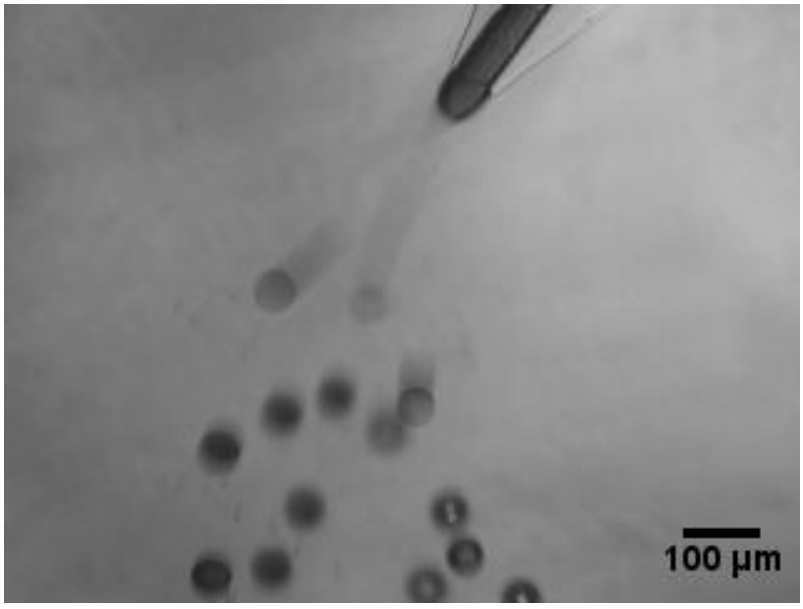

Figure 5.7 : *Droplet generation with a square wave at 30 Hz frequency with a 500 V amplitude.*

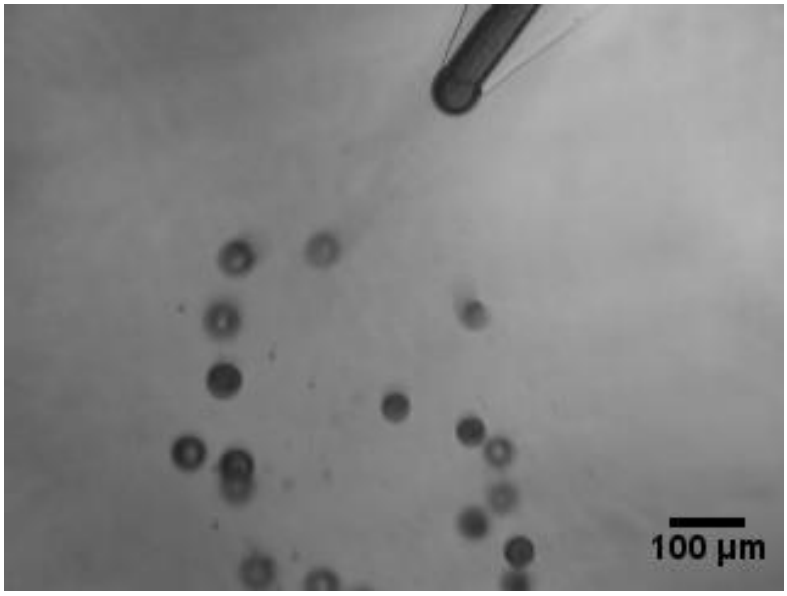

Figure 5.8 : *Droplet generation with a sine wave at 30 Hz frequency with a 500 V amplitude.*

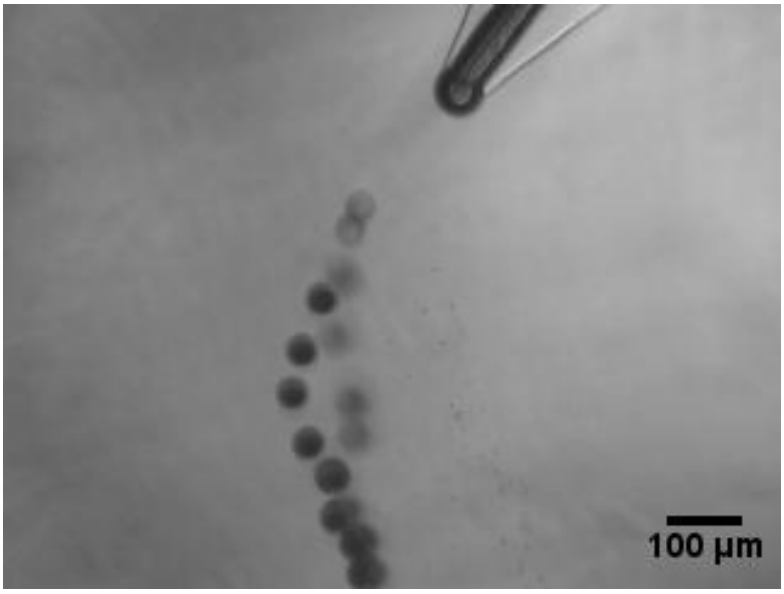

Figure 5.9 : *Droplet generation using a ramping waveform at 30 Hz frequency with a 500 V amplitude.*

5.3.2 AC Signal Droplet Ejection Analysis

A Photron Fastcam Troubleshooter camera was mounted on the microscope in order to observe droplet generation in more detail while using the same voltage (500 V), frequency (30 Hz), and flow patterns (8 mL/hour oil, 1.08 kPa pressure head at capillary) but with the different waveforms of sine, square, and ramping. When utilizing a ramping waveform and a square waveform the number of primary droplet ejection events corresponding to the frequency, which is to say for a 30 Hz frequency, 30 droplet ejection events occurred. The high speed videos show that in case of a square wave, an ejection event begins with ejection of a large droplet (~40 μm) followed by 4 or 5 secondary (<5 μm) droplet ejection events. It is seen in **Figure 5.10**, that the main droplet is much larger than the secondary droplets. This difference in size is due to the meniscus retreating after the primary droplet ejection. Upon measuring the time intervals for droplet ejection under a square wave it is determined that the large droplet is ejected within 1.5 ms of first observing a disturbance in the fluid meniscus (indicating that it is being charged), with the secondary droplets being ejected over a longer period of time of 15.5 ms, followed by a 16 ms "relaxation" time where there is no droplet ejection. The total time period for the entire cycle was measured to be 33 ms which corresponds to a frequency of 30 Hz.

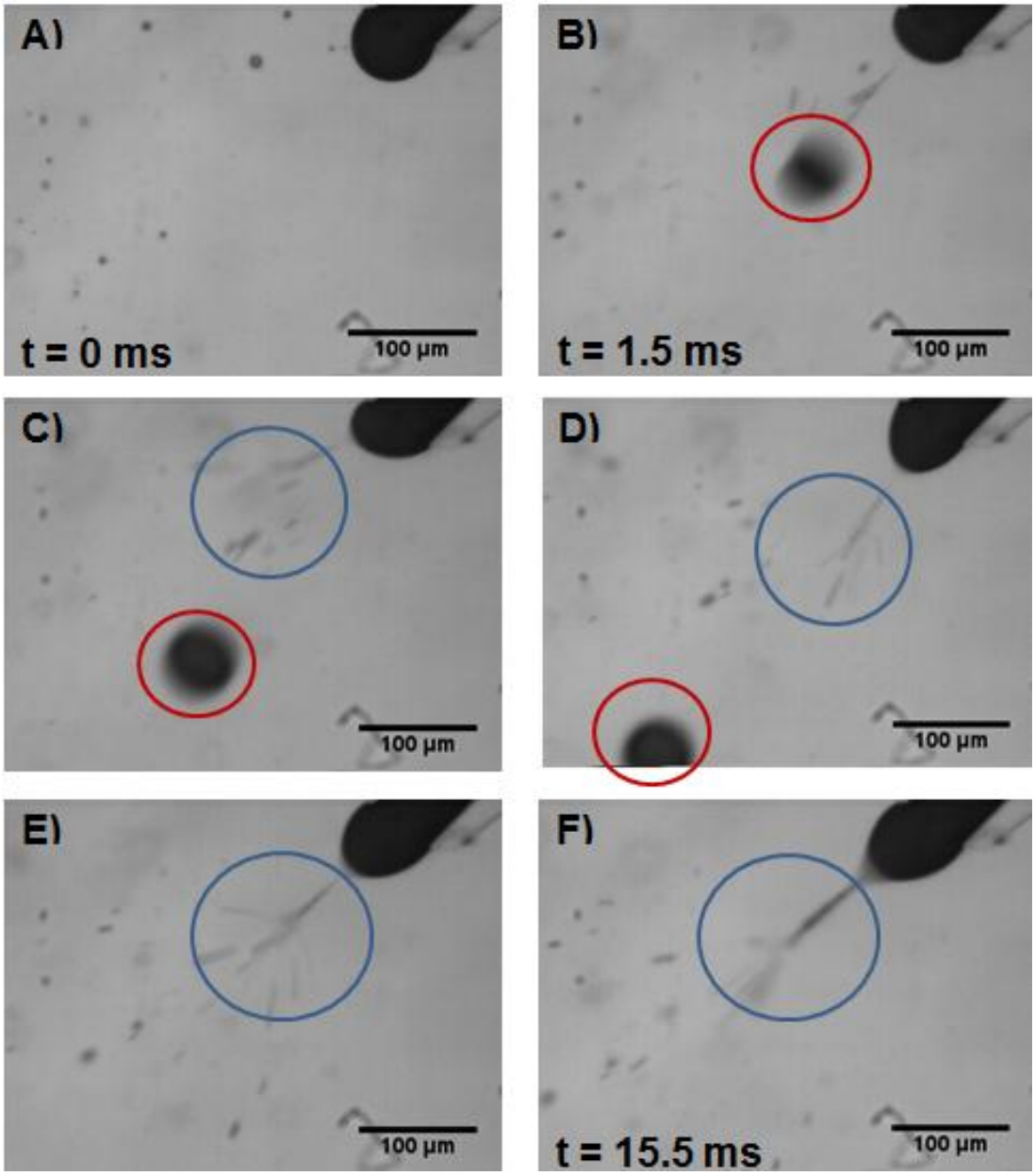

Figure 5.10 : *Droplet generation under a square wave. A) is the primary droplet ejection even with B),C),D), and E) being secondary ejections.Primary droplet is highlighted in red, secondary are highlighted in blue.*

Applying a ramping waveform as illustrated in **Figure 5.11** produces contrasting results. It is observed that initially small droplets are ejected with a large droplet being ejected directly after. After initial meniscus disturbance a small spray of droplets is

ejected and subsequently a large droplet ejection event follows. The ejection process lasted 9.5 ms with a relaxation time of 24 ms after, totalling 33.5 ms. The time interval measured is almost equal to the period of any waveform operating at 30 Hz. The cause of this prolonged relaxation time can be explained by the gradual change of the electric signal. When a ramping waveform is used a secondary droplet ejection occurs before a large droplet is ejected and this contrasts with what is observed when a square waveform is applied. This difference can be explained by observing that for a square wave the electrostatic pressure almost instantly increases past the threshold previously discussed to overcome the capillary pressure causing a large droplet to be ejected. A ramp wave reaches this threshold gradually causing a causing primary droplet ejection to occur some time after the meniscus is initially deformed. The secondary ejections occur due to excess charging causing a repulsive interaction in the fluid meniscus and subsequently ejecting a jet similar to that present in electrospray (Chapter 2). In order to avoid this jetting excess charging must be eliminated via the reduction of the duty cycle or voltage. The results obtained are to be expected for a frequency of 30 Hz.

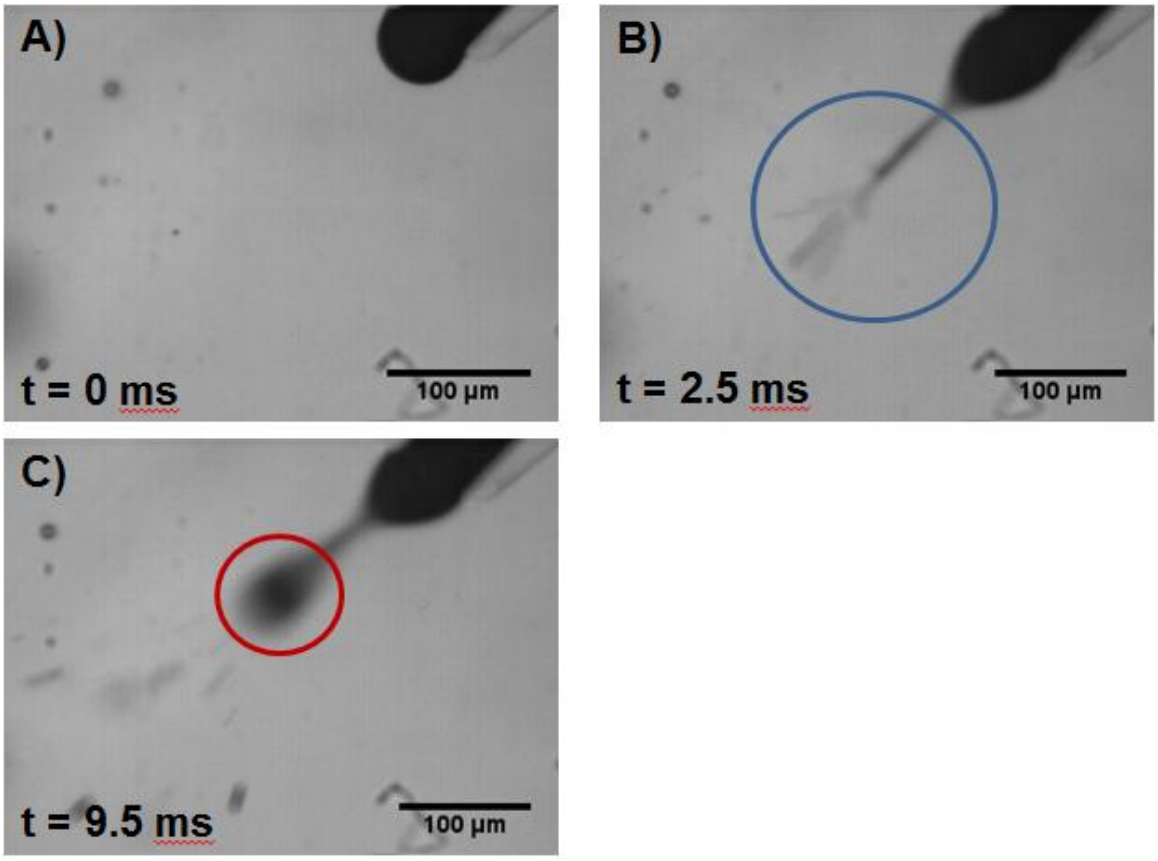

Figure 5.11 : *Droplet generation using a ramping waveform. A) Initial ejection of small droplets. B) Ejection of large droplet (large droplet is highlighted in red whilst smaller ones in blue).*

5.3.3 Analysis of Droplet Generation Utilizing Ramping Waveform

Several experiments were completed in order to analyze the importance of varying parameters when using a ramping waveform, however in this case the signal was purely positive. Initially the voltage was varied from 500 to 2000 V whilst the channel flow rate was held at 4 mL/hour, capillary pressure head was 1.08 kPa, and the frequency constant at 70 Hz. It is seen in **Figure 5.12** that when increasing the voltage there are 4 stages of droplet generation. Initially there are no droplets generated; upon increasing the voltage

droplet generation begins. In this stage the droplet generated are relatively large and have a large size distribution. Upon increasing the voltage further we observe the droplet generation becomes more ordered with large fairly monodisperse droplets being generated and the accompanying satellite droplets being present as well. This area of voltages (500-1500 V) seems to be optimal for droplet generation in the fixed conditions stated earlier. Increasing the voltage even further causes the droplet generation to become chaotic and similar to a spray. The transition from the dripping to spraying is due to increased charge accumulating at the meniscus. Higher voltages cause the electrostatic interactions to dominate the viscous forces. This causes the formation of a Taylor cone which produces a continuous spray of droplets[41].

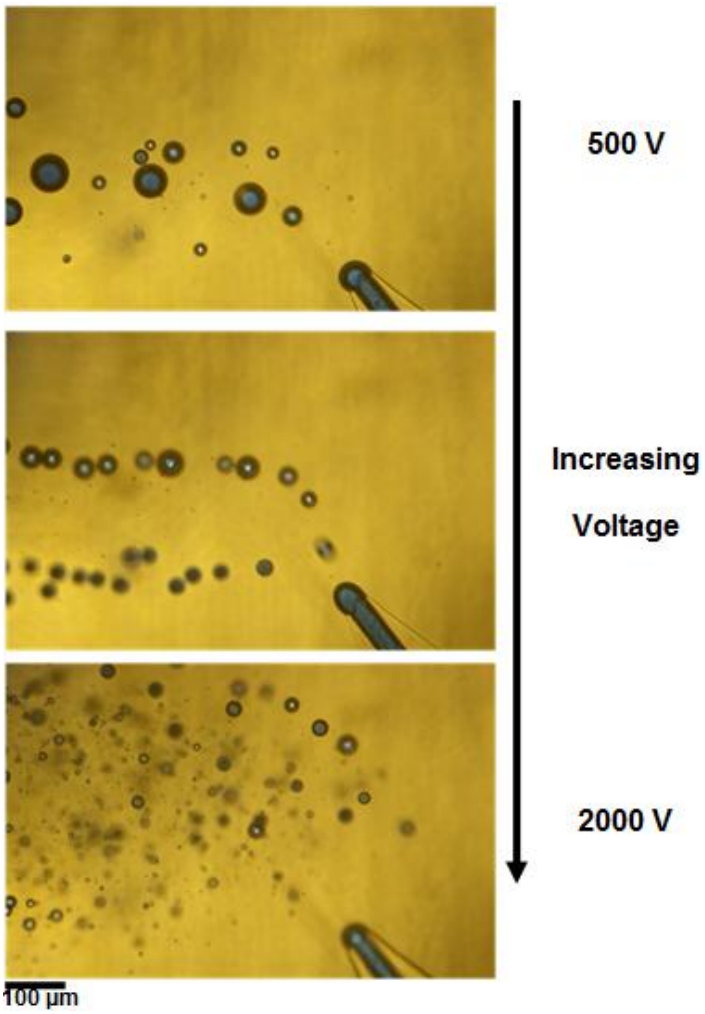

Figure 5.12* : *Effects of increasing voltage from 0-2000 V (70 Hz, 4 mL/hour, 1.08 kPa).

The frequency, voltage and oil flow rate are next fixed (1000 V, 70 Hz, 4 mL/hr) and the effect of changes in the pressure head experienced by the capillary are observed. **Figure 5.13** demonstrates the effects of changing pressure head when increasing pressure. Initially very small droplets are ejected with droplet size increasing as the head is increased. This is easily explained due to the increased flow at the meniscus when increasing the pressure. When making larger droplets it is observed that the droplets generated are deformed. This deformation has previously been analyzed [70] and is a

result of the electrical normal stresses introduced into the droplet by the electric field, an unavoidable consequence of generating droplets via electric field.

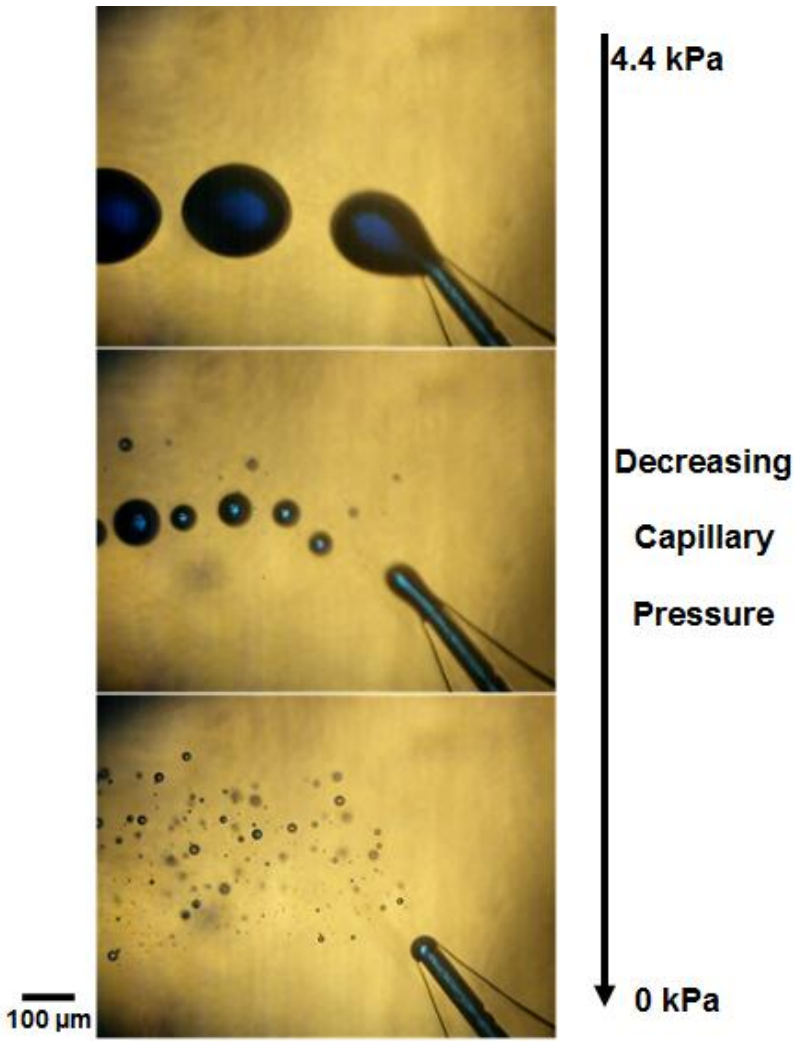

Figure 5.13 : *Effects of increasing the pressure experienced by the capillary (70 Hz, 1000 V, 1.08 kPa).*

Using the same pressure head, flow rate, and voltage (1.08 kPa, 4 mL/hour, 1000 V) the effect of the frequency on droplet generation was analyzed. **Figure 5.14** illustrates the effect of gradually decreasing the frequency on the droplet generation. At higher frequencies droplets being generated are more chaotic in nature with a higher

polydispersity, however decreasing the frequency droplets become larger and more monodisperse. A simple method for determining droplet generation stability with regards to the frequency is to consider the spacing between droplets. When the spacing between droplets is too small due to high frequencies droplets coalesce and cause high polydispersity. To insure adequate droplet spacing and prevent the collision of droplets the following relation which will be called the stability number must be greater than unity:

$$St = \frac{V}{Df} \quad (5.5)$$

Where *V* is the oil channel flow velocity, *f* is the frequency of droplet generation, and *D* is the droplet diameter. This relationship is logical since the flow needs to move a droplet with a diameter D, the same distance (D) away from the region of droplet generation to avoid collision with the next droplet being generated and coalescence. To simplify, the electrostatic effects can be ignored and the droplet diameter can be estimated simply as a function of frequency and the capillary flow rate. The flow rate in the capillary is constant, however the frequency of extracting volume from the meniscus is increasing. It follows that increasing the number of droplets extracted from the same volume will result in smaller volumes extracted per droplet:

$$D = \sqrt[3]{\frac{6Q}{\pi f}} \quad (5.6)$$

where *Q* is capillary flow rate. Combining these two equations the following is obtained:

$$St = \sqrt[3]{\frac{\pi V^3}{6f^2Q}} \quad (5.7)$$

To obtain best droplet generation this dimensionless ratio must be equal or greater than unity.

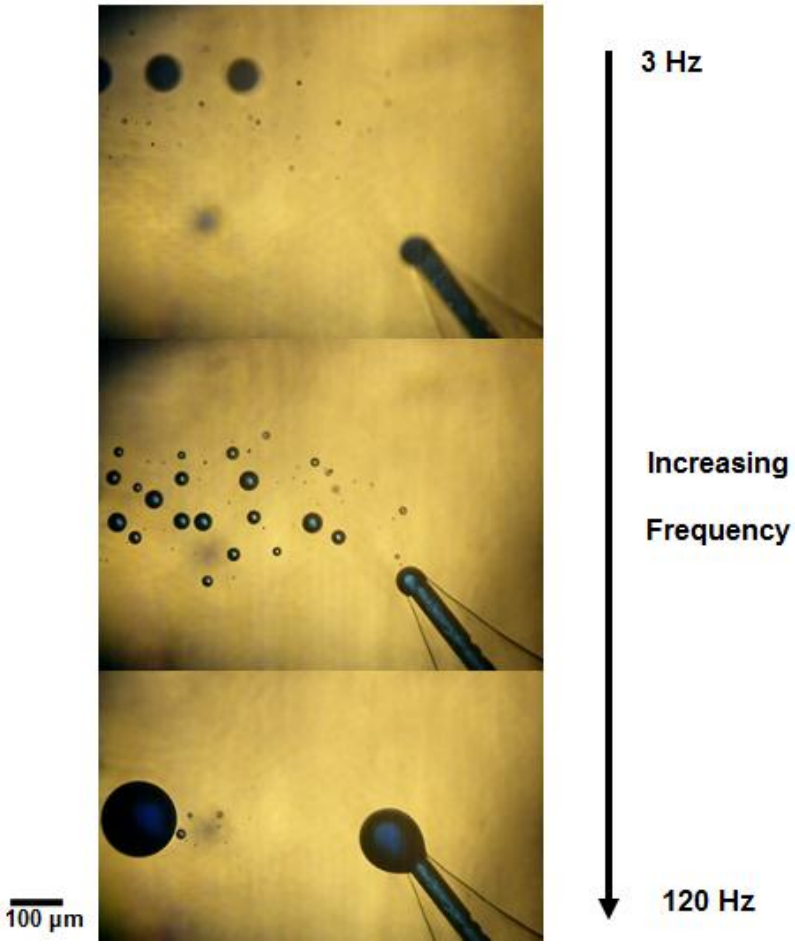

Figure 5.14 : *Effects of increasing frequency (1000 V, 4 mL/hour, 1.08 kPa).*

Figure 5.15 shows droplet generation at a frequency of 4 Hz, it is observed that at such low frequencies it is easy to obtain monodisperse droplets with very few satellites being generated. Completing image analysis on this setting to measure droplet velocity and diameter it is determined that in this case the stability number is greater than unity (St = 1.22). The stability number gives a rough estimate if stability is possible or not. However the application of an electrical signal not only causes changes in droplet sizes

not easily predicted analytically but also promotes droplet coalescence over larger droplet spacing. Indeed a wide array of literature exists in improving droplet coalescence phenomena under AC signals [71] thus it would be preferable to increase the channel flow rates or decrease the frequencies of the electrical signals being applied in order to obtain better droplet size distributions by increasing the stability number much greater than unity.

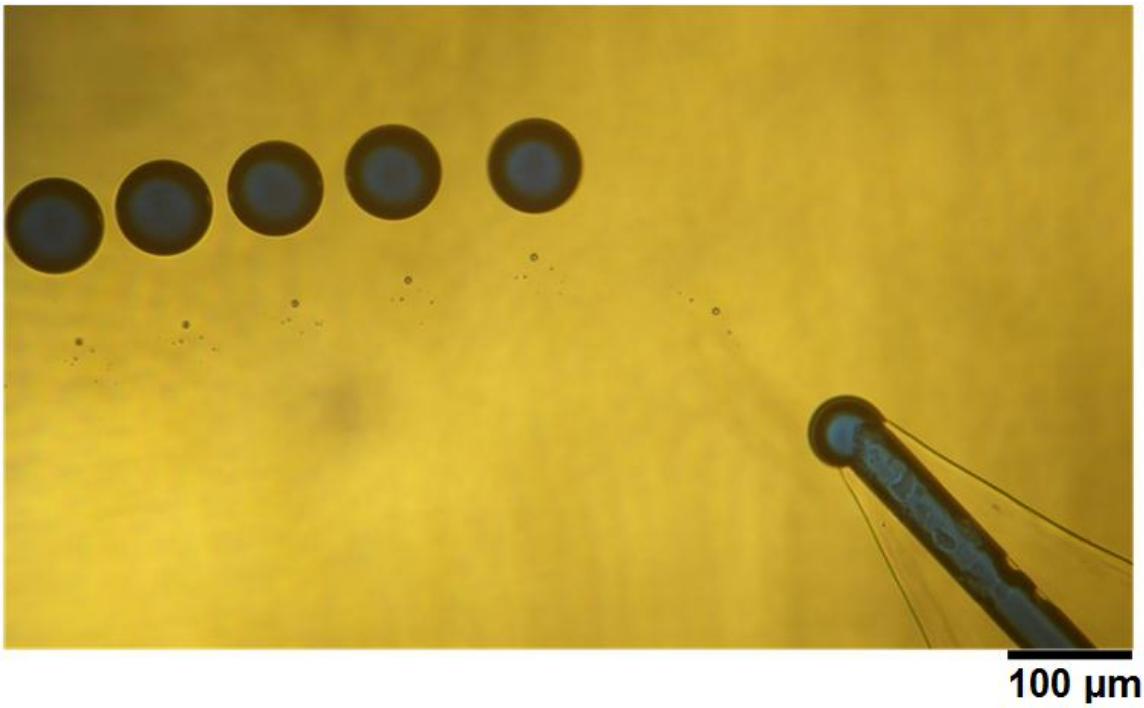

Figure 5.15 : 4 *Hz droplet generation.*

The channel flow rate was increased from 4 to 8 ml/hour in order to increase the spacing between droplets being formed and reduce droplet coalescence due to the AC electric field. Changing the channel flow rate is possible since earlier analysis utilizing the Weber number yielded that the effects of the flow would be minimal on the droplet size.

To summarize the results obtained in this section of the thesis quantitative data was obtained for the effect of the voltage and frequency on the droplet diameter. The channel flow rate and the pressure head were held constant (4 mL/hr, 1.08 kPa) whilst the voltage and the frequency were varied. The results are shown in **Figure 5.16**, it is clear that the droplet size is heavily dependent on the applied frequency. The dependency on frequency was previously explained and this figure further verifies the usage of a stability number.

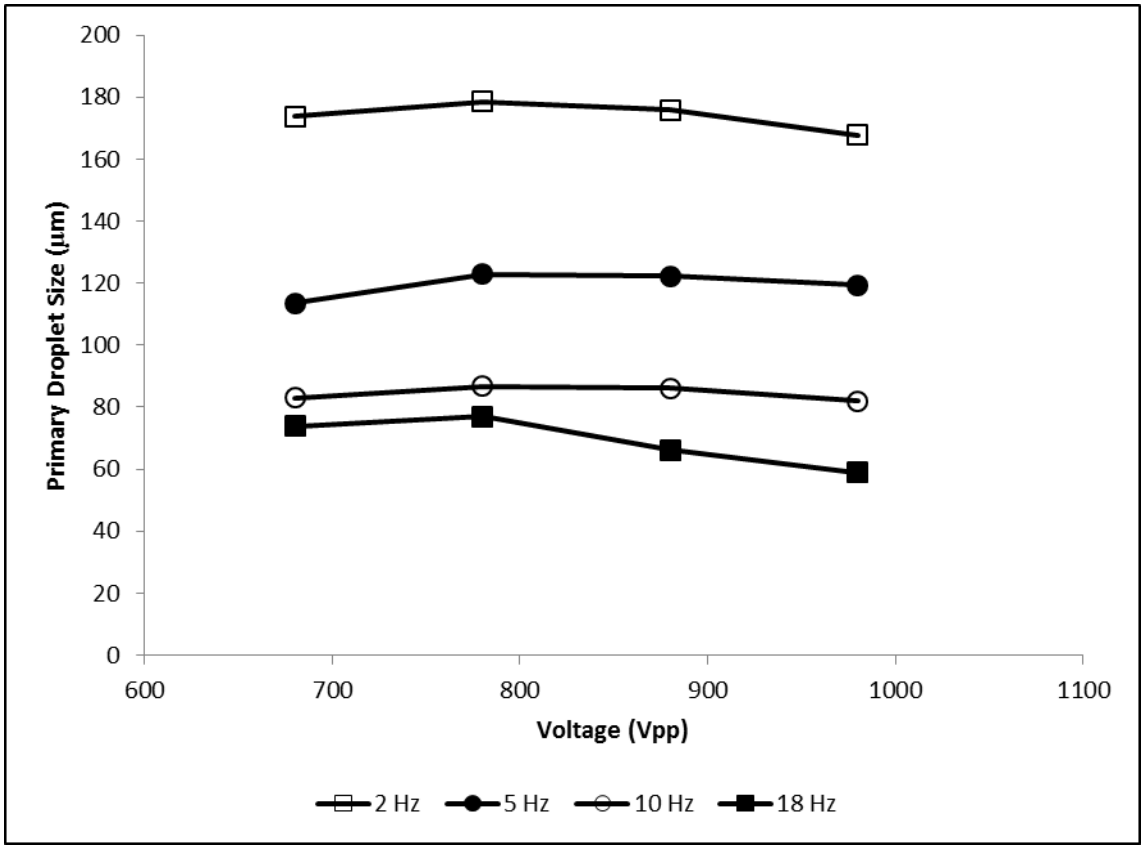

Figure 5.16 : *Droplet size Vs. Voltage at various frequencies when a ramping wave form is applied.*

Surprisingly, there is not much variation in droplet diameter with changes in voltage. This is due to the relatively low potential differences being utilized compared to previous work [49]. In work done by Atten *et al.,* voltages used are considerably lower than this case. Furthermore, these results [49] (**Figure 2.13**) also suggest there are regions where a change in voltage will have little effect on the droplet size. It appears that this result might be in contradiction to results obtained in **Figure 5.12** but this is not the case because the results from **Figure 5.12** are for voltages from 500-2000 where droplet generation will transition to spraying mode generating polydisperse smaller droplets. This experiment utilized the most stable region from **Figure 5.12** (650-1500 V) and analyzed it in greater detail. The ramping waveform gave good results but it is desired to improve upon the process further. When comparing the ramping waveform to a square, a ramping wave generated less satellite droplets. This is due to the fact that the peak voltage is not sustained reducing the charging of the meniscus, taking this one step further would be the usage of low duty cycle high voltage pulses.

5.3.4 Droplet Generation via High Voltage Pulses

Droplet generated was analyzed under the influence of high voltage pulses. These pulses had periods of 1.8, 1, and 0.5 ms and were significantly shorter than the period of the ramping waveforms previously utilized. The advantage of shorter pulse widths is elimination of the secondary droplet spray observed in the previous section with a ramping waveform. It is expected that at the lower end of pulse widths droplet generation will be most stable with a minimum of satellite droplets. Additionally several voltages

(900, 1100, 1400 V) will be utilized. It is expected higher voltages combined with longer pulse widths will cause excess charge build up and secondary droplet generation. Changing the signal to a pulsed waveform an oil flow rate of 8 mL/hour was utilized. A newly purchased high precision syringe pump was used to control the flow rate in the capillary at 2000 pL/s.

When utilizing pulses it is possible for droplet generation to occur in several different modes as shown in **Figure 5.17** and **Figure 5.18**. The first stage occurs when voltage is too low as to not overcome the capillary pressure or if the pulse width is too short and there is not enough flow of ions to the meniscus. In this case droplets with a diameter of 380 μm were generated by only the viscous drag. Increasing the pulse width or the voltage causes droplet generation as demonstrated in **Figure 5.17**. Increasing the pulse width and/or voltage further causes the situation in **Figure 5.18** in which coulombic fission occurs. Coulomb fission is the breakup of droplets due to meeting or exceeding the Raleigh limit of charge. The Raleigh limit of charge is the maximum charge a fluid can maintain before the electrostatic repulsion at the surface overcomes the surface tension and cause fission of the charged fluid volume. This process of breakup of a droplet due to excess electric charging is called Coulomb fission [48]. Furthermore it appears at this channel flow rate there are limitations to increases in frequency. At higher frequencies droplet coalescence is present and causes polydisperse generation thus the channel flow rate must be increased to compensate. In navigating these regions of droplet generation it is possible to change the electrical signal parameters to obtain the best results.

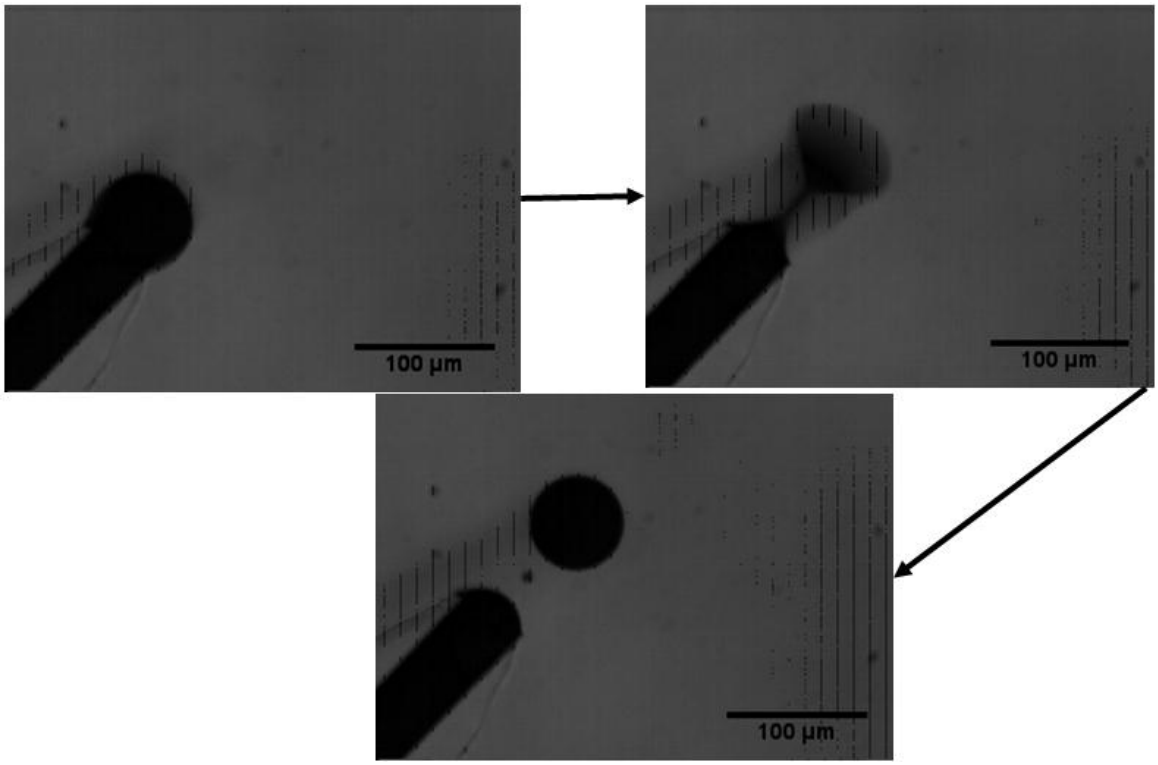

Figure 5.17 : *The first mode of droplet generation.*

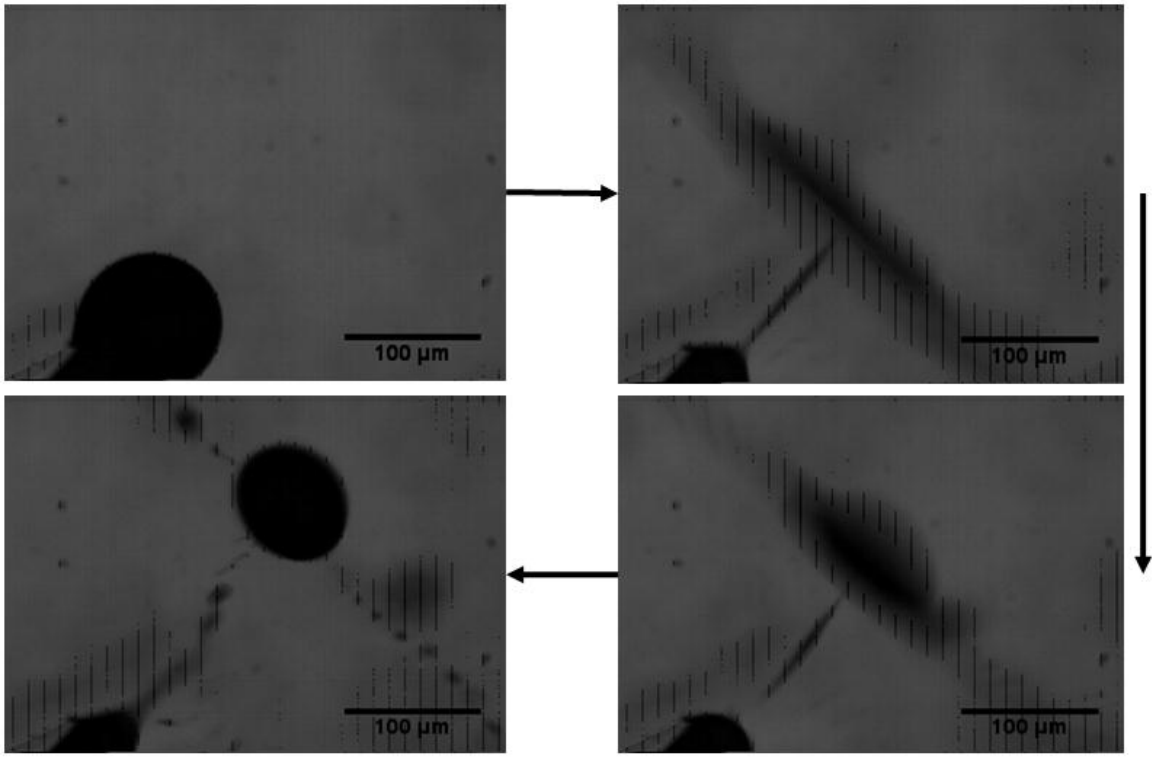

Figure 5.18 : *Coulomb fission occurring to excess charge.*

Experiments were completed in order to obtain the relation between the voltage, pulse width and frequency to the diameter of the droplet generated. These experiments were repeated using the same parameter levels with the addition of a DC bias. A DC bias is essentially an offset applied to a waveform, shifting the curve higher or lower along the voltage axis whilst the waveform remains the same. Two primary regions of droplet generation are observed, stable and unstable. The stable region is where monodisperse droplets with very few satallites are generated uniformly equally spaced apart. Instability means that droplets are generated in a chaotic manner with varying sizes and spacings. When no bias voltage is applied all the three voltages give the same result. As discussed before a change of frequency produces a change in the droplet size. However, in these

cases it was observed that there were changes in size (~10 μm) corresponding with changes in voltage. For longer pulse widths there is little change in size with a change in voltage which matches previous results well. When a 0.5 ms pulse width is applied it is observed that there is little change in size when changing voltage as seen in **Figure 5.19**, **Figure 5.20**, and **Figure 5.21**. At pulse widths of 1 ms for the higher voltages there is little change in size, however for 900 V a significant change in size is present. This resembles the situation occurring at a low pulse width at the higher voltages seen at 0.5 ms in **Figure 5.20** and **Figure 5.21**. It is possible that the 900 V curve (**Figure 5.19**) is similar to that of the higher voltages but merely it is offset along the pulse width axis. It may be that there is a minimum threshold of deformation due to application of the voltage that would enable the droplet to be formed when the pulse is terminated. This situation occurs in lower voltages since the deformation is proportional to the charge (from equation 5) which is directly related to the current which is: $I = \frac{V}{R}$. Given that the resistance remains the same and current is charge per unit time, whilst applying a lower voltage more time is needed in order to accumulate enough charge and cause a force great enough to overcome the surface tension. The reason that the droplet sizes change at the lowest pulse width between different voltages may be due to the pulse width being near the limit where no droplet generation occurs. In this region droplet generation is variable with periods of time when droplets are not being generated and hence unstable; to increase stability the pulse width has to be increased.

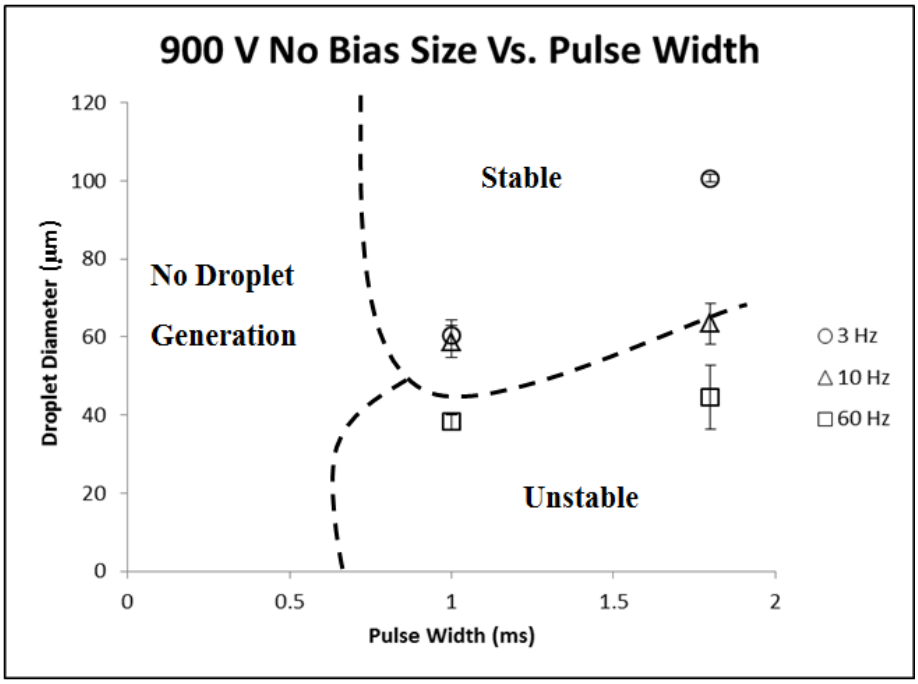

Figure 5.19 : *Droplet Diameter Vs. Pulse width at varying frequencies for a 900 V pulse.*

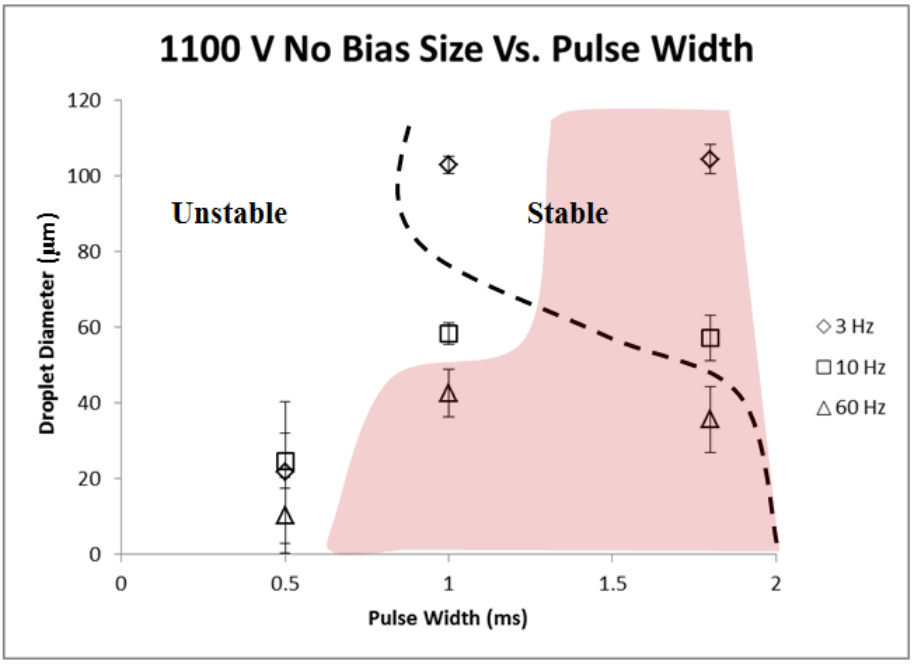

Figure 5.20 : *Droplet Diameter Vs. Pulse width at varying frequencies for a 1100 V pulse (pink shaded area indicates fission is occurring).*

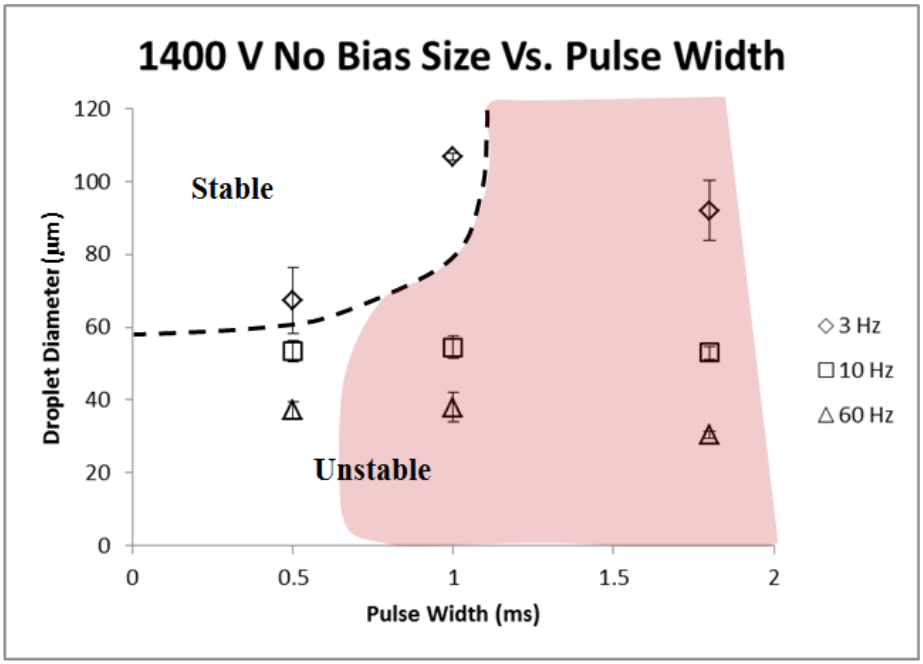

Figure 5.21 : *Droplet Diameter Vs. Pulse width at varying frequencies for a 1400 V pulse (pink shaded area indicates fission is occurring).*

In addition to these experiments a second set was completed to gauge the effects of applying a DC bias voltage when generating droplets. For 900 V there is no obvious change, however for 1100 V it is observed that an area where no droplet generation occurs has arisen. The cause of this is due to the presence of a 300 V bias. This causes the pulse to not have as dramatic change in the surface as would occurred if a bias was not applied. That is to say that at 300 V the meniscus is deformed already, with the pulse deforming it further. Thus when the pulse is terminated the meniscus goes back to a semi deformed state as opposed to when there is no bias voltage where it would have to revert to an undeformed natural state. This reduced gradient in the equilibrium surface tension causes the pulse width required to generate a great enough force and thus disturbance to be longer. At the higher voltage of 1400 V it is clear that there is a change in the

behaviour of the droplet generation when a bias is introduced. When looking to the high speed videos and comparing the droplet generation at 1400 V with and without bias as shown in **Figure 5.21** and **Figure 5.24** a few differences were observed. Without a bias voltage a single droplet is ejected, however with a bias two droplets are ejected in a more ordered fashion. This is caused by the introduction of the bias voltage and increased average voltage. The increase in electrical potential causes the meniscus to approach the Raleigh limit of charge. This can be seen in **Figure 5.18** more clearly where droplets are not generated due to pulse termination but rather ejected due to coulomb fission which is has been documented previously in literature [72].

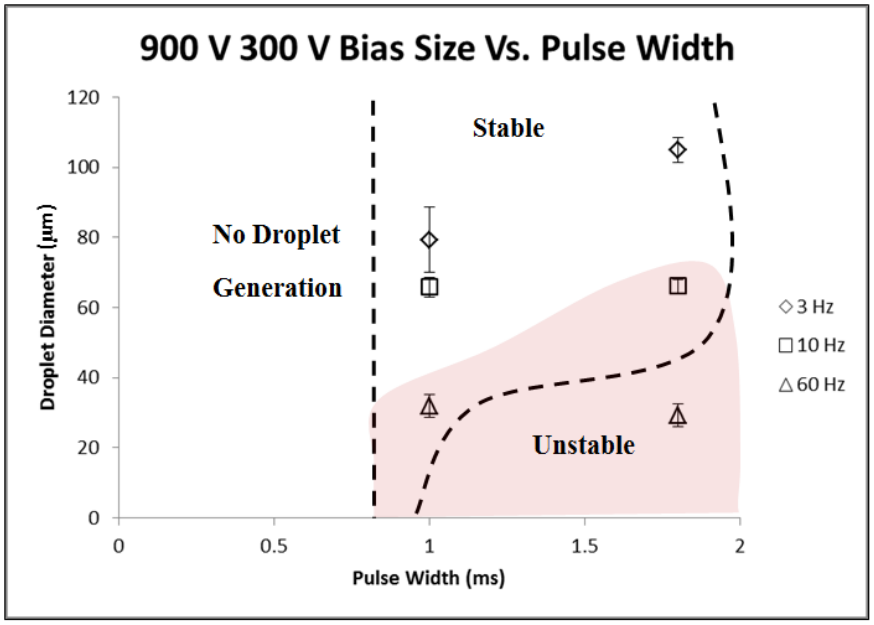

Figure 5.22 : *Droplet Diameter Vs. Pulse width at varying frequencies for a 900 V pulse with a 300 V DC bias (pink shading means fission is occurring).*

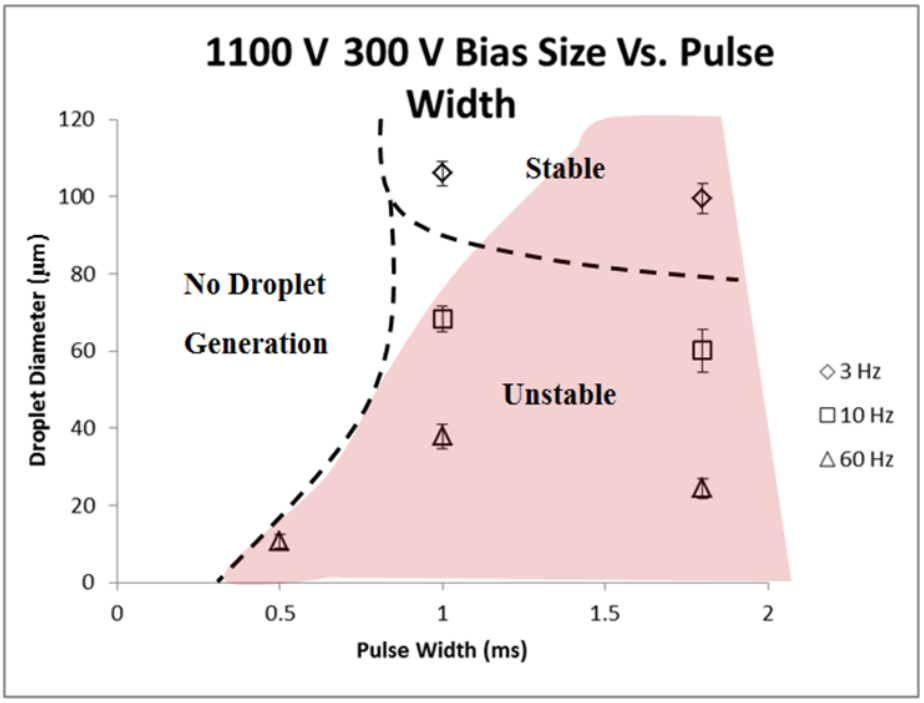

Figure 5.23 : *Droplet Diameter Vs. Pulse width at varying frequencies for a 1100 V pulse with a 300 V DC bias (pink shaded area indicates fission is occurring).*

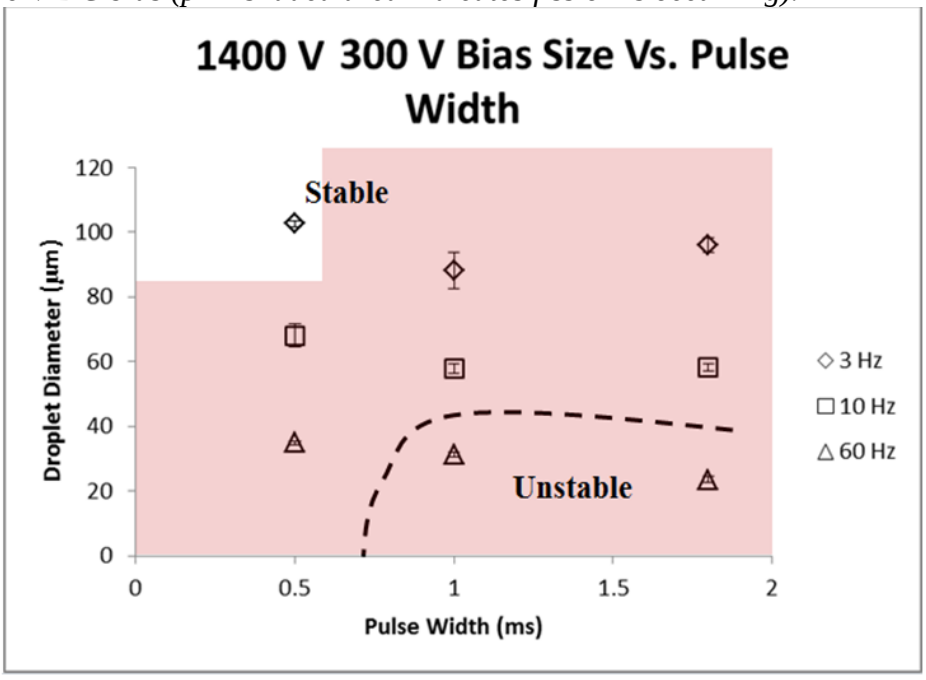

Figure 5.24 : *Droplet Diameter Vs. Pulse width at varying frequencies for a 1400 V pulse with a 300 V DC bias (pink shaded area indicates fission is occurring).*

It is possible to use the results of these experiments to determine optimum droplet generation areas and to tune the parameters to obtain the desirable sizes. **Figure 5.25** demonstrates the wide capabilities of controlling droplet size via electrical signal. Although relatively low frequencies were utilized it is possible to increase the rate of droplet generation by further shrinking down the device which would enable the usage of higher oil flow velocities. Although some characterization has been completed further work is required to gain a complete picture.

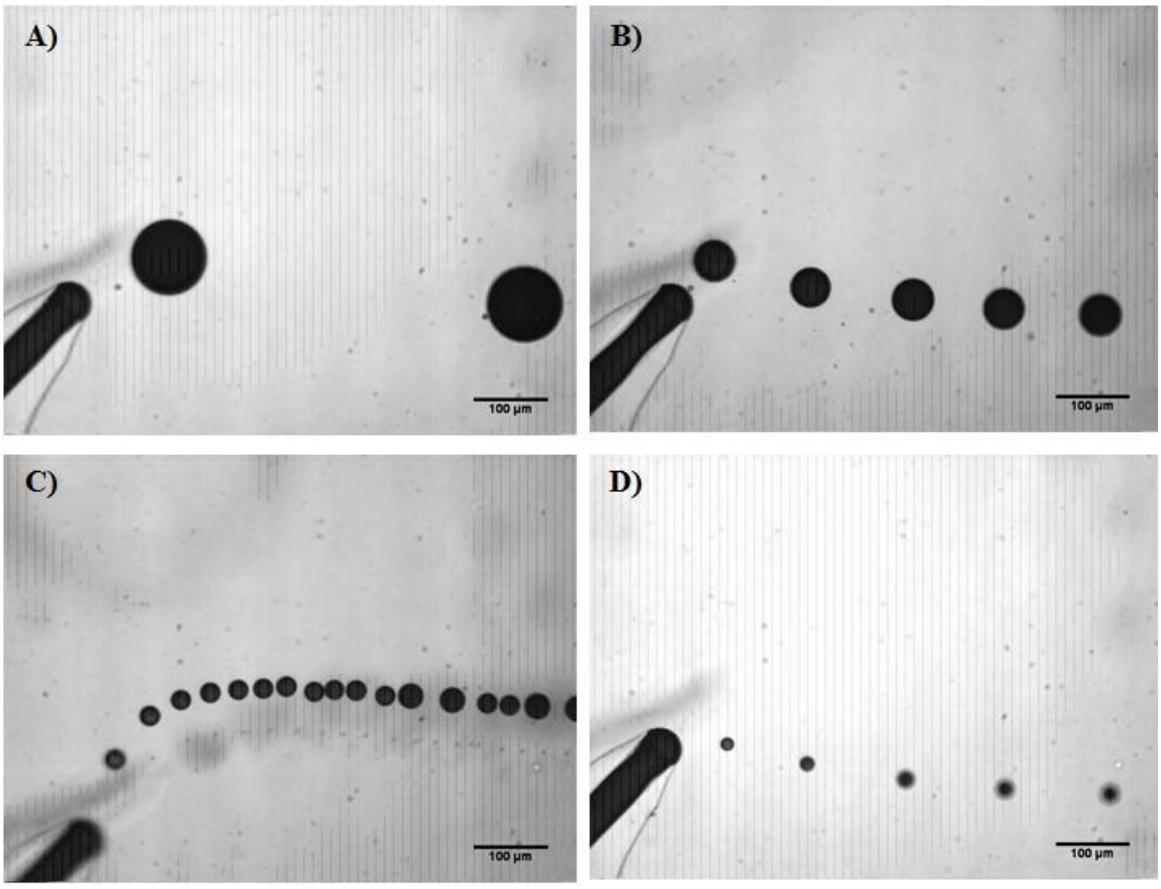

Figure 5.25 : *The possibilities when using electrical control A) 900 V no bias, 3 Hz, 1.8 ms B) 900 V no bias, 10 Hz 1 ms C) 900 V 300 V bias, 60 Hz, 1 ms D) 1100 V no bias, 10 Hz, 0.5 ms. Flow rates constant at: capillary= 2000 pl/s, primary channel 8 mL/hour.*

5.4 Summary

The device designed for electrically driven droplet generation proved to be robust, reliable, reusable, and repeatable. Droplets were generated using varying waveforms including square, ramping, and pulse. AC signals appeared to not give the best results when operated at higher frequencies due to the methylene blue ions large mass. Due to this a pulsing waveform was investigated. Data gained from high speed imaging enabled the analysis of droplet generation modes and the observations of unstable regions where droplet coalescence or coulomb fission occurred. Although fission and jetting can be avoided with proper selection of parameters, satellite droplets still exist to the nature of droplet formation as discussed in Chapter 2. With this knowledge and the careful selection of operation parameters monodisperse droplets were generated at moderate frequencies (1-60 Hz) ranging in size from under 5 μm to over a hundred μm. In summary, we demonstrated in this work the capability to generate large numbers of droplets with narrow size distributions reproducibly and reliably.

Chapter 6 Contributions & Future Work

6.1 Contributions

The contributions of this thesis consist of the design and characterization of two separate microfluidic devices capable of microdroplet generation.

6.1.1 Flow Focusing Device

Design

This research conducted in this thesis involved the design of a flexible microfluidic flow focusing device. This device is capable of creating uniformly mixed droplets of any two miscible fluids in a controlled and repeatable manner. This device eliminates the need of a central buffer stream separating the two miscible streams enabling better control over droplet composition by the design of an appropriate mixing section. Furthermore this device has been proven when used with covalently cross-linked smart polymers as opposed to others which deal with ionically cross-linked alginate. This device was developed for use with rapidly reacting systems and is thus very flexible when generating droplets of any two reagent system. Lastly this device is capable of generating droplets ranging from 10-200 μm via control of flow rates.

Large Quantity Production

The device developed in this work was tested under long term operation with reactive working fluids. The device demonstrated stable droplet generation for durations exceeding 30 hours. The droplet size dispersity was acceptable and comparable to other bulk emulsion production techniques. This long term operation of flow focusing devices dealing with reactive fluids has never been completed before and is unique to this work. Long term operation of this device enables the generation of large volumes of gel or polymer that are required for drug release studies.

6.1.2 Electrical Device

Design

The design that has been presented in this thesis is a novel microfluidic device that is capable of the electrogeneration of microdroplets. Although previous devices have involved the ejection of single droplets or continuous sprays no work had been done on creating a microfluidic device capable of high frequency electrogenerated microdroplets. This design allows for just that with an oil cross-flow clearing droplets away for collection. This device has proven to be robust and reusable providing the same droplet generation results from one device to the next.

Characterization and Modes

The capabilities of the device were characterized as well as the dependence of the droplet generation on varying parameters. Due to the lack of work in this area different

modes of droplet generation were experimentally documented and analyzed with the usage of high speed imaging equipment. This information enabled the optimization of the system and the generation of droplets in a novel microfluidic device with high frequency dynamic control, something which has never been done before. Additionally droplets ranging from under 5 to over 100 μm were generated while work done in literature the droplet sizes were typically limited by device geometry.

6.2 Future Work

In this thesis the base was made for two novel microfluidic droplet generation devices. With these devices a vast array of possibilities exists for research and applications.

Design and Parallel Operation

Both the flow focusing and the electrogenerated droplet devices could benefit from parallel operation. With changes to the design the flow focusing device can be parallelized involving several droplet generation sites increasing chip output and reducing operating times. Such a design involves many complexities and would be a great contribution to this area. Similarly the device for electrogenerated droplets could be improved by further miniaturization, the reduction in channel sizes would increase the flow velocities clearing away droplets and result in the possibility of higher frequency droplet generation. Furthermore the implementation of several capillaries and introduction of a more complex electrical control would allow for the simultaneous

control of various droplet generation sites. This enables the generation of multiple droplet sizes simultaneously which could be useful.

Computational Analytical Modelling

In order to obtain better control over droplet generation in both devices it is required to understand the process more thoroughly. The modelling of both devices would be the best way of gaining this knowledge and subsequently accurately predicting droplet generation. Models could be validated by the comparison to current experimental results and this would allow for further design refinements and increase the ease of use of said devices.

Biomaterial Encapsulation

One of the key applications of microdroplets is in the encapsulation of biomaterials in gels. Although some simple rudimentary experiments were conducted with DNA and mice muscle cell encapsulation, no concrete studies were done. The area of single-cell encapsulation is of most importance and these devices provide a means of accomplishing this task.

Fusion

Ultimately it would be desirable to have a device capable of rapid high frequency mixed droplet generation with dynamic control. The combination of the two principles used in this work would allow for this possibility but would be a difficult task. Fusion of these concepts would be best due to the possibility of reducing the size distributions of

microgels generated when mixed prior to generation. The effect of electric pulses on mixing would also provide another area of analysis.

List of References

[1] L. Rayleigh, "on the instability of jets," *Proc. London Math. Soc*, vol. 1873, no. 1873, 1878.

[2] T. R. A. (MIT), "MIT 1.63 Lecture Notes on Fluid Jets," *MIT Lecture Notes*, pp. 1-8, 2011.

[3] A. Huebner, S. Sharma, M. Srisa-Art, F. Hollfelder, J. B. Edel, and A. J. Demello, "Microdroplets: a sea of applications?," *Lab on a chip*, vol. 8, no. 8, pp. 1244-54, Aug. 2008.

[4] V. Srinivasan, V. K. Pamula, and R. B. Fair, "An integrated digital microfluidic lab-on-a-chip for clinical diagnostics on human physiological fluids.," *Lab on a chip*, vol. 4, no. 4, pp. 310-5, Aug. 2004.

[5] B. Zheng, J. D. Tice, L. S. Roach, and R. F. Ismagilov, "A Droplet-Based, Composite PDMS/Glass Capillary Microfluidic System for Evaluating Protein Crystallization Conditions by Microbatch and Vapor-Diffusion Methods with On-Chip X-Ray Diffraction," *Angewandte Chemie*, vol. 116, no. 19, pp. 2562-2565, May. 2004.

[6] P. Kumaresan, C. J. Yang, S. a Cronier, R. G. Blazej, and R. a Mathies, "High-throughput single copy DNA amplification and cell analysis in engineered nanoliter droplets.," *Analytical chemistry*, vol. 80, no. 10, pp. 3522-9, May. 2008.

[7] H. Search, C. Journals, A. Contact, M. Iopscience, and I. P. Address, "Microfluidic methods for generating continuous droplet streams," *Most*, vol. 319, 2007.

[8] Y.-C. Tan, J. S. Fisher, A. I. Lee, V. Cristini, and A. P. Lee, "Design of microfluidic channel geometries for the control of droplet volume, chemical concentration, and sorting.," *Lab on a chip*, vol. 4, no. 4, pp. 292-8, Aug. 2004.

[9] E. Brouzes et al., "Droplet microfluidic technology for single-cell high-throughput screening.," *Proceedings of the National Academy of Sciences of the United States of America*, vol. 106, no. 34, pp. 14195-200, Aug. 2009.

[10] O. Yogi, T. Kawakami, M. Yamauchi, J. Y. Ye, and M. Ishikawa, "On-demand droplet spotter for preparing pico- to femtoliter droplets on surfaces.," *Analytical chemistry*, vol. 73, no. 8, pp. 1896-902, Apr. 2001.

[11] a Jaworek, "Micro- and nanoparticle production by electrospraying," *Powder Technology*, vol. 176, no. 1, pp. 18-35, Jul. 2007.

[12] B. Kintses, L. D. van Vliet, S. R. a Devenish, and F. Hollfelder, "Microfluidic droplets: new integrated workflows for biological experiments.," *Current opinion in chemical biology*, vol. 14, no. 5, pp. 548-55, Oct. 2010.

[13] B. Zheng, L. S. Roach, and R. F. Ismagilov, "Screening of protein crystallization conditions on a microfluidic chip using nanoliter-size droplets.," *Journal of the American Chemical Society*, vol. 125, no. 37, pp. 11170-1, Sep. 2003.

[14] V. Trivedi, E. S. Ereifej, A. Doshi, P. Sehgal, P. J. Vandevord, and A. S. Basu, "Microfluidic encapsulation of cells in alginate capsules for high throughput screening.," *Conference proceedings : ... Annual International Conference of the IEEE Engineering in Medicine and Biology Society. IEEE Engineering in Medicine and Biology Society. Conference*, vol. 2009, pp. 7037-40, Jan. 2009.

[15] D. Lombardi, "Advances in microfluidics for drug discovery," *Expert Opinion on Drug Discovery*, pp. 1081-1094, 2010.

[16] J. Siepmann, N. Faisant, J. Akiki, J. Richard, and J. P. Benoit, "Effect of the size of biodegradable microparticles on drug release: experiment and theory.," *Journal of controlled release : official journal of the Controlled Release Society*, vol. 96, no. 1, pp. 123-34, Apr. 2004.

[17] C.-H. Choi, J.-H. Jung, Y. W. Rhee, D.-P. Kim, S.-E. Shim, and C.-S. Lee, "Generation of monodisperse alginate microbeads and in situ encapsulation of cell in microfluidic device.," *Biomedical microdevices*, vol. 9, no. 6, pp. 855-62, Dec. 2007.

[18] A. Bransky, N. Korin, M. Khoury, and S. Levenberg, "A microfluidic droplet generator based on a piezoelectric actuator.," *Lab on a chip*, vol. 9, no. 4, pp. 516-20, Feb. 2009.

[19] J. Aden and D. Collins, "The third-generation HP thermal inkjet printhead," *Hewlett Packard*, no. February, pp. 41-45, 1994.

[20] M. Tobío, R. Gref, a Sánchez, R. Langer, and M. J. Alonso, "Stealth PLA-PEG nanoparticles as protein carriers for nasal administration.," *Pharmaceutical research*, vol. 15, no. 2. pp. 270-5, Feb-1998.

[21] M. J. Blanco-Príeto, E. Fattal, A. Gulik, J. C. Dedieu, B. P. Roques, and P. Couvreur, "Characterization and morphological analysis of a cholecystokinin derivative peptide-loaded poly(lactide-co-glycolide) microspheres prepared by a

water-in-oil-in-water emulsion solvent evaporation method," *Journal of Controlled Release*, vol. 43, no. 1, pp. 81-87, Jan. 1997.

[22] S. L. Anna, N. Bontoux, and H. a Stone, "Formation of dispersions using 'flow focusing' in microchannels," *Applied Physics Letters*, vol. 82, no. 3, p. 364, 2003.

[23] H. Liu and Y. Zhang, "Droplet formation in a T-shaped microfluidic junction," *Journal of Applied Physics*, vol. 106, no. 3, p. 034906, 2009.

[24] T. Nisisako, T. Torii, and T. Higuchi, "Droplet formation in a microchannel network.," *Lab on a chip*, vol. 2, no. 1, pp. 24-6, Feb. 2002.

[25] J. Dohnal and F. Štěpánek, "Inkjet fabrication and characterization of calcium alginate microcapsules," *Powder Technology*, vol. 200, no. 3, pp. 254-259, Jun. 2010.

[26] P.-W. Ren, X.-J. Ju, R. Xie, and L.-Y. Chu, "Monodisperse alginate microcapsules with oil core generated from a microfluidic device.," *Journal of colloid and interface science*, vol. 343, no. 1, pp. 392-5, Mar. 2010.

[27] R. P. Dumitriu, G. R. Mitchell, and C. Vasile, "Rheological and thermal behaviour of poly(N-isopropylacrylamide)/alginate smart polymeric networks," *Polymer International*, no. 2010, p. n/a-n/a, May. 2011.

[28] W. Lee, L. M. Walker, and S. L. Anna, "Role of geometry and fluid properties in droplet and thread formation processes in planar flow focusing," *Physics of Fluids*, vol. 21, no. 3, p. 032103, 2009.

[29] P. Garstecki, I. Gitlin, W. DiLuzio, G. M. Whitesides, E. Kumacheva, and H. a Stone, "Formation of monodisperse bubbles in a microfluidic flow-focusing device," *Applied Physics Letters*, vol. 85, no. 13, p. 2649, 2004.

[30] S. L. Anna and H. C. Mayer, "Microscale tipstreaming in a microfluidic flow focusing device," *Physics of Fluids*, vol. 18, no. 12, p. 121512, 2006.

[31] Y. Murakami, T. Arakawa, E. Jeong, J. Go, and S. Shoji, "High Generation Rate of Uniform Oil-In-Water Droplets Formed by Multi-Stage Divergence Microflow Device," in *Solid-State Sensors, Actuators and Microsystems Conference, 2007. TRANSDUCERS 2007. International*, 1982, vol. 129, pp. 171–174.

[32] E. J. Vega, J. M. Montanero, M. a Herrada, and A. M. Gañán-Calvo, "Global and local instability of flow focusing: The influence of the geometry," *Physics of Fluids*, vol. 22, no. 6, p. 064105, 2010.

[33] J. Wacker, V. K. Parashar, and M. a M. Gijs, "Influence of Oil Type and Viscosity on Droplet Size in a Flow Focusing Microfluidic Device," *Procedia Chemistry*, vol. 1, no. 1, pp. 1083-1086, Sep. 2009.

[34] T. Ward, M. Faivre, M. Abkarian, and H. a Stone, "Microfluidic flow focusing: drop size and scaling in pressure versus flow-rate-driven pumping.," *Electrophoresis*, vol. 26, no. 19, pp. 3716-24, Oct. 2005.

[35] J. H. Xu, S. W. Li, J. Tan, and G. S. Luo, "Controllable Preparation of Monodispersed Calcium Alginate Microbeads in a Novel Microfluidic System," *Chemical Engineering & Technology*, vol. 31, no. 8, pp. 1223-1226, Aug. 2008.

[36] Q. Xu et al., "Preparation of monodisperse biodegradable polymer microparticles using a microfluidic flow-focusing device for controlled drug delivery.," *Small (Weinheim an der Bergstrasse, Germany)*, vol. 5, no. 13, pp. 1575-81, Jul. 2009.

[37] S. Xu et al., "Generation of monodisperse particles by using microfluidics: control over size, shape, and composition.," *Angewandte Chemie (International ed. in English)*, vol. 44, no. 5, pp. 724-8, Jan. 2005.

[38] D. Li and Y. Xia, "Electrospinning of Nanofibers: Reinventing the Wheel?," *Advanced Materials*, vol. 16, no. 14, pp. 1151-1170, Jul. 2004.

[39] M. Sato, M. Ieee, T. Hatori, and M. Saito, "Experimental Investigation of Droplet Formation Mechanisms by Electrostatic Dispersion in a Liquid – Liquid System," vol. 33, no. 6, pp. 1527-1534, 1997.

[40] V. N. Gorshkov and M. G. Chaban, "Nonlinear electrohydrodynamic phenomena and droplet generation in charged jets of conducting liquid," *Technical Physics*, vol. 44, no. 11, pp. 1259-1266, Nov. 1999.

[41] M. Cloupeau, "Electrostatic spraying of liquids : Main functioning modes," *Science*, vol. 25, pp. 165-184, 1990.

[42] H. Wang et al., "Electrospun poly(methyl methacrylate) nanofibers and microparticles," *Journal of Materials Science*, vol. 45, no. 4, pp. 1032-1038, Nov. 2009.

[43] G. Meesters, P. Vercoulen, J. Marijnissen, and B. Scarlett, "Generation of micron-sized droplets from the Taylor cone," *Journal of aerosol science*, vol. 23, no. 1, pp. 37–49, 1992.

[44] O. Manuscript, "Design of the Microchannel-Based Electrospray Evaporative Cooling Devices," 2010.

[45] Y. Hong, Y. Li, Y. Yin, D. Li, and G. Zou, "Electrohydrodynamic atomization of quasi-monodisperse drug-loaded spherical/wrinkled microparticles," *Journal of Aerosol Science*, vol. 39, no. 6, pp. 525-536, Jun. 2008.

[46] a Jaworek, "Micro- and nanoparticle production by electrospraying," *Powder Technology*, vol. 176, no. 1, pp. 18-35, Jul. 2007.

[47] J. Xie, W. J. Ng, L. Y. Lee, and C.-H. Wang, "Encapsulation of protein drugs in biodegradable microparticles by co-axial electrospray.," *Journal of colloid and interface science*, vol. 317, no. 2, pp. 469-76, Jan. 2008.

[48] B. Almería, W. Deng, T. M. Fahmy, and A. Gomez, "Controlling the morphology of electrospray-generated PLGA microparticles for drug delivery.," *Journal of colloid and interface science*, vol. 343, no. 1, pp. 125-33, Mar. 2010.

[49] P. Atten, a Ouiguini, J. Raisin, and J.-L. Reboud, "Drop-on-demand extraction from a water meniscus by a high field pulse," *2008 IEEE International Conference on Dielectric Liquids*, pp. 1-4, Jun. 2008.

[50] M. He, J. S. Kuo, and D. T. Chiu, "Electro-generation of single femtoliter- and picoliter-volume aqueous droplets in microfluidic systems," *Applied Physics Letters*, vol. 87, no. 3, p. 031916, 2005.

[51] B. Barbet, P. Atten, and A. Soucemarianadin, "Two-mode EHD stimulation of a continuous jet: Generation of drops and satellites," *The Journal of imaging science and technology*, vol. 41, no. 6, pp. 570–576, 1997.

[52] J. McDonald et al., "Fabrication of microfluidic systems in poly (dimethylsiloxane)," *Electrophoresis*, vol. 21, no. 1, pp. 27–40, 2000.

[53] E. Santini, L. Liggieri, L. Sacca, D. Clausse, and F. Ravera, "Interfacial rheology of Span 80 adsorbed layers at paraffin oil–water interface and correlation with the corresponding emulsion properties," *Colloids and Surfaces A: Physicochemical and Engineering Aspects*, vol. 309, no. 1-3, pp. 270-279, Nov. 2007.

[54] D. N. Sivakumaran, "Injectable In Situ Gellable Hydrogel-Microgel Composites For Drug Delivery," *Open Access Dissertations and Theses. Paper 4439*, 2010.

[55] K. L. Heredia, D. Bontempo, T. Ly, J. T. Byers, S. Halstenberg, and H. D. Maynard, "In situ preparation of protein-'smart' polymer conjugates with retention of bioactivity.," *Journal of the American Chemical Society*, vol. 127, no. 48, pp. 16955-60, Dec. 2005.

[56] Y. Xia, "Soft lithography," *Annual review of materials science*, vol. 11, no. 16, pp. 2772-8, Aug. 1998.

[57] M. a Eddings, M. a Johnson, and B. K. Gale, "Determining the optimal PDMS–PDMS bonding technique for microfluidic devices," *Journal of Micromechanics and Microengineering*, vol. 18, no. 6, p. 067001, Jun. 2008.

[58] G. Mahadevan, "Drug Delivery to the Posterior Eye Using Etched Microneedles," *Open Access Dissertations and Theses. Paper 6145*, 2011.

[59] S. Xu et al., "Generation of monodisperse particles by using microfluidics: control over size, shape, and composition.," *Angewandte Chemie (International ed. in English)*, vol. 44, no. 5, pp. 724-8, Jan. 2005.

[60] T. Ito, Y. Yeo, C. B. Highley, E. Bellas, and D. S. Kohane, "Dextran-based in situ cross-linked injectable hydrogels to prevent peritoneal adhesions.," *Biomaterials*, vol. 28, no. 23, pp. 3418-26, Aug. 2007.

[61] J. Tsai, "Active microfluidic mixer and gas bubble filter driven by thermal bubble micropump," *Sensors and Actuators A: Physical*, vol. 97-98, no. 1-2, pp. 665-671, Apr. 2002.

[62] P. Hiemenz, "Principles of colloid and surface chemistry," 1997.

[63] S. P. Hudson, R. Langer, G. R. Fink, and D. S. Kohane, "Injectable in situ cross-linking hydrogels for local antifungal therapy," *Biomaterials*, vol. 31, no. 6, pp. 1444–1452, 2010.

[64] R. W. Fox, A. T. McDonald, and P. J. Pritchard, *Introduction to fluid mechanics*, Sixth Edit. Wiley, 2004.

[65] A. D. Stroock, S. K. W. Dertinger, A. Ajdari, I. Mezic, H. a Stone, and G. M. Whitesides, "Chaotic mixer for microchannels.," *Science (New York, N.Y.)*, vol. 295, no. 5555, pp. 647-51, Jan. 2002.

[66] F. Blanchette, "Flow lines and mixing within drops in microcapillaries," *Physical Review E*, vol. 80, no. 6, pp. 1-8, Dec. 2009.

[67] T. Nisisako and T. Torii, "Formation of Biphasic Janus Droplets in a Microfabricated Channel for the Synthesis of Shape-Controlled Polymer Microparticles," *Advanced Materials*, vol. 19, no. 11, pp. 1489-1493, Jun. 2007.

[68] G. S. Wright, S. Member, P. T. Krein, J. C. Chato, and S. Member, "Electrical Manipulation of Menisci," *Industry Applications, IEEE Transactions on*, vol. 29, no. 1, pp. 103-112, 1993.

[69] G. S. Wright, P. T. Krein, S. Member, and J. C. Chato, "Self-Consistent Modeling of the Electrohydrodynamics of a Conductive Meniscus," *Time*, vol. 3, no. 4, 1995.

[70] J. S. Eow and M. Ghadiri, "Motion , deformation and break-up of aqueous drops in oils under high electric field strengths," *Chemical Engineering and Processing*, vol. 42, 2003.

[71] J. S. Eow and M. Ghadiri, "Electrostatic enhancement of coalescence of water droplets in oil : a review of the technology," *Chemical Engineering Journal*, vol. 85, pp. 357-368, 2002.

[72] D. Duft, T. Achtzehn, and B. Huber, "Rayleigh jets from levitated microdroplets," *Nature*, vol. 421, no. JANUARY, pp. 128-128, 2003.

Appendix

Flow Focusing Master Mould Fabrication

1. Place the Silicon wafer in oxygen plasma at 50 Watts exposure for 1 minute.
2. Spin Su-8-2075 photoresist on the wafer at 500 rpm for 30 seconds.
3. Ramp the speed up to 4000 rpm at an acceleration of 300 rpm/s and continue spinning for 30 sec at the final speed.
4. Prebake the wafer at 65 C for a time period of 1 minute and 17 seconds.
5. Increase the temperature 10 degrees per minute up to 95 C.
6. Bake at 95 C for a period of 7 minutes and 17 seconds.
7. Check for wrinkles on the wafer, if present return to hot plate until gone.
8. Mount the mask and the wafer on mask aligner and align the mask and wafer.
9. Expose the wafer to UV light for a total exposure energy of 177.86 mJ/cm^2.
10. Post-bake the wafer at 65 C for a time period of 1 minute 25 seconds.
11. Increase the temperature 10 C per minute up to 95C.
12. Bake at 95 C for a time period of 6 minute 25 seconds.
13. Submerge wafer into developer solution until features are clear (~10 minute).
14. Rinse the wafer with Isopropyl Alcohol to ensure complete removal of unexposed photoresist
15. If IPA leaves a white residue on the wafer, re-submerge in developer solution.